Determining the diagnostic accuracy of ^{68}Ga citrate-PET/CT in distinguishing benign from malignant lesions in the lung

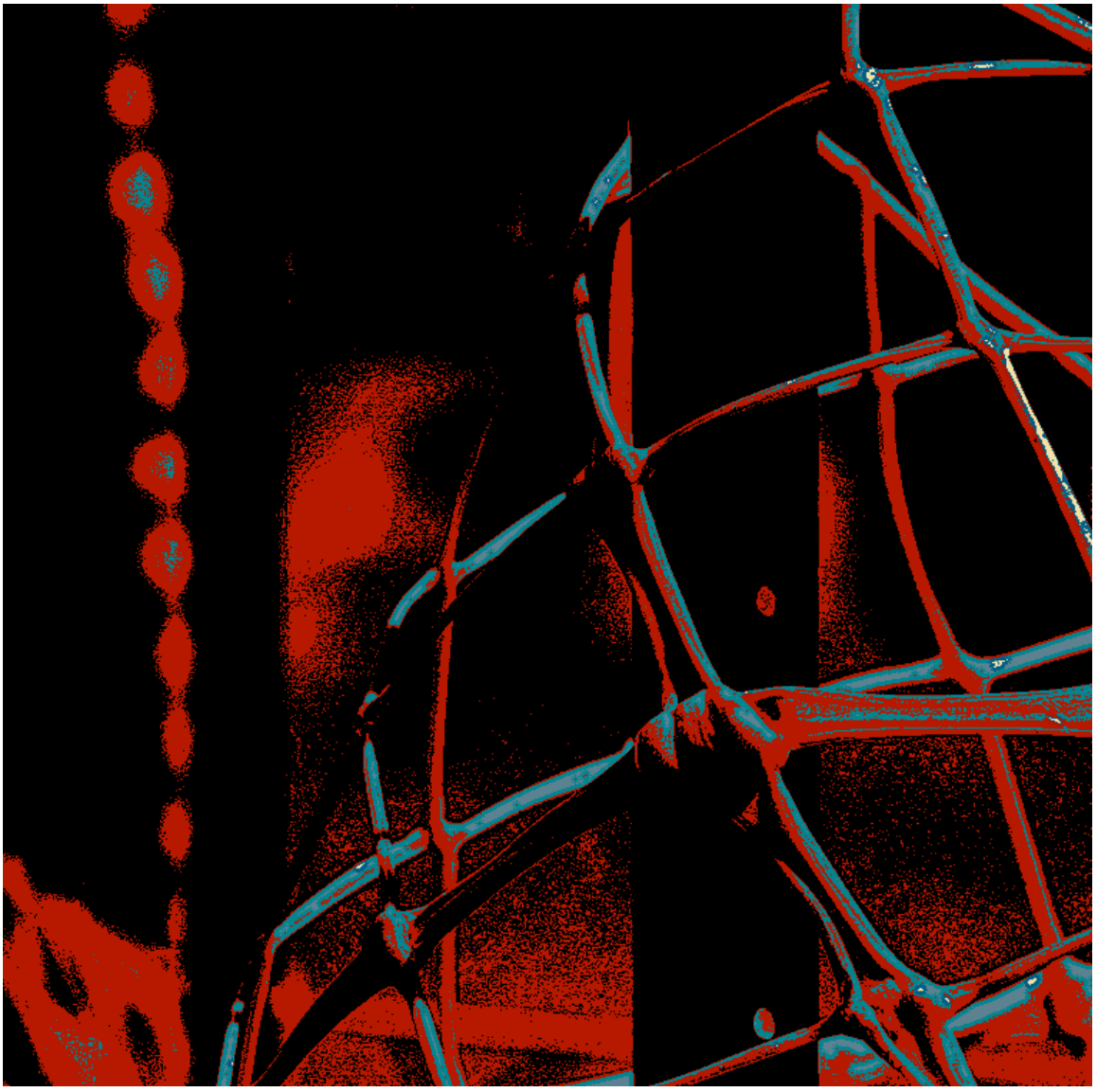

Dr Mariza Vorster
PhD: Medical Nuclear Science

Promoter: Prof MM Sathekge
Co-promoters: Prof A Maes & Prof C Van de Wiele
University of Pretoria (Jan 2014)

This thesis is dedicated to my parents, Quintus & Monica Vorster and to the much-cherished memory of Prof Bern Meyer, whose remarkable legend continues to live on in the hearts and minds of his students.

Thesis submitted to obtain the degree of Doctor in Medical Nuclear Science (PhD Medical Nuclear Science)

Student no 02544601

Examination Board

Internal Examiners

Prof Anton Stoltz
Dr JR Zeevaart

External Examiner

Prof R Dierxx

Promotor

Prof MM Sathekge

Co-Promotors:
Prof C Van de Wiele
Prof Alex Maes

*The content of this Thesis has been publicly defended on 27 Jan 2014 at the University of Pretoria.

Parts of the work contained in this thesis have been presented at the following national and International Scientific Meetings:

Invited speaker to the 16th International Meeting of International Society of Radiolabeled Blood Elements (March 2013)
Faculty Day at the Faculty of Health Sciences, University of Pretoria, Pretoria (Aug 2013) (3rd Prize awarded in Clinical category)
2nd Medical Olympiad in Thessaloniki, Greece (Oct 2013)
(1st Prize awarded in clinical category)

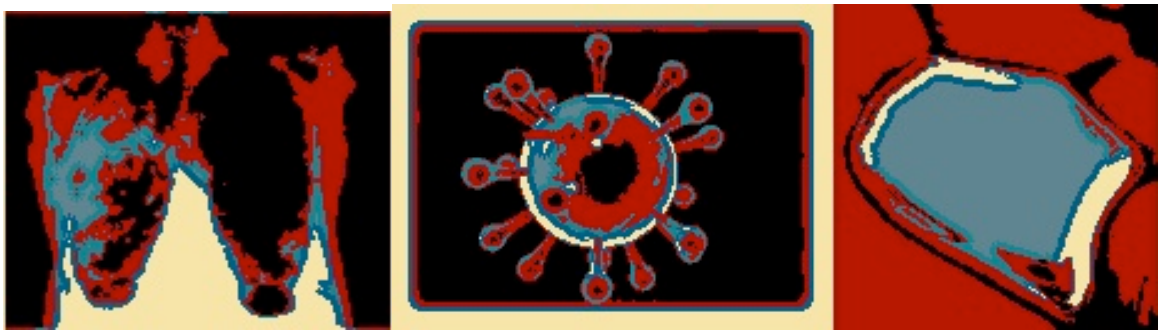

Table of Contents

Chapter 1: Introduction and Thesis Overview

The distinction between benign and malignant lesions in the lung is a commonly encountered clinical problem with important management implications. In the South African setting, this is complicated even further by the high prevalence of Tuberculosis (TB) and Human Immuno-deficiency Virus (HIV) co-infection, which often results in complicated clinical presentations consisting of combinations of simultaneous infective and malignant processes.

This study follows on previous work done at our department by *Sathekge et al.,* and is aimed at trying to improve on some of the limitations experienced with ^{18}F-FDG-PET/CT imaging. Various studies have indicated the inability of ^{18}F-FDG-PET/CT, even with the use of dual phase imaging, to distinguish accurately between benign- and malignant lung lesions in settings with a high TB prevalence. This has also been confirmed in our patient population. In patients with dual infection, early diagnosis of active TB is crucial in order to select the most appropriate treatment regime.

Chapters 2 & 3 form the basis of the **literature review** for this study. In Chapter 2 the importance of distinguishing benign from malignant lesions in the lung is highlighted and some of the major imaging tools and techniques that have been used sofar, is explored. In chapter 3,the application of various ^{68}Ga-labeled tracers is explored in the non-oncological setting.

In **Chapter 4**, the aspects around **^{68}Ga-citrate labeling and adherence to Quality Control** requirements are explored.

The **main study findings** are presented in **Chapters 5, 6** and **7**. In Chapter 5 the use of ^{68}Ga-citrate in distinguishing benign from malignant lung lesions is evaluated in the entire study population, whereas chapters 6 and & 7 deals with two smaller sub-groups of patients with Tuberculosis and pulmonary fibrosis.
Chapter 8 consists of a **case report** of a patient with Tuberculosis imaged with both ^{18}F-Choline and ^{18}F-FDG as an example of another possible novel tracer application.
Chapters **9 & 10** consist of a few **concluding remarks**, **future considerations** and a **Thesis Summary.**

Chapter 2: Distinguishing benign from malignant lesions in the lung: A review of non-invasive diagnostics

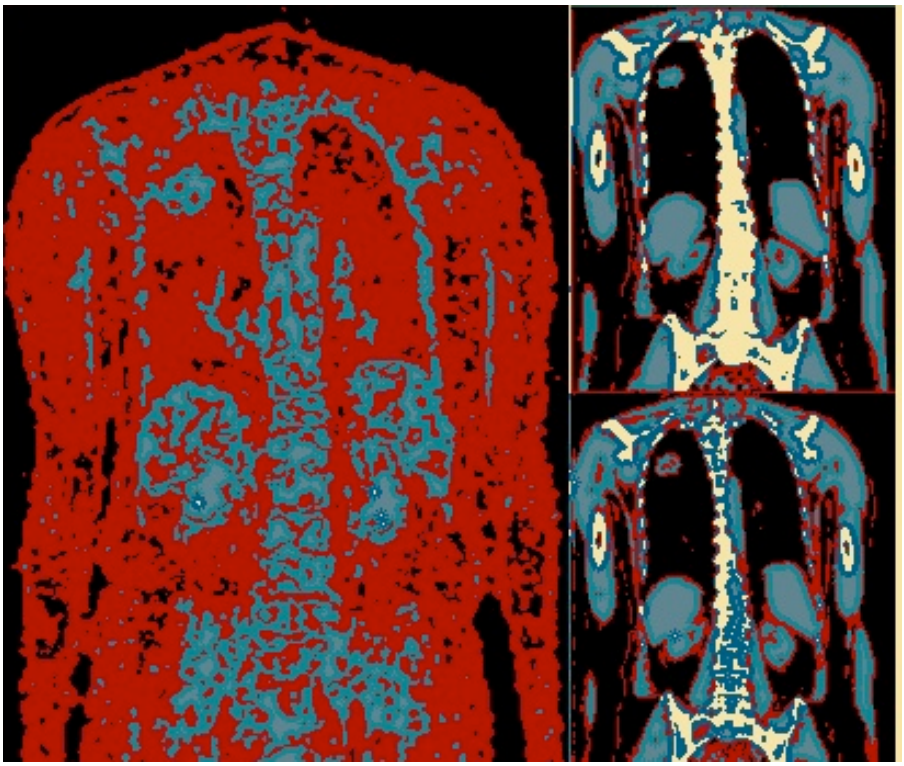

*An amended version of this chapter has been submitted for publication to Molecular Imaging and Biology

Introduction

The distinction between benign and malignant lesions always has important implications with regards to patient management and prognosis. Lung cancer is one of the most common fatal malignancies in both genders globally and therefore early detection is mandatory in order to improve outcomes. On the other hand, there is a clear need to avoid futile invasive diagnostic procedures such as thoracotomies, which often result in increased morbidity and in some cases even increased mortality[1]. In the chest, many different imaging methods have been used to try and avoid unnecessary invasive diagnostic procedures, whilst not missing any malignant ones.

For a diagnostic tool to be truly useful in this context, we would therefor require a test, which is both highly sensitive and specific with an excellent negative predictive value.

The solitary pulmonary nodule (SPN) frequently presents physicians with a diagnostic challenge, since the differential diagnosis includes a wide range of pathologies that ranges from benign causes to malignant ones, and as such it has been the focus of many publications. SPN is defined as a lung nodule less than 3 cm in diameter, which is surrounded by normal lung tissue and is not associated with any mediastinal lymph adenopathy. With advances in the imaging resolution, it is expected that the detection of these lesions will increase, causing diagnostic uncertainty.

Various imaging modalities and a variety of techniques have been employed to try and distinguish benign from malignant lung lesions with no conclusive answer to date. Conventional morphological imaging modalities that have been used in this setting include CT, MRI and ultrasound, all with various adaptations. Physiological imaging, in the form of nuclear medicine, has made use of various SPECT and PET radiopharmaceuticals as well as imaging at various time points. All of the above-mentioned tools suffer from particular limitations, though. It would therefore make sense to combine morphological and physiological imaging in an attempt to maximize the advantages and minimize the limitations. This has resulted in the development of PET/CT and PET/MRI, with rapid increases in availability and clinical demand.

This review will focus on the contributions made by both morphological and physiological imaging modalities in the quest to distinguish benign from malignant lesions in the lung. This has not been restricted to the solitary pulmonary nodule only, and includes any lung lesions of an indeterminate nature.

Search Strategy

Library databases and Google scholar were searched making use of the following **keywords**: **"benign"** and **"malignant"** and **"lung"** or **"thorax"** or **"chest"**

Inclusion criteria: all publications where the focus was on distinguishing benign from malignant lesions in the chest/thorax/lung.

Exclusion criteria: papers where the diagnosis/ distinction was based on an intervention/ procedure, a focus on a specific condition and not a general comparison and any case studies.

In **PubMed**, the above-mentioned search strategy resulted in 44 publications, which were further limited according to the exclusion criteria to result in 15 relevant papers.

An additional search performed on the **Cochrane Library** with the following keywords: benign malignant lung imaging resulted in 14 reviews, which were further limited to 9 relevant articles.
Reviewing the references provided by the above-mentioned publications further augmented the computerized literature search.

Pretest Probabilities

Before having a look at the contributions made by the various imaging disciplines, it may be worthwhile to consider the clinical characteristics of a patient in order to choose the most appropriate investigation The malignant potential of lung lesions vary significantly with patient characteristics such as age, gender, smoking history and history of cancer, amongst others.

The Bayesian theorem requires an estimation of the pre-test probability of a particular disease being present and taking into account whether or not the outcome of the selected test (whether positive or negative) will influence the management in any way. If the patient falls into a very low risk for lung cancer (e.g. young age, non-smoker, no history of cancer and clinical findings more in keeping with an infective cause, follow-up without extensive or invasive investigations would be suitable. However, if a high probability of a malignant process exists (e.g. advanced age, smoker, cancer history) it would be advisable to obtain a definite tissue diagnosis without delay.

Bayes' theorem for SPN requires that the clinician first determine the pre-test probability of any malignancy (based on the history and examination). The Likelihood Ratio (LR) is then multiplied with the pre-test-probability in order to calculate the post-test probability.

It makes sense then, that imaging-especially nuclear medicine plays an important role in the cases with an intermediate probability of malignancy, such as is often encountered with a SPN presentation. Data on the prevalence of SPN in sub-Saharan-Africa is not readily available. In the US a prevalence of 0.2% of all chest radiographs has been reported with cancer present in anything from 10% to 70% of these.[2,3]

Clinical Guidelines

Swensen et al. (1997) [4] derived the predictive value of clinical and CXR findings with multivariate logistic regression in a retrospective cohort consisting of 629 patients with radiologically indeterminate pulmonary nodules. They found that the following three clinical characteristics were independent predictors of a malignant lesion: age, smoking status and a personal history of malignancy. Independent radiological predictors of malignancy were the diameter of the lesion, the presence of spiculation and upper lobe localization. The same group (1999) then continued to test whether their prediction model would improve on the assessments made by physicians, but found that it did not.[5]

The Fleischner Society recently updated their 2005 guidelines[6] for the management of lung nodules, by the inclusion of recommendations specifically for sub-solid nodules. Emphasis is on the importance of the early detection of peripheral adenocarcinomas, which may present as ground glass nodules or opacities. Individualization in the management approach is also emphasized.[7] The authors recommend the use of ^{18}F-FDG-PET for the evaluation of part-solid nodules that are more than 10 mm.

McNulty et al. (2012) suggested CT in the follow-up of evaluation of small lung nodules discovered on chest radiographs, and PET/CT for characterization in certain settings, or where malignancy is strongly suspected in order to accurately stage the disease.[8]

Ost and Gould (2012)[2] reviewed the clinical decision making process in patients with pulmonary nodules by updating the definition of SPN, looking at methods for estimating the probability of cancer, comparing the benefits and harms of current management strategies and integrating risk stratification and alternative management practices into a algorithm. Emphasis is placed on the importance of the use of various thresholds: an observation threshold, and a surgical threshold with a need for further diagnostic testing (with CT-FNA or PET) in between these two thresholds.

In summary

- The investigation of pulmonary nodules is becoming more important with its increased detection due to advances in imaging resolution.
- The most important consideration is not to miss a potentially curable lung cancer at an early stage. (Here possible false negatives should be kept in mind).
- On the other hand, most definitive diagnostic procedures are invasive, costly and may increase morbidity and should therefore be reserved for those with a higher probability of malignancy. A risk/benefit analysis should be made, taking into account patient co-morbidities and preferences, also keeping in mind possible false positive findings on imaging.
- Pre-test probability for a malignancy should be assessed in every case, based on history, clinical examination and available imaging characteristics (no special tools required!).
- Further investigation with non-invasive modalities such as PET/CT, should be reserved for patients with an indeterminate probability for malignancy, and only where this is expected to alter the management.

Contributions from morphological imaging

In the past, conventional imaging such as chest radiographs and CT scans have played a major role in the identification and classification of lung nodules and clinicians are generally familiar with these. Advantages provided by the afore-mentioned imaging modalities include high-resolution images that result in excellent localization capabilities and accurate assessment of the extent of local- and nodal involvement.

A number of widely accepted criteria have been used in order to determine the character of lung lesions. Characteristics that are more in favour of a malignancy include semisolid lesions or those with a pure ground-glass appearance and those with spiculated, lobulated or irregular margins nodules or acentric calcifications. The probability of a malignant lesion increases with increasing lesion diameter. Imaging characteristics that are more in favour of a benign lesion, include the following: smaller size (<1cm), calcifications within the lesion which are central, diffuse, laminar or popcorn in nature and peripheral lesions with smooth margins.[9,10]

Diederich et al. (2005) analyzed 133 pulmonary nodules with the purpose of identifying CT imaging characteristics indicative of resolving lesions. They concluded that resolving (benign) pulmonary nodules are mostly sub-centimeter peripherally located, solid, well-defined, and non-lobulated, but the authors could not identify specific distinguishing demographic or morphologic features.[11] The afore-mentioned patterns, however, are not frequently encountered in clinical practice and more than 40% of non-calcified SPN seen on CXR are benign.[12]

Cronin et al. (2008) conducted a meta-analysis on cross-sectional imaging modalities in the diagnosis of malignancy. They compared the sensitivities and specificities of dynamic contrast-enhanced CT (DCE CT), dynamic contrast-enhanced MRI (DCE MRI), ^{18}F-FDG-PET and ^{99m}Tc-depreotide.[13]

DCE CT evaluates the vascularity of a lesion, which is expected to be higher in malignant disease. Contrast enhancement of nodules is measured by the Hounsfield units (HU) and an increase of 15 HU has been shown to distinguish malignant from benign lesions with high sensitivity and PPV[4]. DCE MRI offers superior tissue contrast resolution to CT and despite being prone to various artifacts, has demonstrated test characteristics similar to that of DCE CT.

Their results demonstrated that nuclear medicine imaging performed the best overall with the following test characteristics: ^{18}F-FDG PET demonstrated a sensitivity of 95% and specificity of 82%, and ^{99m}Tc-depreotide SPECT showed a sensitivity and specificity of 95%and 82% respectively. This was followed by morphological imaging with the following results: DCE MRI sensitivity 94% and specificity 79%, DCE CT sensitivity and specificity of 93% and 76% respectively. Pooled positive likelihood ratios were as follows: ^{18}F-FDG PET 5.44; ^{99m}Tc-depreotide 5.16; DCE MRI 4.57 and DCE CT 3.91. Pooled negative predictive values were as follows: ^{18}F-FDG PET 0.06; 99mTc-depreotide 0.06; DCE MRI 0.08 and DCE CT 0.1. (A high positive LR is required to rule in disease and a low negative LR to rule out disease). This translates to the following: A positive ^{18}F-FDG PET or ^{99m}Tc-depreotide will result in a moderate change in disease likelihood, whereas a positive result on DCE CT- or MRI will result in only a small change in disease likelihood. On the other hand, a negative ^{18}F-FDG PET, ^{99m}Tc-depreotide or DCE MRI will result in a large change in the likelihood of disease. A negative DCE CT will bring about only a moderate change in disease likelihood.[13]

These results provide compelling arguments for the routine use of functional imaging for SPN-either with ^{18}F-FDG/PET or with ^{99m}Tc-depreotide.

Yuan et al. (2013) assessed the diagnostic accuracy of first-pass dual-input perfusion CT in the differentiation of benign from malignant lung nodules in 56 patients. The authors calculated pulmonary blood flow, bronchial flow and a perfusion index in the lung lesions, which were compared to the tissue diagnosis and analyzed using receiver-operating characteristic curve (ROC) analysis. They found that all three vascular parameters differed significantly between benign and malignant lesions, with the biggest differences provided by the perfusion index. The perfusion index represents the fractions of both the pulmonary and the systemic circulation in SPN. The authors concluded that the perfusion index is valuable in the identification of malignant SPN.[14]

Several ongoing European trials are currently evaluating the use of CT as a screening tool in lung cancer. This is in an attempt to address the increasingly high mortality rates and associated costs of this disease. The largest of these trials is the NELSON trial, and findings from this study have suggested that future assessment of lung nodules should preferably be based on 3D-volumetric evaluation in order to improve the accurate assessment of pulmonary nodules. The NELSON criteria states that a volume increase of 26% is hardly appreciated when measuring the diameter, whereas a change of 25% in diameter (current threshold for growth) represents almost a doubling in nodule volume.[15]

In summary

- In the morphological characterization of indeterminate lung lesions, the best documented evidence for a malignant lesion is provided by the following: upper lobe localization, spiculated border, increased lesion diameter, semi-solid nodules and those with a ground glass appearance.
- Various specialized techniques/ capabilities such as dynamic contrast enhancement and first pass dual-input perfusion have been added to CT in order to add functional information. These appear promising, (but may be expensive and not readily available).
- The role of MRI and PET/MRI in this setting is uncertain.

- Meta-analysis comparing morphological imaging to functional imaging has demonstrated the superiority of functional imaging.

Contributions from functional imaging

Nuclear Medicine has employed a variety of tracers and techniques in order to distinguish benign from malignant lesions. SPECT tracers which have been used in this context include ^{99m}Tc-sestamibi, ^{201}Thallium, ^{111}In-octreotide, ^{99m}Tc-depreotide and ^{67}Gallium citrate. The majority of PET work in this setting has made use of ^{18}F-FDG PET, with fewer reports on the use of ^{18}F-FLT, ^{11}C-Methionine and ^{11}C-Choline. Our group has recently evaluated the use of ^{68}Ga-citrate in this setting.

SPECT tracers

^{99m}Tc-depreotide is a synthetic peptide which functions as a somatostatin analogue and is probably the best-documented SPECT tracer used in the setting of SPN. Its use is based on the expression of high-affinity somatostatin receptors (SSTRs) on various malignancies, including small cell lung cancer. There is still some uncertainty with regards to the precise uptake mechanism, as some authors attribute uptake to lymphocytes infiltrating tumours.[16]

Blum et al. (2000) in a multi-center trial, investigated the use of **^{99m}Tc-depreotide** in 114 patients with pulmonary nodules of less than 6 cm and absence of benign calcification patterns on CT. Scintigraphic findings were compared to histopathological diagnoses and this resulted in a **sensitivity of 96.6%** and a **specificity of 73.1%.** There were three false negatives, all due to adenocarcinoma, and seven false positives, the majority of which were due to granulomas. The authors concluded that **^{99m}Tc-depreotide was useful in the evaluation of SPN with sensitivity and accuracy comparable to that of ^{18}F-FDG PET.**[17]

Anther promising SPECT tracer based on somatostatin receptor imaging, is **^{99m}Tc-EDDA-HYNIC-TOC**. This is a hydrazine nicotinic acid-derived somatostatin analogue, in which EDDA is used as a co-ligand to improve both the *in vivo* and the in vitro stability of the complex. It also has fast plasma clearance with predominantly urinary clearance and affinity for various malignant tumours (including both small cell- and non-small cell lung cancer).[18]

Plachcinska and co-workers (2004) evaluated 50 patients who presented with SPN on chest radiograph with the afore-mentioned tracer and compared the findings to histology, cytology or bacteriology. They found increased ^{99m}Tc-EDDA-HYNIC-TOC accumulations in 28/31 (90%) patients with malignant lung lesions, with false negative occurrences noted in liposarcoma and melanoma. No tracer accumulation was detected in 15/19 (79%) patients with benign lesions, with false positives noted in a tuberculoma and a hamartoma. The authors concluded that ^{99m}Tc-EDDA-HYNIC-TOC scintigraphy appears to be effective in the differentiation of SPN.[19]

The use of **^{201}Tl-SPECT** in the setting of SPN is based on the observation that ^{201}Tl demonstrates increased accumulation in malignant tumours on both early and delayed imaging, whereas benign lesions tend to show increased uptake only on early images. Thallium is a potassium analogue and its uptake is related amongst others to perfusion and functioning of the Na/K/ATPase.[20]

^{99m}Tc-MIBI and **^{99m}Tc-tetrofosmin** are both better known for their role in myocardial perfusion imaging, although the role of MIBI in oncology is also well documented. The uptake of both of these lipophilic cations is related to perfusion and the negative mitochondrial- and cytoplasmic cell membrane potential.

Spanu et al. (2006) evaluated the use of **^{99m}Tc-tetrofosmin SPECT** in the characterization of indeterminate nodules on CT in 111 patients. Images were analyzed both qualitatively and semi-quantitatively with tumor/normal tissue ratios and compared to histology. This resulted in a **sensitivity of 91.7%, specificity of 88.9%, accuracy of 91%, PPV of 96.2% and a NPV of 77.4%.**[21]

Nikoletic et al. (2011) evaluated the impact of imaging with **^{99m}Tc-MIBI** in sixty patients with indeterminate pulmonary nodules detected on CT. Early images were acquired at 10 minutes post-injection and delayed images from 60-120 minutes post-injection. Increased MIBI accumulation in the lesions was considered positive and resulted in **sensitivity of 90%, specificity of 76.6%, PPV of 88.5% and NPV of 83.3%.** This provides an attractive, cost-effective alternative to centers without PET. It also offers significant advantages over Tl-201 and Ga-67 in terms of logistics and imaging quality.[22]

In summary

- The following SPECT tracers have been used in the setting of SPN with comparable results: ^{99m}Tc-depreotide, ^{99m}Tc-EDDA-HYNIC-TOC, Thallium-201, ^{99m}Tc-MIBI and ^{99m}Tc-tetrofosmin.
- ^{99m}Tc-Depreotide and ^{99m}Tc-MIBI appear preferable and provide attractive alternatives to centers without access to PET facilities.
- Results with ^{99m}Tc-EDDA-HYNIC-TOC appear promising.

PET tracers

The important role of ^{18}F-FDG-PET in the characterization of in particular SPN is well recognized has been the focus of many studies.^{18}F-FDG-PET is able to distinguish benign from malignant lesions in certain settings, by making use of a SUVmax threshold of 2.5. This is particularly relevant in settings with a low prevalence of granulomatous disease. In a setting such as the South African one, however, findings have to be interpreted with caution, since the physiological behavior of granulomatous lesions is quite similar to that of malignant lesions.[23]

Gupta et al. (1996) investigated the probability of malignancy in SPN using imaging with ^{18}F-FDG PET in 61 patients with radiologically indeterminate nodules. Tracer accumulation was evaluated both qualitatively (compared to background mediastinal activity) and semi-quantitatively and compared to the histological diagnosis. For the detection of malignancy, ^{18}F-FDG PET had a sensitivity of 93%, specificity of 88% and PPV of 92%. By incorporating Bayes' theorem into their analysis, the authors calculated that the probability of malignancy in a PET positive study was 83%, which increased along with the patient's age and the size of the nodule. A negative PET scan was associated with a less than 5% malignancy risk.[24]

Herder et al. (2004) investigated the diagnostic accuracy of ^{18}F-FDG-PET in the evaluation of 36 solitary pulmonary nodules in 35 patients using histology as the gold standard. In this retrospective study, they found that PET accurately classified 30/36 lesions when using moderately increased FDG uptake as the criterion for malignancy. The authors reported a sensitivity of 93%, specificity of 77%, PPV of 72% and NPV of 94%.[25]

Pauls et al. (2008) conducted a large, prospective study on 267 patients with newly diagnosed lung lesions who underwent PET. The aim was to evaluate the performance of PET/CT in the differentiation of benign and malignant lesions and to compare its performance to that of either study alone. Histopathology served as the gold standard, PET was evaluated qualitatively (relative to the mediastinum) and CT according to a five point scale ranging from definitely benign to definitely malignant. The authors concluded that integrated PET/CT was significantly more accurate than CT alone, but did not significantly improve the accuracy of ^{18}F-FDG-PEt al.one. The addition of the metabolic component provided by PET to CT reduced equivocal findings and increased specificity significantly.[26]

In a landmark meta-analysis conducted by Gould et al. (2001), the authors analyzed 40 studies with a total of 1474 lung lesions to determine the accuracy of PET in the diagnosis of pulmonary nodules. They found a maximum pooled sensitivity of 91.2% and specificity of 89.1%, which they estimated in practice to be closer to a sensitivity of 96.8% and specificity of 77.8%. The authors also found no difference in diagnostic accuracy using quantitative or qualitative assessments, regardless of the lesion size.[27]

The above-mentioned studies evaluated only the ability of various imaging techniques to distinguish benign from malignant lesions in the lung. However, there has been several reports on the similar behavior of granulomatous lesions, especially in patients with TB to that of malignant lesions.[23]

Huang et al. (2012) investigated the use of both dynamic- and static ^{18}F-FDG PET in the differentiation of SPN in 34 patients in an area with a high prevalence of granulomatous disease. They made use of the Patlak method in order to calculate the net phosphorylation rate of FDG (Ki) as well as the metabolic rate of glucose (MRGlu) for every nodule. Semi-automatic volumes of interest were used with a 50% threshold of the maximum pixel value within the nodule. A one cm in diameter region of interest was placed over the left ventricle in order to estimate the arterial input. The following parameters were compared between benign and malignant lesions: SUVmax, SUVmean, Ki, MRGlu and the slope of time-activity curves. The authors found that all of the parameters mentioned differed significantly between benign and malignant lesions and could be used in differentiating between these. The combination of Ki and MRGlu from dynamic PET imaging, yielded a specificity of 90% and a sensitivity of 79% in the differentiation of benign from malignant SPN.[28]

Risk stratification and prognosis

Grgic and co-workers (2010) evaluated various SUV thresholds together with the pre-test probability for malignancy in order to improve the accuracy of ^{18}F-FDG in the characterization of SPN. They also evaluated the prognostic value of the SUVmax. A retrospective study was conducted that consisted of a 140 patients who underwent ^{18}F-FDG PET for the characterization of SPN. The final diagnosis was confirmed with histopathology or follow-up over a period of two years. The authors found that the highest accuracy (85%) was achieved by using a SUVmax of 4.0 (sensitivity and specificity of 85%) and that this correlated well with the visual analysis. Where a lung malignancy was diagnosed, a SUVmax of greater than 9.5 was associated with a shorter median survival time (20 months), compared to a longer survival time (more than 75 months) in those with lower FDG accumulation. The authors suggested that a thoracotomy could be omitted in patients who present with a high surgical risk and have low FDG accumulation in the lung lesion.[29]

Other PET tracers

In the largest study of its kind, Hara et al. compared the uptake rates (measured as the SUVmax) of ^{18}F-FDG and ^{11}C-Choline in 116 patients with confirmed lung cancer, pulmonary tuberculosis and atypical mycobacterial lung infections. The authors found that while the SUVmax for ^{18}F-FDG increased with the size of the tumour, the value for ^{11}C-choline appeared more or less stable (around 3.5) in patients with lung cancer. The same held true for tuberculous lesions with a constant value of around 2.0 on ^{11}C-Choline. The authors suggested that sequential imaging with both tracers, together with the knowledge of these trends, could be used to predict the nature of an SPN.[30]

Several reports on the use of ^{18}F-FLT in non-small cell lung cancer (NSCLC) exist where the use of this tracer was compared to ^{18}F-FDG. This tracer functions as a thymidine analogue and is used to image cell proliferation. As such it has also been compared to various indices of cell proliferation, such as Ki-67 and cyclin D_1.

Yamamoto and co-workers (2008) compared ^{18}F-FLT to ^{18}F-FDG in 18 newly diagnosed patients with NSCLC and found a sensitivity of 72% compared to the 89% with 18F-FDG.

The mean SUV with FLT was significantly lower than that of FDG. Both tracers correlated well with Ki-67 with no statistically significant difference noted (FLT r=0.77, FDG r=0.81).[31]

Yang et al. (2010) conducted a similar study on 31 patients and compared the results to Cyclin D_1 immunohistochemistry. This is an important regulator in the cell cycle between G_1 and S and plays an important role in malignant transformation. They found sensitivities of 74% and 94% for FLT and FDG respectively (which is quite similar to the results of Yamamoto et al. FLT correlated well to cyclin D_1 (r=0.644) unlike FDG (r=0.293) and may be useful in predicting treatment response.[32]

Our center is currently working on various promising labeling options with Gallium-68 for the imaging of SPN, Tuberculosis and other lung lesions. These include the labeling of anti-tuberculous drugs, peptides and ^{68}Ga-citrate.

More comparisons within Nuclear Medicine

Halley et al. (2005)[31] compared the efficiency of ^{18}F-FDG PET and ^{99m}Tc-depreotide SPECT imaging in 28 patients who presented with an SPN in the absence of a cancer history. With histology used as the gold standard, the authors concluded that the two modalities were equally sensitive (PET 88.9%; SPECT 94.4%) and specific (85.7%) in both small (<1.5cm) and larger lung lesions (>1.5cm).[33]

Higashi et al. (2001) compared the accuracy of ^{18}F-FDG PET to that of ^{201}Tl-SPECT in the evaluation of 63 patients with 66 pulmonary nodules. Both studies were performed within a week of one another and the authors used SUVmax as well as tumor to non-tumour ratios in order to measure their findings against histopathology. The authors concluded that there were no significant differences in the specificity of ^{18}F-FDG PET and ^{201}Tl-SPECT in the differentiation between benign and malignant lesions. ^{201}Tl-SPECT outperformed ^{18}F-FDG PET in the detection of bronchioalveolar carcinomas as well as a well-differentiated adenocarcinoma, whereas ^{18}F-FDG PET was predictably superior in the detection of smaller nodules.[34]

Sasaki et al. (2001) compared the value of ^{11}C-methionine (MET-PET) with that of ^{18}F-FDG PET in the differentiation between benign and malignant lung lesions. Methionine provides a

measure of amino acid metabolism, which is increased in malignancies, due to either increased amino acid transport or transmethylation. In this retrospective study, the authors analyzed 46 PET studies performed with ^{11}C-Methonine and 94 performed with ^{18}F-FDG. There were no statistically significant differences between the test characteristics of these two tracers with no diagnostic improvement when combining both studies. The authors concluded that both tracers were equally useful in differentiating indeterminate lung lesions.[35]

In Summary

- The use of ^{18}F-FDG PET has been well validated in the setting of SPN with the majority of large studies reporting a sensitivity of above 90% and specificity of around 80%.
- A negative ^{18}F-FDG-PET has an excellent negative predictive value. False negative findings are mainly due to slow-growing- or mucinous tumours, such as neuro-endocrine tumours and broncho-alveolar carcinomas.
- False positives may occur with a variety of infectious and inflammatory conditions, which should be kept in mind in settings with a high prevalence of especially granulomatous diseases.
- Several independent comparisons made between PET, CT and integrated PET/CT have demonstrated the significant added advantage of adding metabolic data to CT and not much benefit by the addition of CT to PET.[24,34,35]. However, these two modalities are clearly complimentary and integrated PET/CT is preferable.
- Comparisons made between ^{18}F-FDG PET and ^{99m}Tc-depreotide have established these as equally accurate.[17,36,38]
- A comparison made between Tl-201 and ^{18}F-FDG revealed a higher sensitivity with Tl-201 in patients with well-differentiated adenocarcinomas (although this was only in a small number of patients).
- The accuracy of Methionine PET appears comparable to that of FDG. Exciting new possibilities may also emerge with Ga-68 labeling.
- Functional imaging offers advantages such as risk stratification, correlation to immunochemistry (Such as Ki-67 and Cyclin D_1) and treatment response evaluation.

How is uptake on PET imaging judged to be benign or malignant?

In order to compare the accuracy of findings on PET to those of other modalities, we need certain measures or criteria according to which PET would be correct in predicting the nature of a particular lesion. This generally consists of a qualitative (visual) assessment and- or a quantitative assessment. Unfortunately, not all of these measures have been standardized, which limits comparisons across various studies.

Various limitations have to be taken into account when evaluating or measuring lesion uptake on PET. The spatial resolution of a PET scanner typically varies from 5-8 mm. This may lead to an underestimation of the intensity of lesions that are less than 1-1.5 cm due to the partial volume effect (PVE).

Lesions with non-uniform tracer distribution presents another quantification problem, since these lesions often have a necrotic center, which appears photopenic and is surrounded by a rim of intense tracer accumulation. Spillover from surrounding structures with high tracer accumulation may also interfere with accurate evaluation.

Some of the most commonly used criteria are discussed below.

Qualitative/visual assessment

Tracer accumulation is generally considered abnormal when it is increased relative to the background. Reference points such as the mediastinal blood pool, contralateral normal lung and the liver have also been used.[24,26,27]

Some authors have reported an improvement in accuracy when using a qualitative scale, rather than a quantitative one. This has been found to be the case especially in small lesions (<1.5 cm). However, this has also been disputed by several studies, including a meta-analysis performed by Gould et al.[27]

Quantification

One of the great advantages of PET imaging, is the ability to quantify metabolic activity. Various methods, ranging from semi-quantification (making use of SUVmax or SUVmean) to quantification with full kinetic modeling, have been employed in order to clearly distinguish benign from malignant lesions in the lung.

The SUVmax is widely accepted and used as a semi-quantitative measure with a threshold value of 2.5 most frequently documented in order to distinguish benign from malignant lesions. However, this should be interpreted with caution, considering that a variety of factors may influence the SUV and its repeatability and that, unfortunately, false positives and negatives do occur. Dual-time point imaging has been suggested as a way of increasing the sensitivity.

When interpreting dual-time point imaging, several authors have made use of an increase of 10% in the mean or maximum SUV as the threshold for a positive scan. Again, no standardized interpretation criteria exist and these variations among study methodologies hinder accurate combination or comparisons of data.

Dynamic- and Dual-time point imaging

Simply stated, these techniques are based on the different ratios of enzymes that are present in benign- and malignant lesions. In benign lesions, the enzyme ratio favors glucose-6-phosphatase, resulting in a (theoretically) quicker washout from lesions. In malignant lesions, however, the ratio favors that of hexokinase, causing an increase in lesion intensity over time. Normal tissue surrounding the lesion will decrease in intensity over time.[39]

Some groups have reported that DTPI is superior to STPI, whereas this has been questioned/ disputed by others.

Lin et al. (2012) conducted a systematic review and meta-analysis on the value of dual-time-point imaging compared to single-time-point imaging of lung nodules with ^{18}F-FDG PET. They included eleven studies with a total of 778 patients and found no statistically significant differences in sensitivity between DTP and SPI. The estimated sensitivity for DTP imaging

ranged from 54-100% and specificity ranged from 14-93%. This suggests that DTPI should be reserved for selected cases and should not be considered for routine clinical practice. Importantly, there was significant heterogeneity present in this meta-analysis due to significant inconsistencies in methodology amongst studies. The main inconsistencies involved inclusion criteria, imaging times and image interpretation. This of course limits the clinical application of the findings. Standardization of methodology should be strongly encouraged across centers.[40] The largest three studies that were included in this meta-analysis are those of Alkhawaldeh et al.[41] with 265 patients ;Suga et al. with 137 participants[42]; and Cloran et al. with 113 patients.[43]

In our institution, where we have a high prevalence of granulomatous diseases, we have not found dual-time point imaging with ^{18}F-FDG PET/CT useful in differentiating benign from malignant lung lesions. This was mainly due to the similar metabolic behavior demonstrated by both tuberculous- and malignant lung lesions.[23]

Another meta-analysis by Zhang et al. (2013) comparing DTPI to STPI in the differential diagnosis of pulmonary nodules included eight studies with a total of 415 patients. The gold standard comprised of pathology or clinical follow-up. The summary sensitivity of dual time point FDG-PET was 79% vs. 77% in single time point imaging. Specificity of DTPI was 73% vs. 59%. These authors also concluded that the accuracy of DTPI with 18F-FDG and single time point imaging resulted in similar accuracy, but that DTPI may offer an increase in specificity. Significant heterogeneity was also present in this meta-analysis and was attributed to differences in diagnostic thresholds and SUV calculation.[44]

Limitations when imaging lung lesions

Imaging of lung lesions are susceptible to a number of well-recognized limitations, which exist to varying degrees in the different diagnostic modalities, the scope of which falls outside of this review.

Due to the breathing process, the location of the lung lesion may vary during the different phases of inspiration and expiration. Also, the depth and breathing rate will influence accurate localization. This phenomenon has led to the development of various modifications during imaging, such as single breath acquisition in CT and respiratory gating in PET. Other issues

include the influence of the regional lung volume/aeration on the level of tracer accumulation and increased background activity in highly vascular regions. Complex compartmental models, normalization or comparison to other regional PET data is often needed.[45]

Another important limitation, especially with regards to metabolic imaging, is the partial volume effect, by which a small lung lesion may appear less intense than a larger lesion, causing a possible false negative in a small malignant lesion when relying on the SUV. These potential inaccuracies have been addressed in various ways.

Hickeson et al. (2002) used the lung lesion size (as measured on CT) to determine the SUVmax corrected for the partial volume effect and compare it to the uncorrected SUVmax in a retrospective study involving 47 patients. The authors concluded that using a corrected SUV max in small lung lesions (2cm or less) improved diagnostic accuracy in differentiating benign from malignant pulmonary nodules.[46]

Comparisons PET vs. CT

A search performed on the Cochrane library revealed only two head to head comparison between CT and PET.

Cronin et al. (2008) conducted a meta-analysis of the diagnostic utility of various imaging modalities in SPN. The purpose was to create a nomogram, which takes into consideration the clinical probability of malignancy together with a positive result in order to provide the clinician with a post-test probability of malignancy. The authors included 44 studies that made use of CT/MRI/PET/SPECT in the evaluation of SPN. All of the afore-mentioned modalities resulted in similar likelihood ratios. The authors therefore concluded that a clinician could confidently select any of the four tests in the evaluation of SPN, but should consider SPECT first when taking into account cost and availability.[13]

Fletcher et al. (2008) compared the diagnostic accuracy of FDG-PET compared to CT in the characterization of 532 participants with SPN.ROC curve analysis demonstrated an area under the curve of 0.9 for PET and 0.82 for CT, which was statistically highly significant. In addition PET was less susceptible to inter- and intra-observer variability.[47]

Combining the best of both

Morphological and metabolic information are synergistic and complementary in the diagnosis and management of a patient with an indeterminate pulmonary lesion. Morphological imaging provides high-resolution images with excellent localization and anatomical detail, whereas functional imaging adds information on the nature of the pathology at molecular level, treatment response and predictions with regards to prognosis and risk stratification. Furthermore, metabolic information may be used to direct biopsies to the areas of most intense activity to ensure that representative tissue is obtained for analysis. In the case of a lung malignancy, PET/CT allows for the accurate whole body staging of the patient in one investigation.

Yi and co-workers (2005) compared the accuracy of integrated PET/CT in the tissue characterization of SPN to that of helical dynamic CT (HDCT) in 119 patients. They found that integrated PET/CT provided the highest sensitivity and accuracy, with similar specificity when compared to dynamic CT. The authors suggested that integrated PET/CT be used as a first-line investigation in the characterization of SPN and that HDCT would be a suitable alternative in the absence of PET/CT facilities.[48]

Kim et al. (2007) conducted a retrospective study on 42 patients with SPN using a qualitative scale (relative to the mediastinum and liver intensity) to evaluate metabolic activity on ^{18}F-FDG PET. PET and CT individually were equally accurate in distinguishing benign from malignant lesions (74%) with a significantly greater combined PET/CT accuracy of 93%. They also found that accuracy did not improve significantly making use of a SUVmax cut-off of 2.0 for malignancy. The authors concluded that combined PET/CT performs significantly better than PET alone with regards to accuracy, sensitivity and specificity and demonstrates better specificity when compared to CT alone.[37]

Chang and co-workers (2010) investigated the incremental value of integrated FDG PET/CT in the evaluation of SPN in a retrospective study, which involved 117 patients with indeterminate pulmonary nodules and no history of malignancy. They demonstrated that PEt al.one had a sensitivity of 90.7% and specificity of 82.4%. Integrated PET/CT had a slightly lower sensitivity of 88.4% with an increased specificity of 89.2%. The authors concluded that

the added benefit of CT was limited, but that it did help in cases where PET was indeterminate.[49]

From the afore-mentioned publications, it is evident that there is sufficient evidence to support the use of integrated ^{18}F-FDG PET/CT in the evaluation of SPN. Where this is available, it may be preferable (and more cost-effective) to start with PET/CT, rather than progressing from CT to PET/CT. It also limits radiation exposure to the patient.

Other advancements

In recognition of the diagnostic challenge in differentiating benign from malignant nodules, various computer-aided diagnostic schemes have been developed. The purpose is to provide the radiologist with a second opinion and to improve accuracy and consistency of reporting.

Suzuki et al. (2005) developed such a tool making use of massive training artificial neural networks (MTANN), which are trainable, non-linear filters. The authors developed multiple MTANNs that consisted of six expert MTANNs arranged in parallel and trained it with CT teaching cases. This diagnostic tool provides the user with a value, which is related to the probability of malignancy. When tested on 342 patients with 76 primary lung cancers and 413 benign nodules, it correctly identified 100% of malignant nodules and 48% of benign nodules, with an area under the ROC of 0.882. The authors concluded that it would be useful in assisting radiologists in differentiating between malignant and benign lung nodules.[50]

Doi (2005) reviewed the status and potential of computer-aided diagnosis in medical imaging considering (amongst others) its use in lung nodules and diffuse lung disease on CXR and CT. The author concluded that computer-aided diagnosis is "likely to have a major impact on medical imaging and diagnostic radiology in the 21st century".[51]

Considering the costs

Finally, it would be important to consider the cost and availability of the various diagnostic modalities.

Current semi-invasive diagnostic procedures include sputum cytology (high specificity, low sensitivity), fiber-optic bronchoscopy, bronchoscopic biopsy, transbronchoscopic biopsy, transthoracic needle aspiration (TTNA) and transthoracic fine-needle biopsy (TTFB). For central lesions bronchoscopic biopsy is preferred with a sensitivity of 65% for malignant nodules. This increases to 79% with transbronchoscopic biopsy[52], although neither method is sensitive enough to exclude malignancy confidently. For peripheral lesions TTNA is preferable with a sensitivity of up to 90%[53]. All of these procedures may result in complications such as bleeding and pneumothoraces. Video-assisted thorascopic surgery and thoracotomies are generally reserved for lesions where a malignancy is judged to be more likely. Most of the above-mentioned procedures are associated with significant costs and morbidity.[54]

Tsushima Y et al. (2004~) demonstrated that ^{18}F-FDG-PET combined with CT-guided needle biopsy was accurate and cost-effective.[55]

Barnett et al. (2010) performed a first of a kind cost and outcome evaluation on 375 patients with SPN and a definitive diagnosis. They hypothesized that despite the relatively high cost of a PET scan; it would probably reduce costs associated with unnecessary surgery or biopsy by identifying "PET negative" patients who are suitable for "watchful waiting". The aim of the study was to evaluate how the PET result influenced management as well as the consequences of both false positive and false negative findings. Hospital, outpatient and pharmacy costs were considered (unadjusted for inflation) and expressed as cost per life-month. The authors found that the care of cost for patients with a malignant SPN was significantly higher than that of a benign outcome ($50233 vs. $22461, $p<0.001$). The risk of mortality was also 5.0 times higher (CI, 3.1-8.2) compared to those with a benign lung nodule. For patients with a malignant nodule and a false negative PET, costs and outcomes were similar to those with true positive PET findings. However, patients with a benign lesion and a false positive result incurred significantly higher costs and a 3.8 times increased risk of mortality, compared to the patients with true negative scans. This is an important point of consideration in any setting

with a high prevalence of granulomatous disease and therefore a high probability of false positive results.[56]

Concluding remarks

The majority of the studies performed on indeterminate lung lesions, have focused on the differentiation of malignant from benign lesions. However, in settings with a high prevalence of granulomatous disease, it is challenging to differentiate malignant lesions from granulomatous ones.

Despite tremendous advances in various imaging modalities, this distinction remains a difficult one. This is especially true in a setting with a high prevalence of granulomatous disease. Presumably, the answer could be found in careful analysis of the pathophysiology that underlies these lesions. Korotkina et al., for example, have observed and described differences in glutathione content and in the membrane-bound activity of glutathione-metabolizing enzymes between benign and malignant lung tumours.[57] Observation and analysis of such findings may be important in selecting a target expressed exclusively in malignant or tuberculous lesions.

It is well known that ^{18}F-FDG-PET imaging is based on increased glucose metabolism. In malignant lesions, increased uptake is mainly due to increased expression of glucose transporters and enzymes such as hexokinase. In infectious or inflammatory conditions, increased uptake is thought to be mainly due to the increased metabolic activity of white blood cells, especially macrophages. Increased blood flow and cytokines play a role in both benign and malignant lesions. The contributions of the various role players are not yet clearly defined. The quest remains to find a tracer that targets a unique component of either benign or malignant lesions.

References

1. Kreider ME, Hansen-Flaschen J,Ahmad NN, Rossman MD, Kaiser LR, Kucharczuk JC, et al. Complications of video-assisted thoracoscopic lung biopsy in patients with interstitial lung disease. The Annals of thoracic surgery.2007;83(3): 1140-44.

2. Ost DE, Gould MK. Decision Making in Patients with Pulmonary Nodules. Am J Respir Crit Care Med. 2012 Feb 15;185(4):363–72.

3. Gould MK, Fletcher J, Iannettoni MD, Lynch WR, Midthun DE, Naidich DP, et al. Evaluation of patients with pulmonary nodules: when is it lung cancer? ACCP evidence-based clinical practice guidelines (2nd edition). Chest. 2007.108S–130S.

4. Swensen SJ. The Probability of Malignancy in Solitary Pulmonary NodulesApplication to Small Radiologically Indeterminate Nodules. Arch Intern Med. 1997 Apr 28;157(8):849.

5. Swensen SJ, Silverstein MD, Edell ES, Trastek VF, Aughenbaugh GL, Ilstrup DM, et al. Solitary Pulmonary Nodules: Clinical Prediction Model Versus Physicians. Mayo Clin Proc. 1999 Apr;74(4):319–29.

6. MacMahon H, Austin JHM, Gamsu G, Herold CJ, JETT JR, Naidich DP, et al. Guidelines for Management of Small Pulmonary Nodules Detected on CT Scans: A Statement from the Fleischner Society. Radiology. 2005 Nov 1;237(2):395–400.

7. Naidich DP, Bankier AA, MacMahon H. Recommendations for the management of subsolid pulmonary nodules detected at CT: a statement from the Fleischner Society. Radiology 266.1(2013): 304-317.

8. McNulty W, Cox G, Au-Yong I. Investigating the solitary pulmonary nodule. BMJ: British Medical Journal.2012:344.

9. Midthun DE, Swensen SJ, JETT JR. Approach to the solitary pulmonary nodule. Mayo Clin Proc. 1993;68(4):378-85.

10. Nicholas E, Braff S, Klein JS. Evaluation of the solitary pulmonary nodule: A practical approach. Appl Radiol. 2011;40(12):6.

11. Diederich S, Hansen J, Wormanns D. Resolving small pulmonary nodules: CT features. Eur Radiol. 2005 Jul 8;15(10):2064–9.

12. Mori K, Saitou Y, Tominaga K, Yokoi K, Miyazawa N, Okuyama A, et al. Small nodular lesions in the lung periphery: new approach to diagnosis with CT. Radiology. 1990 Dec;177(3):843–9.

13. Cronin P, Dwamena BA, Kelly AM, Bernstein SJ, Carlos RC. Solitary pulmonary nodules and masses: a meta-analysis of the diagnostic utility of alternative imaging tests. Eur Radiol. 2008 Sep;18(9):1840–56.

14. Yuan X, Zhang J, Quan C, Cao J, Ao G, Tian Y, et al. Differentiation of malignant and benign pulmonary nodules with first-pass dual-input perfusion CT. Eur Radiol. 2013 Jun:1-6.

15. Field JK, Oudkerk M, Pedersen JH, Duffy SW. Prospects from population screening and diagnosis of lung cancer. Lancet 2013; 382: 732-41.

16. Machac J, Krynyckyi B, Kim C. Peptide and antibody imaging in lung cancer. Semin Nucl Med. 2002 Oct;32(4):276–92.

17. Blum JJ, Handmaker HH, Lister-James JJ, Rinne NN. A multicenter trial with a somatostatin analog (99m)Tc depreotide in the evaluation of solitary pulmonary nodules. Chest. 2000 Apr 30;117(5):1232–8.

18. Plachcinska A, Mikolajczak R, Maecke H, Mlodkowska E, Kunert-Radek J, Michalski A, et al. Clinical usefulness of 99mTc-EDDA/HYNIC-TOC scintigraphy in oncological diagnostics: a pilot study. Cancer Biother Radiopharm. 2004 Apr;19(2):261–70.

19. Płachcińska A, Mikołajczak R, Maecke H, Kozak J, Michalski A, Rzeszutek K, et al. Efficacy of 99mTc-EDDA/HYNIC-TOC scintigraphy in differential diagnosis of solitary pulmonary nodules. Cancer Biother Radiopharm. 2004 Oct;19(5):613–20.

20. Chin BB, Zukerberg BW, Buchpiguel C. Thallium-201 uptake in lung cancer. J Nucl Med.1995;36(8):1514-19.

21. Spanu AA, Schillaci OO, Pietro P Pirina, Arru AA, Madeddu GG, Chessa FF, et al. 99mTc-tetrofosmin SPECT in solitary pulmonary nodule evaluation. Oncol Rep. 2006 Sep 30;16(4):763–9.

22. Nikoletic KK, Lucic SS, Peter AA, Kolarov VV, Zeravica RR, Srbovan DD. Lung 99mTc-MIBI scintigraphy: impact on diagnosis of solitary pulmonary nodule. Bosn J Basic Med Sci. 2011 Jul 31;11(3):174–9.

23. Sathekge MMM, Maes AA, Pottel HH, Stoltz AA, van de Wiele CC. Dual time-point FDG PET-CT for differentiating benign from malignant solitary pulmonary nodules in a TB endemic area. S Afr Med J. 2010 Aug 31;100(9):598–601.

24. Gupta NC, Maloof J, Gunel E. Probability of malignancy in solitary pulmonary nodules using fluorine-18-FDG and PET. J Nucl Med. 1996 Jun;37(6):943–8.

25. Herder G, Golding R, Hoekstra O, Comans E, Teule G, Postmus P, et al. The performance of 18F-fluorodeoxyglucose positron emission tomography in small solitary pulmonary nodules. Eur J Nucl Med Mol Imaging. 2004 Jun 3;31(9).

26. Pauls S, Buck AK, Halter G, Mottaghy FM, Muche R, Bluemel C, et al. Performance of Integrated FDG-PET/CT for Differentiating Benign and Malignant Lung Lesions -Results from a Large Prospective Clinical Trial. Mol Imaging Biol. 2008 Jan 16;10(2):121–8.

27. Gould MK, Maclean CC, Kuschner WG, Rydzak CE, Owens DK. Accuracy of positron emission tomography for diagnosis of pulmonary nodules and mass lesions: a meta-analysis. JAMA. 2001 Feb 21;285(7):914–24.

28. Huang YE, Lu HI, Liu FY, Huang YJ. Solitary pulmonary nodules differentiated by dynamic F-18 FDG PET in a region with high prevalence of granulomatous disease. J Radiat Res.2012;53(2):306-12.

29. Grgic AA, Yüksel YY, Gröschel AA, Schäfers H-JH, Sybrecht GWG, Kirsch C-MC, et al. Risk stratification of solitary pulmonary nodules by means of PET using (18)F-fluorodeoxyglucose and SUV quantification. CORD Conference Proceedings. 2010 May 31;37(6):1087–94.

30. Hara TT, Kosaka NN, Suzuki TT, Kudo KK, Niino HH. Uptake rates of 18F-fluorodeoxyglucose and 11C-choline in lung cancer and pulmonary tuberculosis: a positron emission tomography study. Chest. 2003 Aug 31;124(3):893–901.

31. Yamamoto Y, Nishiyama Y, Kimura N, Ishikawa S, Okuda M, Bandoh S, et al. Comparison of (18)F-FLT PET and (18)F-FDG PET for preoperative staging in non-small cell lung cancer. Eur J Nucl Med Mol Imaging. 2008 Feb;35(2):236–45.

32. Yang W, Zhang Y, Fu Z, Yu J, Sun X, Mu D, et al. Imaging of proliferation with 18F-FLT PET/CT versus 18F-FDG PET/CT in non-small-cell lung cancer. Eur J Nucl Med Mol Imaging. 2010 Jul;37(7):1291–9.

33. Halley A, Hugentobler A, Icard P, Porret E, Sobrio F, Lerochais J-P, et al. Efficiency of 18F-FDG and 99mTc-depreotide SPECT in the diagnosis of malignancy of solitary pulmonary nodules. Eur J Nucl Med Mol Imaging. 2005 May 5;32(9):1026–32.

34. Higashi KK, Ueda YY, Sakuma TT, Seki HH, Oguchi MM, Taniguchi MM, et al. Comparison of [(18)F]FDG PET and (201)Tl SPECT in evaluation of pulmonary nodules. J Nucl Med. 2001 Sep 30;42(10):1489–96.

35. Sasaki MM, Kuwabara YY, Yoshida TT, Nakagawa MM, Koga HH, Hayashi KK, et al. Comparison of MET-PET and FDG-PET for differentiation between benign lesions and malignant tumors of the lung. Ann Nucl Med. 2001 Sep 30;15(5):425–31.

36. Cronin P, Dwamena BA, Kelly AM, Bernstein SJ, Carlos RC. Solitary pulmonary nodules and masses: a meta-analysis of the diagnostic utility of alternative imaging tests. Eur Radiol. 2008 Jul 8;18(9):1840–56.

37. Kim SKS, Allen-Auerbach MM, Goldin JJ, Fueger BJB, Dahlbom MM, Brown MM, et al. Accuracy of PET/CT in characterization of solitary pulmonary lesions. J Nucl Med. 2007 Jan 31;48(2):214–20.

38. Halley A, Hugentobler A, Icard P, Porret E, Sobrio F, Lerochais J-P, et al. Efficiency of 18F-FDG and 99mTc-depreotide SPECT in the diagnosis of malignancy of solitary pulmonary nodules. Eur J Nucl Med Mol Imaging. 2005 May 5;32(9):1026–32.

39. Hamberg LM, Hunter GJ, Alpert NM, Choi NC, Babich JW, Fischman AJ. The dose uptake ratio as an index of glucose metabolism: useful parameter or oversimplification? J Nucl Med. 1994 Aug;35(8):1308–12.

40. Lin Y-Y, Chen J-H, Ding H-J, Liang J-A, Yeh J-J, Kao C-H. Potential value of dual-time-point ^{18}F-FDG PET compared with initial single-time-point imaging in differentiating malignant from benign pulmonary nodules: a systematic review and meta-analysis. Nucl Med Commun. 2012 Oct;33(10):1011–8.

41. Alkhawaldeh K, Bural G, Kumar R, Alavi A. Impact of dual-time-point 18F-FDG PET imaging and partial volume correction in the assessment of solitary pulmonary nodules. Eur J Nucl Med Mol Imaging. 2007 Oct 16;35(2):246–52.

42. Suga K, Kawakami Y, Hiyama A, Sugi K, Okabe K, Matsumoto T, et al. Dual-time point 18F-FDG PET/CT scan for differentiation between 18F-FDG-avid non-small cell lung cancer and benign lesions. Bulletin du Cancer. Springer Japan; 2009 May 13;23(5):427–35.

43. Cloran FJF, Banks KPK, Song WSW, Kim YY, Bradley YCY. Limitations of dual time point PET in the assessment of lung nodules with low FDG avidity. Lung Cancer. 2010 Mar 31;68(1):6–6.

44. Zhang L, Wang Y, Lei J, Tian J, Zhai Y. Dual time point 18FDG-PET/CT versus single time point 18FDG-PET/CT for the differential diagnosis of pulmonary nodules: a meta-analysis. Acta Radiologica. 2013 Mar 25.

45. Schuster DP. The evaluation of lung function with PET. Semin Nucl Med.1998 Oct;28(4):341–51.

46. Hickeson M, Yun M, Matthies A, Zhuang H, Adam L-E, Lacorte L, et al. Use of a corrected standardized uptake value based on the lesion size on CT permits accurate characterization of lung nodules on FDG-PET. Eur J Nucl Med Mol Imaging. 2002 Dec 1;29(12):1639–47.

47. Fletcher JW, Kymes SM, Gould M, Alazraki N, Coleman RE, Lowe VJ, et al. A Comparison of the Diagnostic Accuracy of 18F-FDG PET and CT in the Characterization of Solitary Pulmonary Nodules. J Nucl Med. 2008 Feb 1;49(2):179–85.

48. Chin A Yi, Lee KS, Kim B-T, Choi JY, Kwon OJ, Kim H, et al. Tissue Characterization of Solitary Pulmonary Nodule: Comparative Study Between Helical Dynamic CT and Integrated PET/CT. J Nucl Med.2006;47(3):443-50.

49. Chang C-Y, Tzao C, Lee S-C, Cheng C-Y, Liu C-H, Huang W-S, et al. Incremental value of integrated FDG-PET/CT in evaluating indeterminate solitary pulmonary nodule for malignancy. Mol Imaging Biol. 2010 Apr;12(2):204–9.

50. Suzuki K, Feng Li, Sone S, Doi K. Computer-aided diagnostic scheme for distinction between benign and malignant nodules in thoracic low-dose CT by use of massive training artificial neural network. IEEE Trans. Med. Imaging. 24(9):1138–50.

51. Doi K. Current status and future potential of computer-aided diagnosis in medical imaging. Br J Radiol. 2005 Jan 1;78(suppl_1):S3–S19.

52. Gambhir SSS, Shepherd JEJ, Shah BDB, Hart EE, Hoh CKC, Valk PEP, et al. Analytical decision model for the cost-effective management of solitary pulmonary nodules. J Clin Oncol. 1998 May 31;16(6):2113–25.

53. Klein JSJ, Zarka MAM. Transthoracic needle biopsy: an overview. J Thorac Imaging. 1997 Sep 30;12(4):232–49.

54. Mavi AA, Lakhani PP, Zhuang HH, Gupta NCN, Alavi AA. Fluorodeoxyglucose-PET in characterizing solitary pulmonary nodules, assessing pleural diseases, and the initial staging, restaging, therapy planning, and monitoring response of lung cancer. Radiol Clin North Am. 2004 Dec 31;43(1):1–ix.

55. Tsushima YY, Endo KK. Analysis models to assess cost effectiveness of the four strategies for the work-up of solitary pulmonary nodules. Med Sci Monit. 2004 Apr 30;10(5):MT65–MT72.

56. Barnett PG, Ananth L, Gould MK. Cost and outcomes of patients with solitary pulmonary nodules managed with PET scans.Chest.2010;137(1):53-9.

57. Korotkina RN, Matskevich GN, Devlikanova AS, Vishnevskii AA, Kunitsyn AG, Karelin AA. Activity of Glutathione-Metabolizing and Antioxidant Enzymes in Malignant and Benign Tumors of Human Lungs. Bull Exp Biol Med.2002;133(6):606–8.

Chapter 3: Literature Review on the non-oncological applications of Gallium-68

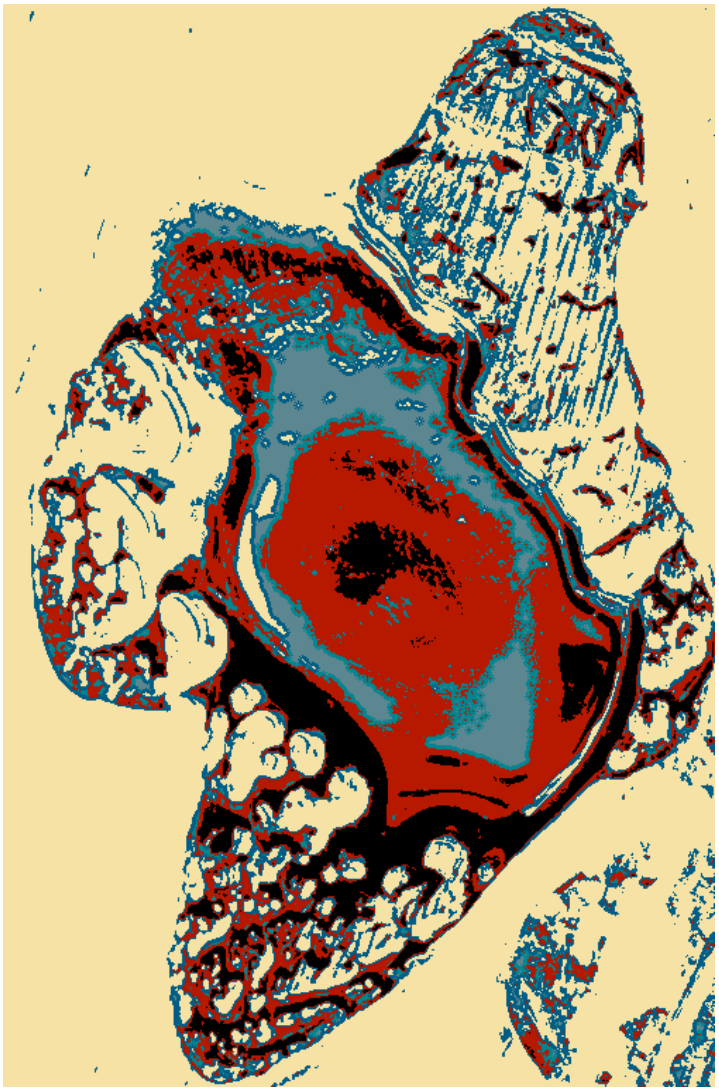

*An adapted version of this chapter was accepted for publication:

Vorster M, Maes A, Van de Wiele C & Sathekge M.

Gallium-68: a systematic review of its nononcological applications. Nuclear Medicine Communications.2013; 34(9): 834-54.

Abstract

Background

The increased availability of PET facilities worldwide has sparked renewed interest in the use of generator-produced tracers such as Ga-68. Imaging with Ga-68 provides exciting opportunities in terms of new ligand labeling possibilities and the exploration of novel clinical applications.

Objective

To summarize and appraise what has been published on the clinical applications of Gallium-68 outside of oncology practice.

Methodology

This systematic review was conducted based on the **PRISMA guidelines**.
Databases searched included PubMed, Medline. Scopus, Web of Science and Google Scholar. **The following search strategy was used:**"Ga-68" OR "Gallium 68" (all fields) NOT the following (title & abstract): Oncology/NET/ neuroendocrine tumour/ tumor/DOTATOC, DOTATATE, DOTANOC. These results were further limited to English publications, which resulted in **205** publications on **PubMed.** After duplicates and irrelevant articles were removed, **72 publications** remained for inclusion.
Inclusion criteria Only those studies were included in which compounds were labeled with Ga-68 for applications other than oncology-related indications.
Exclusion criteria: Publications where the focus was on oncology-related applications of Ga-68 imaging or where the emphasis was on aspects relating to generators, radiochemistry-or physics.

Discussion and limitations

Although a multitude of tracers have been labeled with Ga-68 over several decades, it has not been established in routine clinical practice yet. In addition, neuro-endocrine and other oncological applications have dominated the field until relatively recently following reports of infection and inflammation applications. The majority of publications to date involve small subject numbers in mainly pre-clinical settings. Differences in methodology precludes grouping of studies in order to reach a clear conclusion.

Conclusion

There is a wide scope for ^{68}Ga-tracer application outside of oncological practice, which remains greatly underutilized. Larger clinical trials are needed to validate these applications.

Introduction

Gallium (as ^{67}Ga-citrate) has long provided nuclear physicians with a versatile tool for use over a broad spectrum of clinical applications. The mechanism of action, although incompletely explained, is generally accepted to be the result of various specific and nonspecific factors, which play a role in both infective/inflammatory and malignant processes. It stands to reason that ^{68}Ga would be as useful as ^{67}Ga with the added advantage of improved image resolution gained from PET/CT.

Compared with ^{18}F-FDG, ^{68}Ga provides shorter imaging times and on-demand, year-round tracer availability that negates the need for an onsite or nearby cyclotron. This could have significant financial implications, which may lead to a more cost-effective way of imaging. In addition, the short half-life of 68 min provides attractive peptide-labelling options for novel diagnostic and therapeutic applications.[1]

The majority of published work, however, has focussed on the application of ^{68}Ga in oncology imaging and especially in the setting of neuro-endocrine tumours. This review focuses on the application of ^{68}Ga-labelled tracers in settings other than those that are oncology related. As such, the role of ^{68}Ga tracers in oncology and neuro-endocrine tumours will not be addressed again here, and readers are directed to a number of publications (including a recent meta-analysis by Treglia and colleagues) on this topic.[2-4]

Aim

The aim of the study was to summarize and appraise what has been published on the clinical applications of ^{68}Ga outside oncology practice.

Methodology

The selection of appropriate publications and writing of this review was based on the guidelines contained in the PRISMA statement.[5]

We performed an extensive literature search using the following databases: **PubMed, Medline, Highwire Press, Scopus, Web of Science** and **Google Scholar.**

The following search strategy was used in PubMed: the terms **'Ga-68' OR 'Gallium 68'** was used to search **all fields.** This resulted in a total of 508 publications, which were then further limited to English publications, resulting in 481 publications. Excluding the following terms from both the title and the abstract (by adding 'NOT') resulted in the following numbers of publications in parentheses: 'Oncology' (470), 'NET' (443), 'neuroendocrine tumour' (222), 'DOTATOC', 'DOTATATE' and 'DOTANOC', the results were finally limited to 205 papers. (See Fig 1).

Similar searches were conducted in Medline (142 publications), Google scholar (217 results), Highwire, Scopus and Web of Science (121 results), which yielded an additional 480 publications. Removal of duplicates resulted in 255 papers, which were assessed for relevance and quality by screening the titles and abstracts.

Inclusion criteria: Studies or reports in which compounds were labelled with ^{68}Ga for applications other than in oncology-related indications were included.

Every effort was made to include both the earliest and the most recent publications relating to a particular application, as well as any study with a significant new contribution. The decision to include or exclude an article was made by consensus.

Exclusion criteria: Publications in which the focus was on oncology-related applications of ^{68}Ga imaging or in which the emphasis was on aspects relating to generators, radiochemistry or physics were excluded.

The scope of the literature search was broadened on the basis of the reference lists of all retrieved articles. Publications that were selected for this review were from peer-reviewed indexed journals. Original manuscripts, case reports, case series, abstracts, poster presentations, review articles, editorials, conference proceedings and poster presentations were also included.

After duplicates and irrelevant articles were removed, **72** publications remained for inclusion, of which **63** was included in the qualitative synthesis. (The 9 excluded publications included reviews and editorials, which were referred to, but not analysed as such).

The following search strategy was used for PubMed:

"Ga-68" OR "Gallium 68" (all fields)

The following terms were **excluded** from the title & abstracts: Oncology/neuro-endocrine tumour/tumor/DOTATOC/DOTATATE/DOTANOC

The above-mentioned criteria were further limited to English publications, which resulted in **205 publications** (See figure 1)

The last literature search was performed on 15 January 2013.

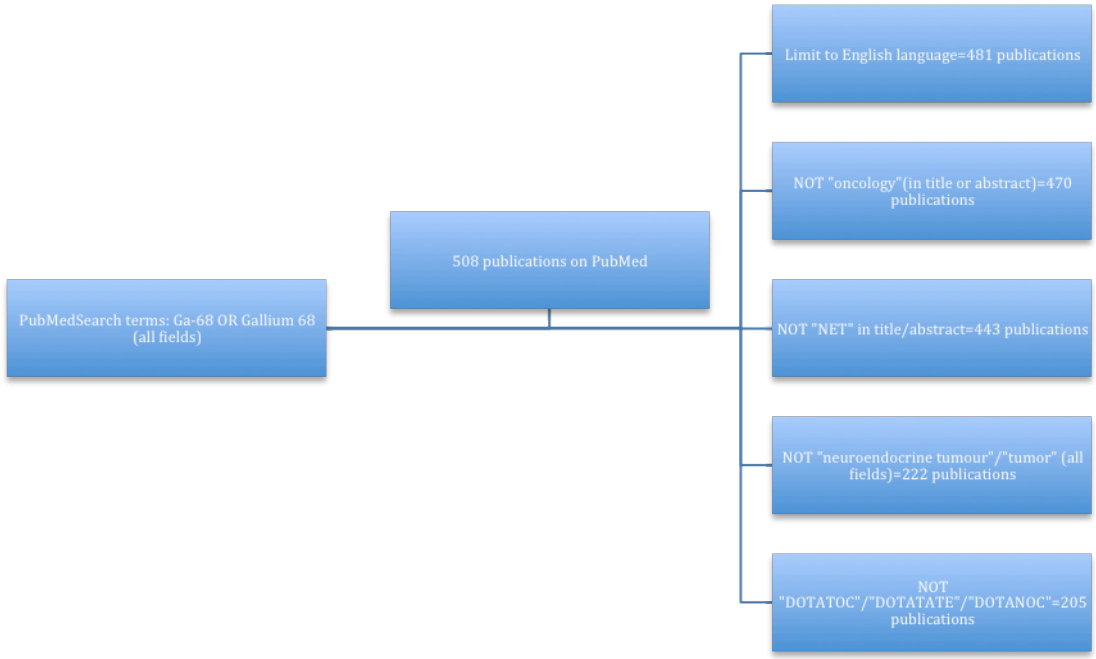

Fig 1: PubMed Search Strategy

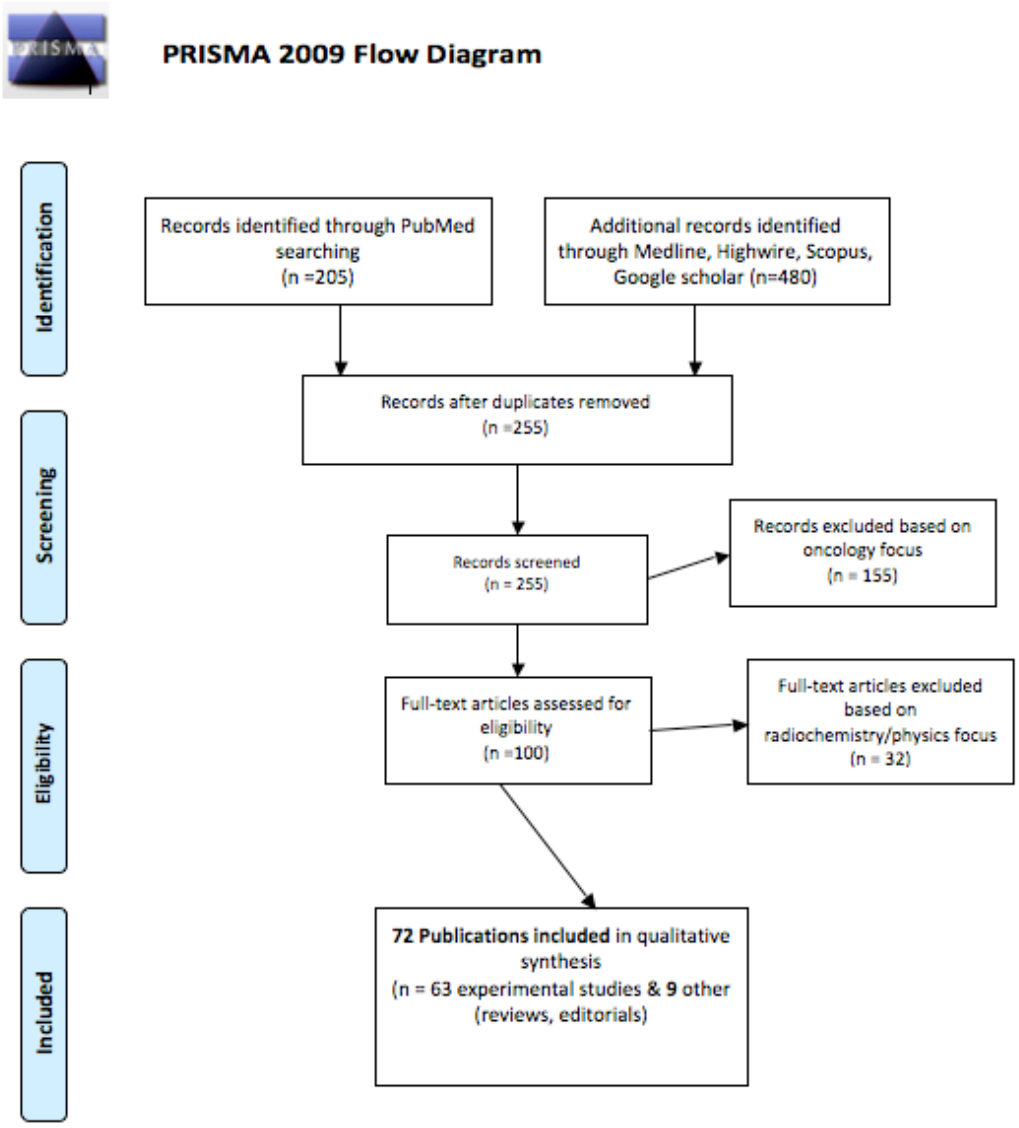

Fig 2: Study selection process.

Clinical applications

During the literature search and article assessment process, it became clear that publications could easily be grouped under the various physiological systems to which they apply. Hence, the selected literature has been organized under the following system headings: Musculoskeletal, Respiratory, Cardiovascular, Central nervous system, Genitourinary, Gastrointestinal and Miscellaneous applications. For the most part, studies under each heading have been discussed in chronological order.

Musculoskeletal system

Perhaps one of the better-known non-oncological applications involves the use of ^{68}Ga in the imaging of musculoskeletal infections.

Despite the fact that ^{18}F-FDG has a well-established role in musculoskeletal infection imaging, imaging with ^{18}F-FDG-PET cannot always clearly differentiate normal healing processes from postsurgical and infective processes.

The following groups have investigated this further between 2005 and 2012:

In 2005, a group from Finland (Mäkinen and colleagues) used a rat model (in a two-part study) to compare the performances of ^{18}F-FDG and **^{68}Ga-chloride ($^{68}GaCl_3$) PET** in the differentiation of experimental osteomyelitis from normal bone healing.[6]

During the first part of the study, 50 rats underwent surgery to the left tibia, with the right tibia serving as the intact control. During the second part of the study, osteomyelitis was induced with Staphylococcus aureus in eight rats and compared with normal bone healing in eight controls. Imaging took place 2 weeks after surgery on consecutive days using both $^{68}GaCl_3$ and ^{18}F-FDG.

Osteomyelitis was confirmed with quantitative bacteriology, and PET imaging was followed by both peripheral quantitative computed tomography (pQCT) and radiography.

The following observations were made:

- Both tracers demonstrated statistically significantly increased uptake in the tibias affected with osteomyelitis compared with the tibias in nonoperated controls. The mean standardized uptake value (SUV) ratio for ^{18}F-FDG was 1.74 (±0.37) and that for $^{68}GaCl_3$ was 1.62 (±0.28).
- ^{18}F-FDG demonstrated increased uptake in control animals (SUV ratio: 1.16) with healing bone, whereas $^{68}GaCl_3$ did not accumulate significantly in these lesions (SUV ratio: 1.02). This difference between ^{18}F-FDG and $^{68}GaCl_3$ was found to be statistically significant.
- $^{68}GaCl_3$ accumulation correlated closely with changes in bone density and area as measured by pQCT, whereas 18F-FDG did not.[6,7]

These findings suggest that imaging with $^{68}GaCl_3$ may result in fewer false-positive findings due to normal postsurgical inflammatory changes.

In two publications by Lankinen and colleagues, the use of **^{68}Ga-DOTAVAP-P1** was evaluated in trying to distinguish inflammation in healing bones from osteomyelitis. The rationale behind the use of this tracer is that vascular adhesion protein-1 (VAP-1) is an endothelial glycoprotein, which plays an important role in the recruitment of CD8 T lymphocytes during inflammatory conditions. As it is basically absent from normal endothelial surfaces and only induced during inflammatory conditions, it should provide a favourable target for imaging of inflammatory processes *in vivo*.[8]

In the first study, the above-mentioned investigators compared two groups of rats using a standardized animal model. The first group represented the infection group and consisted of 34 rats with S. aureus-induced osteomyelitis in the left tibia (with the right tibia serving as the control). In the second group, each of the 34 rats had a healing cortical defect of the left tibia (representing inflammation), with the right tibia used as the control. SUV ratios were used to quantify the PET findings, which were then compared with morphological changes noted on pQCT and radiographs (parameters used included cortical bone area and cortical bone density).

The following observations were made:

- Both groups (infection and inflammation) demonstrated increased ^{68}Ga-DOTAVAP-P1 accumulation for up to 3 h.
- After 36 h, only the infection group demonstrated increased tracer accumulation.
- Statistically significant differences in SUV ratios allowed for differentiation between infection and inflammation at 7 days after intervention.
- Immunohistological evaluation of VAP-P1 allowed for differentiation between normal healing and infection as early as 24 h after surgery, whereas cortical bone area and density could reliably discriminate between the two at 7 days after surgical intervention.[8]

These findings suggest that ^{68}Ga-DOTAVAP-P1 may be able to differentiate bone infection with S. aureus from normal bone healing as early as 7 days after surgery. It may also be useful in determining the phase and rate of infectious and inflammatory processes and as such is anticipated to play a role in monitoring treatment response. Limitations of this study included the use of a clinical PET scanner rather than a micro-PET scanner, which may have had an impact on the image resolution.

In a follow-up study in 2009 from the same group, Ujula and colleagues further evaluated the labelling and biodistribution of **^{68}Ga-DOTAVAP-P1.** The authors noted that ^{68}Ga-DOTAVAP-P1 binds to VAP-P1-infected cells more efficiently than to normal cells. ^{68}Ga-DOTAVAP-P1 is cleared quickly from the blood pool to be excreted into the urine and has an in-vivo half-life of around 26 min in rats. They concluded that infection-induced VAP-P1 can be targeted successfully with ^{68}Ga-DOTAVAP-P1 and suggest that this novel tracer could be the first in a series of similar VAP-P1-specifific imaging agents for the diagnosis of osteomyelitis.[9]

A recent study by Kumar and colleagues investigated the potential use of **^{68}Ga-apo-transferrin (^{68}Ga-TF)** in the detection of S. aureus infection. They injected five rats with S. aureus and found that the site of infection could be imaged within an hour after injection using a dose of 10–15 MBq. Infected lesions could be visualized as early as 20 min after injection for up to 4 h with improving target-to-background ratios (TBRs). This was in contrast to the results obtained with the use of $^{68}GaCl_3$, which did not demonstrate any remarkable uptake for up to 2 h after injection. This study suggests that ^{68}Ga-apo-TF may be valuable in the imaging of S. aureus (and possibly other anaerobic bacterial infections) and also supports the hypothesis that gallium uptake depends more on transferrin binding than on vasodilatory changes.[7,10]

In the authors' experience with ^{68}Ga imaging, the image quality deteriorates significantly after 2 h, which casts some doubt over the repeatability of these results in the clinical setting.

Nanni et al. in 2010 assessed the accuracy of **^{68}Gallium-citrate** in the evaluation of skeletal infections. A total of 31 patients (with 40 scans in total) were enrolled with either acute (n=18) or chronic osteomyelitis (n=4) or diskitis (n=9) and findings were validated with the results of combinations of MRI, CT, radiographs, white blood cell scintigraphy, biochemistry, biopsy results and follow-up data (up to 1 year).
All patients underwent biopsy, but only 11 turned out to be diagnostic.

An average dose of 4.5 MBq was injected and imaging followed an uptake period of 60 minutes. Tracer bio-distribution revealed relatively high vascular activity (mean SUVmax: 1.5) with mild hepatic and bone marrow uptake and absence of bowel activity. All patients with proven infection demonstrated increased tracer accumulation at the infection site with a mean SUVmax of 4.4 (+/- 1.8).

The following observations were made:

- The diagnostic accuracy of ^{68}Ga-citrate for musculoskeletal infection (90% overall) imaging is similar to that of other modalities currently in use.
- Sensitivity was 100%, specificity was 76%, positive predictive value was 85% and negative predictive value was 100%.
- Imaging with ^{68}Ga-citrate has a very high negative predictive value and no false positives occurred as a result of implants.
- It may be used to evaluate treatment response.
- Added value includes being a simple and fast imaging procedure with low dosimetry and no contraindications to scanning.[11]

To the best of the authors' knowledge, this is the first study of its kind to involve the imaging of patients. Possible limitations of this study include the small number of patients and no inclusion of patients who had sustained recent trauma or who had undergone recent surgery.

Mitterhauser and colleagues sought to develop a simple preparation method for **^{68}Ga-EDTMP** as a PET bone-imaging agent. This was done in anticipation of making use of the superior resolution of PET imaging together with the convenience of a generator-based tracer. They demonstrated that a simple kit preparation was plausible and that binding of ^{68}Ga-EDTMP to bone mineral was irreversible. However, the uptake and image quality were inferior to that of ^{18}F-fluoride, and therefore the advantages of this tracer were not clear.[10]

Suzuki and colleagues investigated the use **of ^{68}Ga-NOTA-Bisphosphonate (^{68}Ga-NOTA-BP)** as an alternative to imaging with ^{99m}Tc-MDP in a rat model. Although their study involved the use of this novel ^{68}Ga tracer in the setting of metastatic bone disease evaluation, its application could easily be extended to include the nononcological indications for conventional bone imaging and therefore deserves a brief mention here. The authors compared **^{68}Ga-NOTA-BP** with **^{99m}Tc-MDP** and **^{18}F-NaF** and found that ^{68}Ga-NOTA-BP cleared faster from the blood, had higher bone-to-blood ratios and allowed imaging as early as 1 h after injection. This study was conducted primarily to overcome some of the limitations experienced with ^{18}F-NaF imaging (such as the higher costs of a cyclotron-produced tracer) and to find a generator-based alternative in light of the molybdenum shortage. Other tracers evaluated by various groups before **^{68}Ga-NOTA-BP** included **^{68}Ga-citrate, ^{68}Ga-tripolyphosphate** and **^{68}Ga-EDTMP,** which did not demonstrate sufficient efficacy for clinical application.[12]

Riss and colleagues in 2008 developed two **NODAPA-glucosamine derivatives for ^{68}Ga-labelling** for another novel musculoskeletal application. Glucosamine forms part of the normal cartilage and synovial fluid and therefore may be useful in the imaging of osteoarthritis. *To the authors' best knowledge, no clinical data on this application are available to date.*[13]

Summary

- The limitations of imaging with ^{18}F-FDG in the setting of musculoskeletal infections are well known. Of greatest significance clinically is the difficulty to differentiate normal bone healing or inflammation from infected bone using this tracer.

- Imaging with ^{68}Ga may provide attractive alternatives such as $^{68}GaCl_3$, ^{68}Ga-DOTAVAP-P1, ^{68}Ga-apo-transferrin, ^{68}Ga-citrate and ^{68}Ga-NOTA-BP.
- A simple kit formulation was plausible with ^{68}Ga-EDTMP, although the tracer did not provide any advantages over those already in existence.

The majority of publications relating to this application involves limited subject numbers and relate to pre-clinical settings. They also focused mainly on infection with *Staph Aureus* only.

The outcomes of preclinical studies are as follows:

- Bone infection imaging with **$^{68}GaCl_3$** appears to yield fewer false positives due to postsurgical inflammatory changes.
- Differentiation between infection and inflammation is possible as early as 7 days after intervention with **^{68}Ga-DOTAVAP-P1.**
- **^{68}Ga-apo-transferrin** imaging allows the detection of infection with S. aureus and other anaerobic infections as early as 1 h after injection.
- Work on **^{68}Ga-NODAPA-glucosamine** derivatives for possible osteoarthritis imaging is still in a preclinical phase.

The only study that involved humans suggested a diagnostic accuracy for **^{68}Ga-citrate** similar to that of currently used gold standards with additional practical advantages such as shorter imaging times and lower dosimetry.

Many exciting opportunities for tracer development exist with the emergence of novel applications such as in osteoarthritis imaging. More studies in clinical settings involving larger numbers of patients are clearly needed.

Respiratory system

In the preclinical setting of lung pathology, ^{68}Ga has been labelled mostly to albumin microspheres, to **macroaggregates of albumin (MAA)** or to **transferrin.** These have been applied in various studies to evaluate pulmonary blood flow, calculate lung water compartments and assess pulmonary capillary permeability (PTCER). In the clinical setting, ^{68}Ga has been labelled successfully to siderophores and microspheres. In addition, several studies have made use of **'Galligas'**, wherein **$^{68}GaCl_3$** is labelled to carbon particles in a manner similar to technegas production.

Many lung conditions result in an increase in pulmonary capillary permeability and extravascular lung water. PET imaging allows for the quantification of the rate at which intravenously injected radiolabelled proteins escape into the extravascular space, which is then expressed as the pulmonary transcapillary escape rate (PTCER). This provides an estimate of the severity of lung injury. It could potentially be used to differentiate cardiogenic from noncardiogenic causes of pulmonary oedema and may find clinical application in such conditions as acute respiratory distress syndrome (ARDS), pneumonia, acute interstitial lung disease, reimplantation response and acute ejection after lung transplantation.

Accurate quantification of lung function, however, remains difficult for several reasons. Tracer activity is typically expressed per millilitre of tissue (SUV) and as such changes in values may result from differences in regional lung volumes, rather than from any real change in tracer concentration. Other drawbacks include the high pulmonary blood flow, which results in high background activity and movement during breathing, which may result in various artifacts. Therefore, the use of a SUV alone in the setting of lung disease appears inadequate.[14]

As early as 1987, Mintun and colleagues measured pulmonary vascular permeability using **^{68}Ga-transferrin.** They imaged six dogs injected with oleic acid to induce lung injury, as well as two patients with ARDS and two healthy volunteers. ^{68}Ga-citrate was injected

intravenously and was followed by sequential 1–5-min PET scans taken over 1 h using a two-compartment model for analysis. They found that the PTCER was increased 10-fold in the lungs affected by oleic acid injury and four-fold in patients with ARDS (compared with normal lung values).[15]

Mintun's study provides proof-of-concept for the use of ^{68}Ga-citrate PET in the measurement of pulmonary vascular permeability. Further generalizations or applications are not really possible in light of the small size of the samples and because of the discrepancies between the protocols used in animals and humans.

Schuster and colleagues in 1998 compared PTCER values obtained with **^{68}Ga-transferrin** (370–555 MBq) and **^{11}C-methylalbumin** (185 MBq) in the evaluation of lung injury. The authors imaged two groups of dogs (seven in total): one group with normal lungs (n=3) and the other group with lung injury induced by injection of oleic acid (n=4). Imaging and plasma samples were obtained 2 min after tracer injection for up to 45 min. Blood and tissue samples were used in a two- compartment analysis to calculate the PTCER.
They concluded that the two tracers correlated strongly over a wide range of values and that either tracer could be used to evaluate the severity of lung injury. Labelled transferrin, however, provided significant practical advantages, such as availability from a generator.[16]

In a follow-up study by the same group published in 2002, Schuster and colleagues evaluated the use of **^{68}Ga-transferrin PET** and **^{99m}Tc-albumin** single-photon emission computed tomography (SPECT) in the detection of acute lung injury in a group of patients. They imaged 38 patients in total, of whom 21 patients had noncardiogenic pulmonary oedema, seven had hydrostatic forms of pulmonary oedema and 10 were healthy volunteers. All patients were selected on the basis of radiological criteria and imaged within 24 h of symptom onset. Their aim was to compare the values of PTCER obtained with gamma imaging (^{99m}Tc-albumin SPECT) with the values obtained with PET imaging (222 MBq of ^{68}Ga-transferrin).[17]

They made the following observations:

- PTCER could not reliably distinguish noncardiogenic pulmonary oedema from hydrostatic pulmonary oedema.
- PTCER and the normalized slope index are strongly correlated.
- Gamma-obtained PTCER correlated better with PET PTCER and PaO_2/FIO_2 than with normalized slope index.

They concluded that, on the basis of the (limited) available data, gamma camera methods should probably not be used as a screening tool in acute lung injury trials.[17]

In 2010, Kotzerke and colleagues evaluated the use of **^{68}Ga-microspheres** and **Galligas** for PET imaging of lung function. This was done in an attempt to deal with the worldwide shortage of molybdenum by finding a suitable alternative. Galligas could be produced in a relatively simple manner, similar to the procedure used for technegas production. The greater than 3.5 h in-vivo stability allowed for PET imaging with a dose of 5–10 MBq of ^{68}Ga. They found that ^{68}Ga-DOTA microspheres were rapidly filtered from venous blood in rats and accumulated in the lungs in a manner that allows for quantification.[18]

In 2011, Borges and colleagues compared the PET acquisition of ventilation images using 'Galligas' with those acquired using conventional techniques (consisting of technegas and SPECT imaging). They made use of a porcine model and imaged 12 piglets in total, all of which underwent sequential SPECT and PET imaging. The animals were divided into three groups: those with lobar obstruction (a balloon catheter was used to occlude the lower main bronchus), those with diffuse airway obstruction (continuous metacholine infusion used to cause bronchoconstriction) and those with normal lung function. 'Galligas' was prepared using the same technique and equipment as those used for the production of technegas, with the substitution of technetium-99m with a $^{68}GaCl_3$ solution that was inhaled within 10 min of preparation. Image analysis revealed similar tracer distribution in both studies for the normal group as well as for those with lobar obstruction. With diffuse ventilation involvement, however, nonuniformity on PET images appeared more pronounced and was confirmed by a statistically significant difference in tracer count variability.[19] (The authors implemented

correcting measures to overcome the limitation of differences in acquisition times.)

The rationale for imaging with a positron emitter includes better resolution and the possibility of rapid, repeated studies if needed. In this study, the authors concluded that PET imaging provides a more accurate picture of ventilation distribution in the setting of diffuse bronchoconstriction and that 'Galligas' is a 'promising new diagnostic tool for the assessment of ventilation distribution'.[19]

Hofman and colleagues in 2011 investigated the use of ^{68}Ga PET as a high-resolution alternative to ventilation perfusion imaging with SPECT. In this prospective pilot study, they imaged 10 patients suspected of having pulmonary embolism using both SPECT and PET. '**Galligas'** was used for PET ventilation, and **^{68}Ga-MAA** was injected before PET perfusion image acquisition.

Five out of the 10 patients underwent SPECT and PET imaging on the same day, with the rest of the patients undergoing both studies within a period of 1–8 days apart.

Interpreting physicians were blinded to the results of other investigations and had to make use of a scoring system in their image evaluation. Image quality was then rated on a scale of 1 (poor) to 10 (very high) judged on the uniformity of tracer distribution. The number of matched and mismatched defects in each lobe was counted and characterized as segmental, subsegmental or nonsegmental. In conclusion, a remark of testing positive or negative for pulmonary embolism was made.

The following observations were made:

- PET images demonstrated a more homogeneous tracer distribution compared with SPECT images and were judged to be of superior quality compared with SPECT in all patients ($P<0.01$).
- Matched and mismatched defects were similar (in terms of number and localization) in eight out of 10 studies.
- Advantages of PET over SPECT imaging included higher resolution, the possibility of better regional lung function quantification, greater flexibility in image acquisition

protocols and less time (3–6 min/study) with a similar effective radiation dose of 3–5 mSv.

The authors concluded that ^{68}Ga PET imaging of ventilation and perfusion is clinically feasible.[20]

An important limitation of this study is the fact that half of the participants underwent the comparative studies several days apart (1–8 days), during which time the pathology may have changed.

Ament and colleagues recently confirmed the clinical feasibility of ^{68}Ga-PET ventilation perfusion imaging in a 2012 publication. They concluded that imaging with ^{68}Ga aerosol (Galligas) and ^{68}Ga-MAA provides an interesting alternative with high accuracy to ^{99m}Tc-labelled tracers. This is relevant especially in times of molybdenum shortage and in light of the increasing availability and use of PET/CT scanners and ^{68}Ga generators.[21]

In 2010, Ambrosini and colleagues investigated the novel use of **^{68}Ga-DOTA-NOC** PET/CT in the imaging of idiopathic pulmonary fibrosis (IPF). This condition remains difficult to diagnose and has rapid progression with poor prognosis. The diagnosis is based on radiological and clinical criteria with a pathophysiologic hallmark of fibroblast foci. These fibroblast aggregates express somatostatin receptors that can be imaged with ^{68}Ga-DOTA-NOC because of the tracer's affinity for somatostatin receptors 2, 3 and 5. Because healthy lungs demonstrate no ^{68}Ga-DOTA-NOC, any tracer accumulation may be regarded as abnormal.[22] The authors imaged 14 patients in total, half with a diagnosis of IPF and the other half with nonspecific interstitial pneumonia (NSIP). All patients were imaged with ^{68}Ga-DOTA-NOC PET/CT (185 MBq, 60 min uptake time) and high-resolution CT (HRCT) within a 3-week time frame. The severity of the lung involvement on CT was scored visually according to a five-point scale. The sites and extent of the abnormal tracer accumulation on PET/CT were then compared with the areas of pathology on HRCT. All of the study participants (with the exception of one) were undergoing treatment at the time of the investigations. Treatment included administration of steroids, cyclophosphamide, azathioprine, methotrexate and various combinations thereof.

Their findings were as follows:

- In patients with IPF, abnormal ^{68}Ga-DOTA-NOC correlated with areas of reticular fibrosis and honeycombing noted on HRCT and was typically located in the subpleural and peripheral regions.
- A linear correlation was found between SUV_{max} and the extent of disease noted on CT.
- Patients with NSIP demonstrated less intense uptake in the areas of ground-glass opacification.

The authors concluded that somatostatin overexpression in IPF could be imaged with ^{68}Ga-DOTA-NOC with the potential for future treatment response evaluation.[22]

In a series of publications between 2010 and 2012, Petrik and colleagues investigated both the in-vitro and in-vivo potential of **^{68}Ga siderophores** to diagnose invasive pulmonary aspergillosis.

Aspergillus fumigatus is one the most common airborne fungi and, although easily eliminated in the immunocompetent host, infection with this pathogen in the immunocompromised individual remains potentially fatal. Diagnosis of this increasingly prevalent serious condition using conventional investigations remains suboptimal. Iron plays an essential role in the nutrition and survival of the causative pathogen A. fumigatus and is crucial to its virulence. Many of its siderophores (which function as iron transporters in most bacteria and fungi) demonstrate an affinity for ^{68}Ga similar to that for iron.[22]

The above-mentioned group from Innsbruck labelled two different siderophores from A. fumigatus (desferri-triacetylfusarinine C/TAFC and desferriferricrocin/FC) with ^{68}Ga. They injected it into a group of immunosuppressed mice as well as into a healthy group and **found the following:**

- Both ^{68}Ga siderophores demonstrated high ^{68}Ga affinity, stability, specific activity and hydrophilic properties.
- Tracer uptake in the lungs depended on the severity of the infection, with no uptake

noted in the lungs of the control group and rapid accumulation noted in mice with severe infection. This was observed in particular with ^{68}Ga-TAFC.

- Tracer accumulation was highly dependent on the iron load, which could be blocked by administering high amounts of siderophores or NaN_3. This suggests the presence of a specific energy-dependent uptake mechanism.[23]

In a 2012 publication, the same group (Petrik and colleagues) compared various siderophores in the PET imaging of A. fumigatus infections. They found significant differences in the stability and labelling efficiencies and discovered that uptake in A. fumigatus cultures was dependent on both the iron load and the siderophore type. Normal, uninfected mice were injected with around 2 MBq of ^{68}Ga and evaluated at 30 and 90 min after injection. Biodistribution varied according to the siderophore type, with ^{68}Ga-TAFC and ^{68}Ga-ferrioxamine (FOXE) demonstrating low plasma values early after injection with rapid renal excretion.

^{68}Ga-ferricrocin and **^{68}Ga-ferrichrome** showed high blood retention, and **^{68}Ga-fusarinine** demonstrated very high renal retention.

According to their experiments, **^{68}Ga-TAFC** and **^{68}Ga-FOXE** showed the most promise as PET imaging tools in invasive pulmonary aspergillosis with high, specific uptake and favourable biodistribution.[24]

In the latest publication by Petrik and colleagues, the two tracers mentioned above were further evaluated both in vitro and *in vivo* using rat models.

In-vitro studies were used to evaluate the uptake of ^{68}Ga siderophores using A. fumigatus in iron-sufficient medium (30 mmol/l $FeSO_4$ added) compared with iron-deficient medium (no iron added) after 45 min of incubation at room temperature.[24]

In-vivo biodistribution was evaluated in two groups of rats – a group of neutropenic rats infected with A. fumigatus and a normal comparison group. Imaging was carried out with ^{68}Ga-TAFC in 20 rats and with ^{68}Ga-FOXE in 19 rats. The acquisition of dynamic PET/CT images started with intravenous injection and continued for up to 60 min, whereas static images were acquired after 30 min for 30 min.

The following observations were made:

- The uptake of both ^{68}Ga-TAFC and ^{68}Ga-FOXE was increased in iron-deficient cultures and could be blocked with excess ferrisiderophore and sodium azide.
- The intensity of the tracer accumulation correlated with the severity of the infection (and abnormal CT findings) and was not significantly decreased by iron preloading.
- Both tracers demonstrated early (10–20 min after injection for up to 60 min) selective uptake in infective lung lesions with rapid renal elimination.[25]

Summary

The following trends were observed:

- The PTCER can be determined using ^{68}Ga-citrate or ^{68}Ga-MAA and appears valuable in the assessment of various types of lung injury.
- Unfortunately, the use of PTCER does not help to differentiate cardiogenic pulmonary oedema from cardiogenic oedema.
- Imaging with ^{68}Ga-transferrin PET/CT appears to be of value in distinguishing sterile induced lung injury from ARDS with higher tracer accumulation indicating a more severe injury.
- With regard to imaging parameters, a dose of 185–370 MBq with an uptake time of 45–60 min and a two-compartment model for analysis appear sufficient for accurate image interpretation.
- Promising results have been found with ^{68}Ga-DOTA-NOC imaging of IPF, which may find clinical application especially in the evaluation of treatment response.
- For lung infection imaging, promising results have been found with ^{68}Ga-TAFC and ^{68}Ga-FOXE in Aspergillosis imaging. These tracers have been shown to accumulate selectively in infective lung lesions in animal models, with a correlation noted between tracer intensity and severity of infection.

- 'Galligas' and ^{68}Ga-MAA provide an attractive, clinically feasible alternative for lung ventilation and perfusion imaging that offers advantages such as improved resolution with faster, more flexible imaging protocols.

Readers are also referred to a review published in 2011 by Bomanji and colleagues on the use of PET/CT in imaging pulmonary infections and inflammation.[26]

Cardiovascular system

Publications focussing on the cardiovascular applications of ^{68}Ga began to appear during the early 1980s. These papers focussed mainly on the search for suitable ligands, on kit development and refinements and on clinical application of ^{68}Ga-labelled tracers as perfusion or blood pool agents. More recently, however, interest has been rekindled with a new focus on the application of ^{68}Ga-labelled tracers as atherosclerotic plaque agents and on its emerging role in interventional cardiology.

The search for an appropriate ligand, kit development and refinements

The development of cardiac PET tracers was pursued with the aim of improving the resolution and quantification of myocardial imaging and started with the search for appropriate ligands.

In 1993, Green and colleagues evaluated four novel gallium complexes as potential PET myocardial perfusion tracers. The four ligands (n-BuO–, iso-BuO, sec-BuO– and n-PrO) were labelled to ^{67}Ga and then used to image rat hearts. From these initial experiments, **^{68}Ga-[(sal)3tame-O-iso-Bu]** was selected as the most promising complex for further evaluation in PET studies and was used on a healthy dog. This study was conducted to improve upon previous poor results obtained with uncharged ^{68}Ga complexes that tend to resist ligand exchange with transferrin. Previous work carried out with ^{68}Ga [(5-MeOsal)3tame] demonstrated a flow-dependent extraction fraction and clearance that required correction for tracer activity remaining in the ventricle.[27]

The following observations were made:

- The ^{68}Ga complexes demonstrated rapid plasma clearance with good myocardial accumulation, significant (unwanted) liver accumulation and, despite the lipophilic nature, no penetration of the blood–brain barrier.
- The suboptimal pharmacokinetics of all these complexes were still considered to be superior to those of **^{68}Ga-[(5-MeOsal)3tame],** which was previously regarded as the most promising tracer.
- PET images of a healthy dog using **^{68}Ga-[(sal)3tame-O-iso-Bu]** were of high quality as early as 2–10 min after injection.[27]

Good results had been found with **^{68}Ga-BAPEN** as a myocardial imaging agent in terms of stability and biodistribution.[28]However, its complicated and time-consuming preparation prompted Yang and colleagues in 2010 to develop a simple, two-step labelling kit for ^{68}Ga with this ligand. This involves adding eluted ^{68}Ga to the BAPEN kit, followed by a filtering step. Labelling is carried out at room temperature and this kit provides a relatively quick and simple way of labelling salicylaldimine ligands to ^{68}Ga with a high labelling efficiency and radiochemical purity. Imaging with ^{68}Ga-BAPEN provides high myocardial uptake, which decreases slowly over time.[29]

Hoffend and colleagues investigated the use of **^{68}Ga-DOTA-RSA** (rat serum albumin) as an alternative PET blood pool tracer. They made use of a rat model and analysed the biodistribution, making use of volumes of interest and time–activity curves at 10 and 60 min after injection. ^{68}Ga-DOTA-RSA demonstrated long plasma retention; it remained stable and was considered a suitable alternative to ^{15}O-H_2O in centres without an onsite cyclotron. The authors evaluated the use of ^{68}Ga-DOTA-RSA in the setting of tumour angiogenesis, but broader applications should also be considered.[30]

Plössl and colleagues developed a new gallium compound for myocardial perfusion imaging. They made use of an N_2S_2 chelating core to which they added three cyclohexyl rings. Again, the rationale was to improve resolution and quantification and provide a generator-based PET tracer with ^{68}Ga should labelling with ^{67}Ga prove successful. These studies followed on previous work conducted with N_2S_2 and NS_3-based compounds. The added cyclohexyl rings

lead to added stability and an increase in both lipophilicity and first-pass extraction. The radiochemical purity achieved was greater than 92%. Biodistribution was determined using a rat model, which demonstrated high cardiac tracer accumulation with retention of 2.1% and 0.9% of the initial dose (10–100 μCi) at 2 and 60 min after injection, respectively. Autoradiography was then used to evaluate the feasibility of **gallium-bisamino-isthiolate** as a myocardial perfusion tracer in two groups of rats, and comparisons were made with equal doses of ^{99m}Tc-sestamibi. The first group consisted of healthy rats (n=3) and the second had undergone surgical ligation of the LAD (n=3). Imaging demonstrated even uptake in the heart, which was retained at 30 min in the healthy group and showed a marked decrease in the areas affected by LAD ligation. Limitations of this tracer included the high liver uptake as well as the kinetics that showed that the tracer was neither trapped nor feely diffusible. Despite the limitations, this compound could potentially be used as an alternative generator-based PET myocardial perfusion imaging agent.[31]

Tarkia and colleagues recently evaluated the use of several ^{68}Ga tracers as alternatives to currently used PET perfusion tracers. These consist of nitrogen-13-ammonia, rubidium-82 chloride and ^{15}O-H_2O. Despite the fact that these current PET tracers have been validated for the quantification of myocardial perfusion, widespread application thereof has been limited by the short physical half-lives and the need for an onsite cyclotron. The investigators selected four hexadentate salicylaldimine ligands derived from bis(3-aminopropyl)ethylenediamine (BAPEN), which has shown promise in previous rat experiments, to be compared with ^{15}O-H_2O in 14 healthy pigs. Dynamic PET images were acquired for 90 min and analysed in combination with the results from serial arterial blood collections. The authors found that myocardial uptake with all four ^{68}Ga tracers was too slow for clinical application. **^{68}Ga[Ga-(sal)2BAPDMEN]** demonstrated the highest myocardial uptake but did not correlate with myocardial perfusion as quantified by ^{15}O-H_2O. They thus concluded that none of the tested ^{68}Ga tracers would be suitable for clinical application.[32]

The vulnerable plaque

The vulnerable plaque presents an exciting target for research and is generally accepted to be a plaque with a lipid-rich core, a thin fibrous cap and inflammatory infiltrates. Macrophages have clearly been implicated in culprit lesions leading to cardiac events and tend to express

somatostatin receptors (subtypes 1 and 2), which may be detected with ^{68}Ga-DOTA-TATE as a marker of plaque vulnerability. Increased expression of certain integrins such as $\alpha v\beta_3$ / $\alpha v\beta_5$ have also been demonstrated, which has generated novel imaging possibilities for both the diagnosis and treatment of atherosclerosis.

Currently, there is no generally accepted accurate, noninvasive way to identify vulnerable plaques, and it seems that markers of inflammation or remodelling would be ideal. Early identification of vulnerable plaques with such tracers may lead to early intervention with improved outcomes.

In a 2009 publication, Haukkala and colleagues investigated the feasibility of occlusive atherosclerotic imaging with the use of **^{68}Ga-DOTA-RGD peptide**. Atherosclerotic lesions are associated with increased microvessel formation within the vessel walls with migration of activated endothelial cells, which is regulated partly by the $\alpha v\beta_3$ / $\alpha v\beta_5$ integrin. The expression of the aforementioned integrin is also increased in CD-68-positive macrophages, in the necrotic core of atherosclerotic lesions and in the shoulder of advanced plaques, which makes it an attractive target in cardiovascular disease. The authors evaluated the uptake of intravenously administered ^{68}Ga-DOTA-RGD peptide *in vivo* in excised tissue samples and aortic sections of LDLR$^{-/-}$ApoB$^{100/100}$ atherosclerotic mice (n=12).

^{68}Ga-DOTA-RGD peptide is known to bind to $\alpha v\beta_3$ / $\alpha v\beta_5$ integrin with high affinity and showed rapid plasma clearance with renal excretion and high uptake in the lungs, liver, spleen and bowel. Tracer biodistribution was examined *in vivo* in mice with atherosclerotic plaques (n=6) combined with immunohistological analysis. Findings were compared with those in control rats (n=6) and expressed as a ratio of atherosclerotic to normal vessel uptake. Results showed statistically significantly higher tracer accumulation in atherosclerotic plaques compared with normal vessels (mean ratio value of 1.4), suggesting the feasibility of imaging with this tracer. Confirmatory studies are needed to assess the clinical relevance.[33]

Substitution of the –DOTA ligand with –NOTA has resulted in some practical and imaging advantages. Initial work, which involved PET imaging with **^{68}Ga-NOTA-RGD,** was done in the setting of oncology in which it has been used as an angiogenesis imaging agent.[34]

Recently, however, Caforio and colleagues in a 2012 review on myocarditis suggested its application in the imaging of myocarditis on the basis of the promising results published from studies conducted on animal models of myocardial infarction imaging with ^{68}Ga-DOTA-TATE and **^{68}Ga-NOTA-RGD.**[35]

More recently, Rominger and colleagues retrospectively evaluated the use of ^{68}Ga-DOTA-TATE in imaging of the coronary arteries in 70 consecutive oncology patients. They assessed the tracer uptake in the LAD, which they then correlated with coronary calcium burden and cardiac risk factors.[36]

^{68}Ga-DOTA-TATE uptake was quantified in the following novel manner: fixed-sized regions of interest (ROIs) were placed manually on the LAD of all patients, which was chosen to match the lumen of the vessel. A mean blood pool SUV was calculated from three ROIs placed in the mid-lumen of the superior and inferior vena cava. The SUV_{max} from the LAD was subsequently divided by the blood pool SUV_{max} to yield a TBR. A TBR of at least 1.5 was considered as high uptake and a TBR less than 1.5 constituted low tracer accumulation. Patients were divided into those with and without calcified plaques based on the Hounsfield units obtained from the CT part of each study.

The authors found a significant correlation between increased tracer accumulation and the presence of vessel wall calcifications. They also found a significant correlation between increased ^{68}Ga-DOTA-TATE uptake in the LAD and the presence of prior cardiovascular events. They suggested that ^{68}Ga-DOTA-TATE might be useful in the imaging of coronary artery plaques.[36]

It is not clear from the methodology whether the authors considered the effect of attenuation correction on the intensity of the tracer accumulation. It is well known that areas of calcification might falsely increase the SUV in such areas.

On the basis of the accepted inflammatory nature of atherosclerosis and the increased number of activated macrophages in rupture-prone plaques, Silvola and colleagues evaluated the uptake of **^{68}Ga-Cl** in atherosclerotic plaques. They used two groups of mice: nine with

LDLR$^{-/-}$ApoB$^{100/100}$ and six normal mice as controls. All the mice were injected with ~17 MBq of ^{68}Ga-Cl and killed 3 h after injection.[37] Blood and tissue samples were measured for radioactivity using a gamma counter, and aortic tissue was evaluated with a combination of digital autoradiography and hematoxylin and eosin staining. Image analysis consisted of four ROIs, which were analysed on each aorta as follows: (a) plaque excluding media; (b) healthy vessel wall; (c) adventitia with adjacent fat; and (d) muscle for internal control tissue. Tissue staining with Mac-3 was used to grade plaques into the following categories: (a) no inflammation=no macrophages; (b) mild inflammation=occasional macrophages; (c) moderate inflammation=occasional and groups of macrophages; and (d) abundant macrophage infiltrations.

They imaged an additional three LDLR$^{-/-}$ApoB$^{100/100}$ mice with a micro-PET scanner. These were injected with a mean dose of 16 MBq of ^{68}Ga-Cl, which was followed by acquisition of a contrasted CT angiography. PET findings were quantified by drawing same-sized ROIs over the following areas: the left ventricle, the aortic arch and the brachiocephalic artery (as identified on CT angiography).

Their results were as follows:

- Autoradiography demonstrated significantly increased ^{68}Ga activity (1.8±0.2) in areas of (especially macrophage rich) atherosclerotic plaques compared with healthy vessels (P=0.0002).
- PET/CT imaging demonstrated high tracer accumulation in the heart and the aorta.
- The high plasma activity and slow blood clearance, combined with the short half-life, may limit the clinical applicability of 68Ga as an atherosclerotic plaque-imaging agent.[37]

Interventional cardiology

Unfortunately, restenosis follows angioplasty all too often because of factors such as elastic recoil, proliferation and migration of smooth muscle, synthesis of extracellular matrix and late constrictive remodelling, among others.

Various investigators have tried to combat this by means of medicated stents and brachytherapy. In the early 2000s, intracoronary radiation therapy was considered a promising novel approach in the prevention of restenosis. Initial commercial systems made use of solid sources emitting [beta]-radiation or [gamma]-radiation. This has the advantage of avoiding any radioactive spill in case of damage but poses the problem of proper centring within the coronary arteries and ensuring a uniform field of radiation.

Stoll et al.[38] proposed the use of ^{68}Ga (with its convenient 68 min half-life) for intracoronary radiation therapy with liquid-filled balloons in restenosis prevention. They made use of in-vitro studies on bovine aortic smooth muscle cells to ascertain the antiproliferative efficacy of positrons emitted by ^{68}Ga. They found that cellular proliferation rates were inversely proportional to the radiation dose in cultures irradiated with both gamma and positron radiation and that they were equally effective as reflected by the similar ED_{50} and ED_{80} values.

Phantom studies were performed with standard angioplasty balloon catheters, which were inflated with various liquid positron emitters and used to quantify the radiation tissue penetration. Modelling of balloon rupture and spills was also performed. The rationale behind this study was that balloon catheters with short-lived liquid radioisotopes would provide a homogeneous, readily available dose that would be safer than the conventionally used ^{186}Re and ^{188}Re in case of rupture or spillage.

The authors concluded that under a worst-case scenario a balloon rupture with ^{68}Ga would result in a maximal whole-body dose of 50 mSv and that ^{68}Ga could therefore be considered a safe alternative for coronary radiation therapy.[35,36]

Platelet and thrombus imaging

Imaging of platelet behaviour in thrombosis in the presence or absence of atherosclerosis provides an interesting target for understanding the pathophysiology of cardiovascular disease. Platelets play an important role in the development of atherosclerosis and tend to accumulate only in active thrombi; incorporation of thrombi into the vessel wall represents a potentially fatal complication of atherosclerosis. Imaging of platelets provides the location of thrombi and also provides a noninvasive functional assessment of thrombotic activity.

Karanikas and colleagues set out to identify the best chelate for the radiolabelling of platelets with gallium as this could prove to be a useful probe in the imaging of platelet behaviour both in thrombosis and atherosclerosis. Blood for platelet labelling was obtained from 172 healthy volunteers without any cardiovascular risk factors. The platelet-labelling characteristics of ^{67}Ga was evaluated with oxine, tropolone and MPO, and ^{67}Ga-MPO of autologous platelets was finally selected as the most appropriate agent to substitute for platelet imaging. This could easily be substituted with ^{68}Ga, resulting in **^{68}Ga-MPO platelets** for PET imaging.[39]

Jalilian and colleagues evaluated the early detection of thrombi through imaging by labelling streptokinase with ^{67}Ga for possible application in stroke management. Streptokinase imaging acts as a probe for plasminogen detection in thrombi or emboli. A rat thrombosis model was used and ~50 μCi of **^{67}Ga-DTPA-streptokinase** was injected into the tail vein, followed by SPECT imaging. The best time to image was determined as 1–2 h after injection, as enzymatic degradation of the protein starts after 80 min.

The authors suggested that, in light of the promising imaging results with ^{67}Ga, ^{68}Ga-streptokinase could also be considered a potentially useful tracer for thrombus detection, providing better resolution and a more suitable half-life.[40]

Summary

- Several interesting tracer possibilities with ^{68}Ga for cardiovascular imaging exist. In particular, ^{68}Ga-[(sal)3tame-O-iso-Bu],^{68}Ga-BAPEN and ^{68}Ga-bisamino-isthiolate appear promising for myocardial imaging and ^{68}Ga-DOTA-RSA seems to be a reliable alternative PET blood pool tracer. Refinements of tracers with development of kits should accelerate once clinical applications and demand increase.
- Many novel and exciting applications for ^{68}Ga-labelled tracers have emerged, which are not limited to diagnosis only. Imaging of the ‘vulnerable plaque’ and the processes of atherosclerosis and thrombus formation provide insight into the pathophysiology of these processes, which may find broader clinical application.
- For the imaging of vulnerable plaques and atherosclerosis the following tracers have shown the most promise: ^{68}Ga-DOTA-TATE and ^{68}Ga-DOTA-RGD. With regard to

thrombus imaging (for possible application in stroke management) ^{68}Ga-MPO platelets/^{68}Ga-streptokinase shows some promise.

- Interventional cardiology provides a whole new field for ^{68}Ga tracer applications. Intracoronary balloon catheters filled with short-lived radioisotopes such as ^{68}Ga have been proven to be safe and effective in preventing restenosis following vascular intervention.

Central nervous system

Various disease processes (such as brain tumours and dementia) affect the functioning of the blood–brain barrier. **^{68}Ga-EDTA** is an ideal tracer for the evaluation and quantification of these changes as its permeability of the blood–brain barrier under normal circumstances is low. ^{68}Ga-EDTA has also been applied in the evaluation of cerebrospinal fluid flow as early as 1970.[42]

In 1984, Hawkins and colleagues used ^{68}Ga-EDTA to estimate the permeability of the blood–brain barrier and the local cerebral blood volume in 12 patients with primary or metastatic brain tumours. They made use of a two-compartment model and arterial blood samples to calculate values for the forward (k_1) and reverse (k_2) transverse constants, and patients were imaged for up to 2 h after injection.[43]

Friedland and colleagues in 1985 evaluated the permeability of the blood–brain barrier in Alzheimer's disease (AD) using dynamic PET imaging with both ^{82}Rb and ^{68}Ga-EDTA making use of a two-compartment model.

Imaging was performed on a group of patients diagnosed with AD and the results were compared with those of a group of healthy participants. A total of 17 patients were imaged. The k_1 values calculated using both tracers did not deviate significantly from zero and the affected areas in AD did not demonstrate any increase in permeability.[44]

Pozzilli and colleagues sought to quantify the increase in blood–brain barrier permeability in patients with multiple sclerosis (MS), which was noted in previous studies conducted with contrasted CT scans. To do so, they injected 15 patients having confirmed MS with 6–8 mCi of ^{68}Ga-EDTA, followed by PET/CT imaging. Quantification was performed using multiple-

time graphical analysis, which allowed for simultaneous calculation of the blood to brain influx (K_i) and plasma volume (V_p).[45]

The following observations were made:

- Four patients with clinical exacerbation of disease demonstrated focal areas of increased ^{68}Ga-EDTA, which corresponded to the areas of enhancement noted on CT (both in terms of localization and extent).
- A moderate increase in the K_i value was found in the areas of pathology, with no corresponding increase in V_p values.[45]

Although this study suffers from several limitations, with many questions remaining, it does provide some insight into the function of the blood–brain barrier in patients with MS. Further studies would be of value. To the authors' knowledge no similar studies have been attempted with ^{68}Ga-based compounds.

In 1999, Cutler and colleagues investigated the potential of **^{68}Ga-S_3N** as a possible cerebral blood flow tracer. This amine complexed to ^{68}Ga demonstrates ideal properties for blood–brain penetration, as it is small, neutral, lipophilic and kinetically stable. Biodistribution studies demonstrated significant brain, cardiac and liver uptake, and the authors concluded that ^{68}Ga-S_3N could be promising in terms of cerebral blood flow imaging.[46]

In 2002, McCarthy and colleagues labelled leptin to **^{68}GA-DTPA** to assess whether intrathecal administration of leptin could achieve therapeutic levels at the site of action in the hypothalamus. They injected the tracer into the intrathecal space of the lumbar spine of three baboons and compared it with unconjugated ^{68}Ga-DTPA. They found that the ^{68}Ga-labelled leptin compound reached the arcuate nucleus between 90 and 140 min after injection at levels 40 times higher than normal levels, whereas the unconjugated ^{68}Ga-DTPA was resorbed back into the blood. These findings could have important implications for the management of obesity, as it has long been accepted that leptin plays a major role in weight control. Finding a suitable route of administration, however, is problematic, primarily because of the saturability of the transport system over the blood–brain barrier.

The authors suggest that the intrathecal method of administration may potentially overcome this problem.[47]

Summary

- The blood–brain barrier remains an important imaging target in the evaluation of central nervous system disorders. A few investigators have made use of ^{68}Ga-EDTA in this setting for possible application in Alzheimer's dementia and MS. Studies have been small (involving 12–17 patients) and have centred around the period 1984–1988, after which it seems that these applications were abandoned.
- ^{68}Ga-S_3N demonstrated promise as a cerebral perfusion agent.
- Other unusual applications such as ^{68}Ga-DTPA-leptin in the investigation of obesity management appear to be limited to a single study only with the most recent publication seen in 2002

Genitourinary system

Renal imaging has been performed with the use of ^{68}Ga since the late 1960s. The first ^{68}Ga/^{68}Ga generator was eluted with an EDTA solution, which resulted in **^{68}Ga-EDTA** for application in glomerular filtration rate (GFR) determination mostly. It is only recently that the attention has shifted away from renal function quantification towards infection imaging.

One of the first publications on the use of ^{68}Ga in renal imaging reported on renal imaging with ^{68}Ga in the form of **^{68}Ga-polymetaphosphate**. The authors concluded that the high kidney accumulation and the short half-life would make ^{68}Ga-polymetaphosphate a useful tracer in renal imaging.[48]

In 1988, Yamashita and colleagues evaluated renal function with the use of **^{68}Ga-EDTA** in six healthy male volunteers. Organ activity was corrected for blood content with the use of ^{15}C-O gas. They found the blood volume to be around 12 ml/100 g kidney and the GFR to be around 30 ml/min/100 g kidney.

As these values corresponded well to those published in standard physiology textbooks, the authors concluded that PET studies could find a valuable clinical application in the measurement of GFR.[49]

In a 2006 publication, Szabo and colleagues discussed the future direction of renal PET and attributed the slow development thereof to the success of planar and SPECT renal imaging and to the usefulness of other noninvasive imaging modalities such as ultrasound, CT and MRI. Despite the infrequent use of ^{68}Ga, its value in the determination of GFR was again emphasized. When labelled to EDTA, its kinetics are described by a noncompartmental impulse response function, which is identical to that of ^{99m}Tc-DTPA (which has been studied extensively).[50]

In a 2008 publication by the same authors, Szabo and colleagues again mentioned the role of ^{68}Ga-EDTA in renal imaging and the use of **^{68}Ga-labelled alizarin red S.** This radiopharmaceutical accumulates in the renal cortex within 90 min after injection in a way similar to DMSA but has a lower urinary excretion. It appears promising as an imaging agent for acute pyelonephritis, for determination of anatomical kidney defects and for relative blood flow assessment.[51]

In a 2009 publication, Nanni and colleagues investigated the use of **^{68}Ga-Cl** in the imaging of genital infection. The group sought to assess the feasibility of ^{68}Ga-Cl in an animal model of genital infection induced with Chlamydia muridarum. Eleven infected mice (as well as three controls with inflammation and one healthy control) were imaged on several occasions (with ^{68}Ga-Cl and small animal PET) for up to 19 days after vaginal inoculum with C. muridarum. The results from this study demonstrated increased tracer accumulation in the infected mice, which was not seen to the same extent in controls. Cervical swabs and in-vivo analysis validated the PET findings, and the authors concluded that ^{68}Ga-Cl may be a suitable marker for genital infection assessment in a mouse animal model. In the light of the inability of ^{68}Ga-Cl to distinguish clearly between infection and sterile inflammatory changes, the authors suggested that ^{68}Ga-citrate may be a promising agent in this setting because of the more stable nature of the compound.[52]

Summary

- With regard to renal imaging, ^{68}Ga-based alternatives are available for most of the commonly used ^{99m}Tc-based tracers.
- ^{68}Ga-EDTA has been shown to be as accurate in the assessment of GFR as ^{99m}Tc-DTPA.
- ^{68}Ga-alizarin red S can be used as an alternative to ^{99m}Tc-DMSA in the imaging of anatomical kidney abnormalities, pyelonephritis imaging and split function assessment.

Future developments may include the ability to distinguish between genital infections and inflammatory changes with the use of ^{68}Ga-Cl or ^{68}Ga-citrate.

Despite the above-mentioned possibilities, imaging with ^{68}Ga in this setting remains underutilized for reasons that are not quite clear. Possible explanations include dosimetry considerations and lack of knowledge and/or expertise.

Liver and gastrointestinal applications

Alizarin and alizarin red S had been labelled with ^{68}Ga as early as the late 1970s for visualization of the reticuloendothelial system (RES) and kidneys. Alizarin is known to form stable compounds with gallium in neutral or slightly acidic conditions, whereas alizarin red S stains calcifying tissues a fluorescent red.

Schuhmacher and colleagues in 1980 investigated these two substances coupled to ^{68}Ga. In their investigation, both groups of animals (rats and dogs) and the single healthy volunteer studied demonstrated high tracer accumulation in the liver and spleen within 5 min of injection of **^{68}Ga-alizarin**, whereas **^{68}Ga-alizarin red S** demonstrated high renal accumulation 2 h after injection. These features, combined with the resolution advantages of PET/CT and the simple and fast preparation, rendered them promising imaging agents of the RES and kidneys.[53]

In 1983, Schuhmacher and colleagues described the use of **^{68}Ga-BP-IDA** for the evaluation of hepatobiliary function using PET to try and overcome some of the inaccuracies experienced with SPECT tracers when subtle changes in hepatic excretion or comparisons among patients had to be evaluated. The compound was tested in a rat model (n=7) and in two healthy human volunteers. It provided good stability, favourable kinetics and biodistribution, and competition from exogenous bilirubin was low. These findings led the authors to conclude that the use of ^{68}Ga-BP-IDA for quantitative evaluation of hepatobiliary function would be feasible.[54]

In a 2009 publication by Rizzello and colleagues on the synthesis and quality control of **^{68}Ga-citrate**, the authors included an image from a patient with inflammatory bowel disease that demonstrated increased tracer accumulation in the descending bowel. This suggests that an application for the use of ^{68}Ga-labelled radiotracers also may exist in the imaging of inflammatory bowel disease.[56]

Several studies involving ^{68}Ga compounds for application in the liver or gastrointestinal system were published in 2011. Haubner et al.[55]developed the ^{68}Ga compound for liver function imaging based on receptor density determination of a glycoprotein receptor (ASGP-R). They found that **^{68}Ga-GSA** could be produced relatively easily with high radiochemical purity and yield. Rat biodistribution studies demonstrated a favourable biodistribution.[58]

Zimny et al. [59] investigated the imaging of **sulphonylurea receptor 1 (SUR-1)** for the purpose of imaging β-cell masses. This could potentially play an important role in the success of β-cell transplantation in type I diabetes mellitus. ^{18}F-FDG-based tracers are limited by high liver uptake that precludes adequate pancreas visualization, which leads to the successful development of ^{68}Ga-NODAPA-NCS-glibenclamide by this group.[60]

Kumar and colleagues in a 2012 publication further investigated the possibility of using ^{68}Ga in the imaging of intra-abdominal infections. The authors induced infection with S. aureus in rats and found increased tracer accumulation as early as 5 min after injection, with intense uptake noted between 30 min and 6 h at the site of infection. Increased tracer accumulation was also present in a patient with postoperative intra-abdominal infection, highlighting the possible clinical role of this tracer in infection imaging.[57]

The use of **^{68}Ga-MAA** in the assessment of extrahepatic shunts before selective internal radiation therapy (SIRT) has also been successfully evaluated.[61]

Summary

- Many interesting ^{68}Ga-based imaging options exist for application in routine liver and gastrointestinal imaging. These include the use of ^{68}Ga-MAA for extrahepatic shunt evaluation before SIRT and the use of ^{68}Ga-alizarin red and alizarin red S for RES and kidney function imaging.
- In the imaging of hepatic function, ^{68}Ga-PP-IDA may overcome some of the limitations of ^{99m}Tc-IDA agents and provide quantification options. Recent advances include imaging of liver function with ^{68}Ga-GSA based on ASGP receptor density.
- Recent publications have revealed novel imaging possibilities such as the use of ^{68}Ga-citrate in the evaluation of inflammatory bowel disease and postoperative abdominal infections as well as the ability to image SUR-1 to determine the [beta]-cell mass of the pancreas with the use of ^{68}Ga-NODAPA-NCS-glibenclamide. These are mainly case reports, which will require validation in larger studies before routine clinical application.

Miscellaneous applications

The recent worldwide shortage of molybdenum has sparked interest in the search for alternative generator-based radiopharmaceuticals such as ^{68}Ga for a multitude of routine clinical and novel indications. Various reports, case studies and short communications have reported on new ^{68}Ga compounds and applications, some of which are mentioned here.

Folate receptors tend to be overexpressed in many malignant processes as well as on activated macrophages. Often, these activated macrophages either cause, or contribute significantly to, various debilitating illnesses such as rheumatoid arthritis, Crohn's disease, atherosclerosis, lupus, inflammatory osteoarthritis, diabetes, ischaemia–reperfusion injury, glomerulonephritis, sarcoidosis, psoriasis, Sjogren's disease and vasculitis.

^{68}Ga-deferoxamine-folate has been developed and tested in tumour-bearing animals, and thus far folate-receptor PET imaging appears to be promising both as a diagnostic and as a therapeutic target for potential application in the nononcological indications mentioned above.[62,63]

Necrosis has also become an interesting target for the diagnosis of, and for monitoring the therapeutic effect on, several conditions in which excessive cell death plays a role. This occurs, for example, in myocardial infarction, chronic heart failure, transplant rejection, neurodegenerative conditions and stroke, among others. However, molecular imaging of this process has proven troublesome so far, because of the many substances that are released following cell membrane integrity loss. Prinsen and colleagues evaluated **^{68}Ga-bis-DTPA-PA** as a potential tracer for necrosis imaging. This compound demonstrated significantly higher uptake in necrotic tissues compared with viable tissue and was able to differentiate between apoptosis and necrosis. Findings were validated in vitro, ex vivo and .[64]

Despite the well-established role of sentinel lymph node imaging, no PET tracers had been developed until 2010 when a group from Seoul National University developed ^{68}Ga-mannosylated human serum albumin (MSA) for this purpose. They successfully developed a PET sentinel lymph node imaging tracer, **^{68}Ga-NOTA-MSA,** with high stability and labelling efficiency at room temperature. The imaging target here is the mannose binding protein, which is expressed by the RES. After subcutaneous injection of 7.4 MBq into the footpads of mice, which were imaged with micro-PET, persistent increased activity was noted in the inguinal lymph nodes as early as 1 min after injection. In addition, biodistribution studies demonstrated high hepatic uptake with mild splenic and bone marrow accumulation. The authors concluded that sentinel lymph node imaging with ^{68}Ga-NOTA-MSA would be feasible with rapid lymph node migration and early imaging possibilities. A [beta] probe (proven to be superior to [gamma] probes) has also been developed that can detect positron and [beta] emissions from lymph nodes intraoperatively.[65]

Pichler and colleagues recently published an image of a 53-year-old woman with Graves' orbitopathy. PET/CT images with **^{68}Ga-DOTA-NOC** showed increased uptake in the right inferior rectus muscle, which corresponded to morphological muscle changes noted on CT and MRI and which represented active endocrine orbitopathy.[66]

Infection/inflammation imaging

The field of infection and inflammation imaging is an interesting and rapidly growing one, and therefore it was felt that certain aspects needed to be highlighted despite some overlap with various sections of this review. Recently, Roivainen and colleagues published a comprehensive review on gallium-labelled peptides for inflammation imaging, which readers are directed to.[67]

Infection/inflammation imaging has always suffered from the limitation of being unable to clearly distinguish between these two processes, as so many aspects concerning their pathophysiology overlap. There is a definite need for tracers that target processes or cells, which are expressed exclusively during infection or inflammation.

Thus far, one of the promising radiopharmaceuticals that has emerged is ^{99m}Tc-ubiquicidin. This is a bacteria-specific peptide that has been proposed as an infection-specific agent.[68] The development of a new radiotracer based on an antibiotic derivative, the assessment of its biodistribution and binding to the target bacteria are also of interest to our group and hence our work on **^{68}Ga-NOTA-UBI30-41**.[69]

The biodistribution of **^{68}Ga-ubiquicidin** in rabbits infected with S. aureus demonstrates increased tracer uptake in infected muscles when compared with healthy and inflamed muscles. This increased accumulation in infected muscles therefore supports an argument for a mechanism that, at least partly, involves bacteria-specific binding. This correlates well with our in-vitro results, which demonstrated binding to bacteria. Further, the results of our recent study (which involved injecting **^{68}Ga-NOTA-UBI30-41** into healthy monkeys) revealed no activity in target organs, such as the lungs, the musculoskeletal system or the abdomen, revealing potential infection (e.g. TB). In-vivo results demonstrated compound blood clearance within 60 min of injection through renal excretion and transient liver metabolism.[70]

Certain common potentially debilitating conditions have an inherently inflammatory nature, such as atherosclerosis, obesity and diabetes. These and other conditions such as musculoskeletal infections and cardiovascular, lung and abdominal inflammatory or infectious processes would potentially benefit from infection and inflammation imaging.

Earlier discussions have highlighted that **^{68}Ga-labelled siderophore desferri-triacetylfusarinine C** can display highly selective accumulation by *Aspergillus fumigatus in vivo*. This is potentially useful for imaging invasive pulmonary aspergillosis, which may benefit patients who are immunosuppressed.[25]

In the musculoskeletal section, Kumar and colleagues demonstrated the potential use of **^{68}Ga-apo-transferrin (^{68}Ga-TF)** in the detection of S. aureus infection and Gram-negative *Proteus mirabilis* with highly promising results.[7]

One tracer that appears particularly promising in this regard is **^{68}Ga-DOTA-VAP-P1.** This tracer targets VAP-1, which is normally stored in intracellular granules within the endothelial cells to be released to the endothelial surface only when inflammation occurs. VAP-1 promotes leucocyte adhesion, mediates various leucocyte interactions and also has some mono-amine-oxidase activity. These properties provide an imaging target for inflammation as well as for the monitoring of anti-inflammatory treatment. Tumour expression of VAP-1 also occurs and varies considerably among the different tumour types. Therefore, knowledge of VAP-1 expression for the various malignancies is required for accurate interpretation in the oncology setting.

^{68}Ga-DOTA-VAP-P1 was the first tracer to be developed for the imaging of VAP-1 and has since been applied in the setting of musculoskeletal infections, with promising results seen in the studies by Lankinen et al. [8]and Silvola et al. [41]as discussed earlier.

Autio and colleagues investigated the use of ^{68}Ga-DOTAVAP-P1 to distinguish between inflammation and malignant processes. They made use of an animal model with two groups of rats. Human pancreatic adenocarcinoma cells were implanted subcutaneously into a group of athymic rats, whereas turpentine oil was used to induce sterile skin or soft tissue inflammation in the other group. The biodistribution of ^{68}Ga-DOTAVAP-P1, ^{18}F-FDG and ^{11}C-choline was compared using an experimental rat model.

Their findings were as follows:

- Imaging with ^{68}Ga-DOTAVAP-P1 was 'more inflammation-selective' than that with ^{18}F-FDG or ^{11}C-choline.
- ^{68}Ga-DOTAVAP-P1 could differentiate inflammatory foci from malignant ones with sensitivity similar to that of ^{18}F-FDG.
- ^{11}C-Choline was found to be the most tumour-selective tracer compared with ^{18}F-FDG and ^{68}Ga-DOTAVAP-P1.[71]

Attempts to improve the biochemical properties of ^{68}Ga-DOTAVAP-P1 have led to the development of **^{68}Ga-DOTAVAP-PEG-P2.** This compound has a significantly longer metabolic half-life, with slower renal excretion and a higher TBR. It has a radiochemical purity of more than 95% and has been shown to be stable in vitro for around 2 h in human plasma.[41]

^{68}Ga-Siglec-9 is another new compound, which is based on a granulocyte ligand for VAP-1 for the detection of vascular inflammation and malignant tumours.[67]

Another promising target for labelling with ^{68}Ga is $\alpha v\beta_3$, which is increased in malignant cells and tumour neovasculature as well as in chronic inflammatory conditions such as inflammatory bowel disease and inflamed synovial tissues in rheumatoid arthritis. Integrin $\alpha v\beta_3$ mediates intercellular adhesion of all proteins in which arginine–glycine–aspartic acid (RGD) is exposed. **^{68}Ga-RGD peptides** provide an imaging tool for the above-mentioned processes, which are relatively fast and simple to synthesize and image. Haukkala et al.[33]evaluated the use of ^{68}Ga-DOTA-RGD in an animal model of atherosclerosis with promising results.

Silvola et al. [37] evaluated inflammation imaging with ^{68}Ga in vulnerable atherosclerotic plaques with promising results (as described earlier).

^{68}Ga-NODAGA-RGD is a new RGD peptide with a high affinity for $\alpha v\beta_3$ integrin. This can be prepared relatively fast and easily at room temperature and has improved imaging characteristics when compared with ^{68}Ga-DOTA-RGD on micro-PET[72]

Ambrosini et al. [22] have found **^{68}Ga-DOTA-NOC PET** imaging to be useful in the evaluation of IPF and NSIP as described earlier.

Several authors have investigated the use of ^{68}Ga-citrate in the evaluation of various infectious and inflammatory conditions. So far, the most promising results have been found in the imaging of musculoskeletal infections.[6,11]

Summary

- ^{68}Ga-Transferrin appears to be capable of detecting both Gram-positive S. aureus and Gram-negative P. mirabilis, thus justifying further investigations.
- ^{68}Ga-DOTAVAP-P1, a peptide inhibitor of vascular adhesion protein-1/semicarbazine sensitive amine oxidase (VAP-1/SSAO), is a promising target molecule for the assessment of inflammatory reaction, more so in healing bones.
- Preliminary data confirm the possible role of ^{68}Ga-citrate for the diagnosis of bone infections, with reliable negative predictive value and overall accuracy.

Inflammatory and infectious diseases are a heterogeneous class of diseases that continue to be imaged with nonspecific radiopharmaceuticals. Thus, accelerated research and development with a ^{68}Ga-labelled tracer may help address this poor record.

So, why are we not using it every day?

Clearly, many convincing and compelling reasons and indications exist for the use of ^{68}Ga in various nononcological (and of course all of the better-known oncological) settings. The convenient in-house supply, the multitude of labelling possibilities and the prospects of freeze-dried kits with ^{68}Ga makes it a very attractive option for PET imaging.

Its advantages over both ^{67}Ga and ^{18}F-FDG are well known and include improvements in resolution, labelling possibilities, lower radiation burden and faster and more cost-effective imaging. It may also overcome some of the limitations of ^{18}F-FDG, such as false negatives in highly differentiated tumours with low growth rates, the inability to evaluate lesions

located close to tissues with high metabolic activity and limited ability to distinguish malignant processes from inflammation or infection in certain settings.

Why then has it failed to find widespread clinical application despite publications as early as the 1950s and despite constant improvements in generator design, labelling techniques and options and a host of clinical application possibilities? Several authors have addressed the issues that have so far prevented widespread clinical application.

In a 2007 editorial, Breeman and colleagues attributed the lack of widespread clinical application of ^{68}Ga to (among others**) the following issues:**

The requirements imposed by pharmaceutical legislations on the generator, the ligands and on the final compound are very complex, entailing a lengthy process in obtaining marketing authorization. In addition, there is a perception of limited returns on investment by investors. The authors proposed some solutions to the above-mentioned problems, including the need for manufacturers of medicinal products to obtain marketing authorization for ^{68}Ga-labelling kits. This would, however, still be a lengthy process involving extensive clinical trials. Alternatively, physicians could be allowed the autonomy to take personal responsibility for radiopharmaceuticals administered, which in their opinion would potentially benefit the patient.[73]

In a recent editorial, Ballinger and Solanki reflected on the progress made in the preceding 4 years and the obstacles that remain and concluded that the use of ^{68}Ga will never be as simple as that of technetium-99m for the **following reasons:**

- ^{68}Ga generators continue to be labelled as ‘not for human use’ despite following good manufacturing practices.
- The short half-life of ^{68}Ga may lead to the need for several elutions per day.
- There are concerns over long-term generator sterility.
- It is the opinion of the above-mentioned authors that manual labelling cannot be performed safely and that automated or remote-controlled labelling procedures are essential.
- The HCl needed for elution of the generator requires pharmacological formulation.

- There is a lack of licensed kits and reagents for labelling with 68Ga and a need for chelators that can be labelled rapidly at room temperature and at a neutral pH.[74]

Dosimetry

Rizello et al. [56] in their landmark paper reported the effective dose per unit of administered activity for ^{68}Ga-citrate as 2.6×10^{-2} mSv/MBq, compared with 1.1×10^{-1} mSv/MBq for ^{67}Ga-citrate.This calculation was based on data gathered from human subjects using a dynamic bladder model with a 4.8-h voiding interval, and our initial calculations have yielded comparable results.

Conclusion

Many exciting imaging opportunities exist for ^{68}Ga tracer applications outside oncological practice, most of which remain greatly underutilized. Larger clinical trials are needed to validate these applications for future use in routine clinical practice.

References

1. AL-Nahhas A, Win Z, Szyszko T, Singh A, Khan S, Rubello D.What can gallium-68 PET add to receptor and molecular imaging?Eur J Nucl Med Mol Imaging.2007 Aug 23;34:1897–1901.

2. Treglia G, Castaldi P, Rindi G, Giordano A, Rufini V.Diagnostic performance of gallium-68 somatostatin receptor PET and PET/CT in patients with thoracic and gastroenteropancreatic neuroendocrine tumours: a meta-analysis.Endocrine.2012 Feb 20;42:80–87.

3. Khan MU, Khan S, El-Refaie S, Win Z, Rubello D, Al-Nahhas A.Clinical indications for gallium-68 positron emission tomography imaging.Eur J Surg Oncol.2009 Jun 1;35:561–7.

4. Al-Nahhas A, Win Z, Szyszko T, Singh A, Nanni C, Fanti S, et al.Gallium-68 PET: a new frontier in receptor cancer imaging.Anticancer Res.2007 Nov;27:4087–94.

5. Moher D, Liberati A, Tetzlaff J, Altman DG, Group TP.Preferred reporting items for systematic reviews and meta-analyses: the PRISMA statement.Ann Intern Med.2009 Jul 21;151:264–9.

6. Mäkinen TJ, Lankinen P, Pöyhönen T, Jalava J, Aro HT, Roivainen A.Comparison of ^{18}F-FDG and ^{68}Ga PET imaging in the assessment of experimental osteomyelitis due to Staphylococcus aureus.Eur J Nucl Med Mol Imaging.2005 Nov 9;32:1259–68

7. Kumar V, Boddeti DK, Evans SG, Roesch F, Howman-Giles R.Potential use of ^{68}Ga-apo-transferrin as a PET imaging agent for detecting Staphylococcus aureus infection.Nucl Med Biol.2011 Apr 1;38:393–8.

8. Lankinen PP, Mäkinen TJT, Pöyhönen TAT, Virsu PP, Salomäki SS, Hakanen AJA, et al.(68)Ga-DOTAVAP-P1 PET imaging capable of demonstrating the phase of inflammation in healing bones and the progress of infection in osteomyelitic bones.Eur J Nucl Med Mol Imaging.2008 Jan 31;35:352–64.

9. Ujula TT, Salomäki SS, Virsu PP, Lankinen PP, Mäkinen TJT, Autio AA, et al.Synthesis, ^{68}Ga labeling and preliminary evaluation of DOTA peptide binding vascular adhesion protein-1: a potential PET imaging agent for diagnosing osteomyelitis.Nucl Med Biol 2009 Jul31;36:11–21.

10. Mitterhauser M, Toegel S, Wadsak W, Lanzenberger RR, Mien L-K, Kuntner C, et al.Pre vivo, ex vivo and in vivo evaluations of [^{68}Ga]-EDTMP.Nucl Med Biol.2007 May;34:391–7.

11. Nanni C, Errani C, Boriani L, Fantini L, Ambrosini V, Boschi S, et al.^{68}Ga-Citrate PET/CT for evaluating patients with infections of the bone: preliminary results.J Nucl Med.2010 Dec 1;51:1932–36.

12. Suzuki K, Satake M, Suwada J, Oshikiri S, Ashino H, Dozono H, et al.Synthesis and evaluation of a novel ^{68}Ga-chelate-conjugated bisphosphonate as a bone-seeking agent for PET imaging.Nucl Med Biol.2011 Sep 30;38:83–90.

13. Riss PJ, Kroll C, Nagel V, Rösch F.NODAPA-OH and NODAPA-(NCS)n: synthesis, ^{68}Ga-radiolabelling and in vitro characterisation of novel versatile bifunctional chelators for molecular imaging.Bioorg Med Chem Lett.2008 Oct;18:5364–67.

14. Schuster DP.The evaluation of lung function with PET.Semin Nucl Med.1998 Oct;28:341–51.

15. Mintun MA, Dennis DR, Welch MJ, Mathias CJ, Schuster DP.Measurements of pulmonary vascular permeability with PET and gallium-68 transferrin.J Nucl Med.1987 Nov 1;28:1704–16.

16. Schuster DP, Markham J, Welch M.Positron emission tomography measurements of pulmonary vascular permeability with Ga-68 transferrin or C-11 methylalbumin.Crit Care Med.1998 Sept 17;26:518–25.

17. Schuster DP, Stark T, Stephenson J, Royal H.Detecting lung injury in patients with pulmonary edema.Intensive Care Med.2002 Sept;28:1246–53.

18. Kotzerke J, Andreeff M, Wunderlich G.PET aerosol lung scintigraphy using Galligas.Eur J Nucl Med Mol Imaging.2010;37:175–77.

19. Borges JB, Velikyan I, Langstrom B, Sorensen J, Ulin J, Maripuu E, et al.Ventilation distribution studies comparing Technegas and 'Gallgas' using $^{68}GaCl_3$ as the label.J Nucl Med.2011 Jan 26;52:206-9.

20. Hofman MS, Beauregard J-M, Barber TW, Neels OC, Eu P, Hicks RJ.^{68}Ga PET/CT ventilation–perfusion imaging for pulmonary embolism: a pilot study with comparison to conventional scintigraphy.J Nucl Med.2011 Oct 3;52(10):1513–19.

21. Ament SJ, Maus S, Reber H, Buchholz HG, Bausbacher N, Brochhausen C, et al.PET lung ventilation/perfusion imaging using (68)Ga aerosol (Galligas) and (68)Ga-labeled macroaggregated albumin.Recent Results Cancer Res.2013;194:395–423.

22. Ambrosini V, Zompatori M, De Luca F, Antonia D, Allegri V, Nanni C, et al.^{68}Ga-DOTANOC PET/CT allows somatostatin receptor imaging in idiopathic pulmonary fibrosis: preliminary results.J Nucl Med.2010 Nov 23;51:1950–55.

23. Petrik M, Haas H, Dobrozemsky G, Lass-Florl C, Helbok A, Blatzer M, et al.^{68}Ga-Siderophores for PET imaging of invasive pulmonary aspergillosis: proof of principle.J Nucl Med.2010 Mar 29;51:639–45.

24. Petrik M, Haas H, Schrettl M, Helbok A, Blatzer M, Decristoforo C.In vitro and in vivo evaluation of selected ^{68}Ga-siderophores for infection imaging.Nucl Med Biol.2012 Apr;39:361–69.

25. Petrik MM, Franssen GMG, Haas HH, Laverman PP, Hörtnagl CC, Schrettl MM, et al.Preclinical evaluation of two (68)Ga-siderophores as potential radiopharmaceuticals for Aspergillus fumigatus infection imaging.Eur J Nucl Med Mol Imaging.2012 Jun 30;39:1175–83.

26. Bomanji J, Almuhaideb A, Zumla A.Combined PET and X-ray computed tomography imaging in pulmonary infections and inflammation.Curr Opin Pulm Med.2011 May 1;17:197–205.

27. Green MAM, Mathias CJC, Neumann WLW, Fanwick PEP, Janik MM.Deutsch EAE. Potential gallium-68 tracers for imaging the heart with PET: evaluation of four gallium complexes with functionalized tripodal tris(salicylaldimine) ligands.J Nucl Med.1993 Jan 31;34:228–33.

28. Tsang BW, Mathias CJ, Green MA.A gallium-68 radiopharmaceutical that is retained in myocardium: ^{68}Ga[(4,6-MeO_2sal)2BAPEN].J Nucl Med.1993 Jun 30;34:1127–31.

29. Yang BY, Jeong JM, Kim YJ, Choi JY, Lee Y-S, Lee DS, et al.Formulation of ^{68}Ga BAPEN kit for myocardial positron emission tomography imaging and biodistribution study.Nucl Med Biol.2010 Feb 1;37:149–55.

30. Hoffend J, Mier W, Schuhmacher J, Schmidt K, Dimitrakopoulou-Strauss A, Strauss LG, et al.Gallium-68-DOTA-albumin as a PET blood-pool marker: experimental evaluation in vivo.Nucl Med Biol2005;32:287–292.

31. Plössl K, Chandra R, Qu W, Lieberman BP, Kung M-P, Zhou R, et al.A novel gallium bisaminothiolate complex as a myocardial perfusion imaging agent.Nucl Med Biol.2008 Jan;35:83–90.

32. Tarkia M, Saraste A, Saanijoki T, Oikonen V, Vähäsilta T, Strandberg M, et al.Evaluation of ^{68}Ga-labeled tracers for PET imaging of myocardial perfusion in pigs.Nucl Med Biol.2012 Jul;39:715–23.

33. Haukkala J, Laitinen I, Luoto P, Iveson P, Wilson I, Karlsen H, et al.^{68}Ga-DOTA-RGD peptide: biodistribution and binding into atherosclerotic plaques in mice.Eur J Nucl Med Mol Imaging.2009 Dec 23;36:2058–67.

34. Jeong JM, Hong MK, Chang YS, Lee YS, Kim YJ, Cheon GJ, et al.Preparation of a promising angiogenesis PET imaging agent: ^{68}Ga-labeled c(RGDyK)-isothiocyanatobenzyl-1,4,7-triazacyclononane-1,4,7-triacetic acid and feasibility studies in mice.J Nucl Med.2008;49:830–836

35. Caforio ALP, Marcolongo R, Jahns R, Fu M, Felix SB, Iliceto S.Immune-mediated and autoimmune myocarditis: clinical presentation, diagnosis and management.Heart Fail Rev.2012 Nov 1:1–18.

36. Rominger A, Saam T, Vogl E, Ubleis C, La Fougere C, Forster S, et al.In vivo imaging of macrophage activity in the coronary arteries using ^{68}Ga-DOTATATE PET/CT: correlation with coronary calcium burden and risk factors.J Nucl Med.2010 Feb 1;51:193–7.

37. Silvola JM, Laitinen I, Sipilä HJ, Laine VJO, Leppänen P, Ylä-Herttuala S, et al.Uptake of ^{68}gallium in atherosclerotic plaques in LDLR$^{-/-}$ApoB$^{100/100}$ mice.EJNMMI Res.2010 Dec 31;1:14–24.

38. Stoll H-P, Hutchins GD, Winkle WL, Nguyen AT, Appledorn CR, Janzen I, et al.Advantages of short-lived positron-emitting radioisotopes for intracoronary radiation therapy with liquid-filled balloons to prevent restenosis.J Nucl Med.2001;42:1375–83.

39. Karanikas G, Schmaljohann J, Rodrigues M, Chehne F, Granegger S, Sinzinger H.Examination of co-complexes for radiolabeling of platelets in positron emission tomographic studies.Thromb Res.1999 Apr;94:111–15.

40. Jalilian AR, Mirazizi F, Nazem H, Shafaii K, Nasserian B, Sadeghpour H.Evaluation of radiolabeled streptokinase for thrombosis imaging.Iran J Nucl Med.2008;16:34–40.

41. Silvola J, Autio A, Luoto P, Jalkanen S, Roivainen A.Preliminary evaluation of novel ^{68}Ga-DOTAVAP-PEG-P2 peptide targeting vascular adhesion protein-1.Clin Physiol Funct Imaging.2010;30:75–78.

42. James AE, DeLand FH, Hodges FJ, Wagner HN.Cerebrospinal fluid (CSF) scanning: cisternography.Am J Roentgenol.1970 Sept;110:74–87.

43. Hawkins RA, Phelps ME, Huang SC, Wapenski JA, Grimm PD, Greenberg P, et al.Simultaneous estimations of blood brain barrier (BBB) permeability and local cerebral blood volume (CBV) in human brain tumors with positron tomography and Ga-68 EDTA.J Nucl Med.1984 Jan 1;25:5.

44. Friedland RP, Jagust WJ, Budinger TF, Yano Y, Huesman RH, Knittel B.Dynamic PET studies of blood–brain barrier permeability in Alzheimer's disease.J Nucl Med.1985 May 1;26:5.

45. Pozzilli C, Bernardi S, Mansi L, Picozzi P, Iannotti F, Alfano B, et al.Quantitative assessment of blood–brain barrier permeability in multiple sclerosis using 68-Ga-EDTA and positron emission tomography.J Neurol Neurosurg Psychiatry.1988 Aug 1;51:1058–62.

46. Cutler CS, Giron MC, Reichert DE, Snyder AZ, Herrero P, Anderson CJ, et al.Evaluation of gallium-68 tris(2-mercaptobenzyl)amine: a complex with brain and myocardial uptake.Nucl Med Biol.1999 May 21;26:305–16.

47. McCarthy TJ, Banks WA, Farrell CL, Adamu S, Derdeyn CP, Snyder AZ, et al.Positron emission tomography shows that intrathecal leptin reaches the hypothalamus in baboons.J Pharmacol Exp Ther.2002 Jun;301:878–83.

48. Anghileri LJL.A new Ga68-compound for kidney scanning.Int J Appl Radiat Isot.1968;19:421–22.

49. Yamashita M, Inaba T, Kawase Y, Iiorii H, Wakita K, Fujii R, et al.Quantitative measurement of renal function using Ga-68-EDTA.Tohoku J Exp Med.1988;155:207–8.

50. Szabo Z, Xia J, Mathews WB, Brown PR.Future direction of renal PET.Semin Nucl Med.2006;36:36–50.

51. Szabo Z, Xia J, Mathews WB.Radiopharmaceuticals for renal positron emission tomography imaging.Semin Nucl Med.2008 Jan;38:20–31.

52. Nanni C, Marangoni A, Quarta C, Di Pierro D, Rizzello A, Trespidi S, et al.Small animal PET for the evaluation of an animal model of genital infection.Clin Physiol Funct Imaging.2009 May 1;29(3):187–92.

53. Schuhmacher JJ, Maier-Borst WW, Wellman HNH.Liver and kidney imaging with Ga-68-labeled dihydroxyanthraquinones.J Nucl Med.1980;21:983–987.

54. Schuhmacher J, Matys R, Hauser H.Ga-68-labeled tetrabromophthalein (Ga-68 BP-IDA) for positron imaging of hepatobiliary function: concise communication.J Nucl Med.1983 Oct 1;24:593–602.

55. Haubner R, Vera DR, Farshchi-Heydari S, Helbok A, Rangger C, Putzer D, Virgolini IJ.Development of (68)Ga-labelled DTPA galactosyl human serum albumin for liver function imaging.Eur J Nucl Med Mol Imaging.2013[Epub ahead of print].

56. Rizzello A, Di Pierro D, Lodi F, Trespidi S, Cicoria G, Pancaldi D, et al.Synthesis and quality control of ^{68}Ga citrate for routine clinical PET.Nucl Med Commun.2009 Jul;30 (7):542–45.

57. Kumar V, Boddeti DK, Evans SG, Angelides S.(68)Ga-Citrate-PET for diagnostic imaging of infection in rats and for intra-abdominal infection in a patient.Curr Radiopharm.2012 Jan;5:71–5.

58. Galibert M, Sancey L, Renaudet O, Coll J, Dumy P, Boturyn D.Application of click–click chemistry to the synthesis of new multivalent RGD conjugates.Org Biomol Chem.2010;8:5133–38.

59. Zimny MJ, Fellner M, Rosch F, Thews O.In vitro evaluation of ^{68}Ga-Schiff bases for myocardial imaging.Nucl Med Biology.2010;37:691.

60. Hany TF, Strobel K.PET/CT in pancreatic cancer. New concepts in diagnosis and therapy of pancreatic adenocarcinoma.2010.91–9.

61. Gartenschlaeger MM, Maus SS, Buchholz HH, Reber HH, Pitton NN, Schreckenberger MM.Investigation for extrahepatic shunt before SIRT by PET/CT with ^{68}Ga-MAA.Nuklearmedizin.2010 Dec31;50:37–8.

62. Mathias CJ, Lewis MR, Reichert DE, Laforest R, Sharp TL, Lewis JS, et al.Preparation of ^{66}Ga- and ^{68}Ga-labeled Ga(III)-deferoxamine-folate as potential folate-receptor-targeted PET radiopharmaceuticals.Nucl Med Biol.2003;30:725–31.

63. Low PS, Henne WA, Doorneweerd DD.Discovery and development of folic-acid-based receptor targeting for imaging and therapy of cancer and inflammatory diseases.Acc Chem Res.2008 Jan;41:120–29.

64. Prinsen KK, Li JJ, Vanbilloen HH, Vermaelen PP, Devos EE, Mortelmans LL, et al.Development and evaluation of a ^{68}Ga labeled pamoic acid derivative for in vivo visualization of necrosis using positron emission tomography.Bioorg Med Chem.2010 Jul 14;18:5274–81.

65. Choi JYJ, Jeong JMJ, Yoo BCB, Kim KK, Kim YY, Yang BYB, et al.Development of ^{68}Ga-labeled mannosylated human serum albumin (MSA) as a lymph node imaging agent for positron emission tomography.Nucl Med Biol.2011 Mar 31;38:371–79.

66. Pichler R, Sonnberger M, Dorninger C, Assar H, Stojakovic T.Ga-68-DOTA-NOC PET/CT reveals active Graves' orbitopathy in a single extraorbital muscle.Clin Nucl Med.2011 Sep 30;36:910–11.

67. Roivainen AA, Jalkanen SS, Nanni CC.Gallium-labelled peptides for imaging of inflammation.Eur J Nucl Med Mol Imaging.2012 Jan 31;39SupplS68–S77.

68. Welling MM, Lupetti A, Balter HS, Lanzzeri S, Souto B, Rey AM, et al.^{99m}Tc-Labeled antimicrobial peptides for detection of bacterial and Candida albicans infections.J Nucl Med.2001;42:788–94.

69. Ebenhan T, Chadwick N, Govender T, Kruger HG, Sathekge M, Zeevaart JR.Gallium-68 labelling of NOTA-peptide conjugates for imaging infection – especially tuberculosis.World J Nucl Med.2011;10:73–89.

70. Ebenhan T, Govender T, Kruger G, Pulker T, Zeevaart JR, Sathekge M.Synthesis of Ga-68-NOTA-UBI-30-41 and in vivo bio-distribution in vervet monkeys towards potential PET/CT imaging of infection.J Nucl Med.2012;53Suppl1520.

71. Autio AA, Ujula TT, Luoto PP, Salomäki SS, Jalkanen SS, Roivainen AA.PET imaging of inflammation and adenocarcinoma xenografts using vascular adhesion protein 1 targeting peptide ^{68}Ga-DOTAVAP-P1: comparison with ^{18}F-FDG.Eur J Nucl Med Mol Imaging.2010 Sep 30;37:1918–25.

72. Knetsch PA, Petrik M, Griessinger CM, Rangger C, Fani M, Kesenheimer C, et al.[^{68}Ga]NODAGA-RGD for imaging [alpha]v[beta]3 integrin expression.Eur J Nucl Med Mol Imaging.2011 Apr 13;38:1303–12.

73. Breeman WAP, Verbruggen AM.The ^{68}Ge/^{68}Ga generator has high potential, but when can we use ^{68}Ga-labelled tracers in clinical routine?Eur J Nucl Med Mol Imaging.2007 Jul;34:978–81.

74. Ballinger JR, Solanki KK.What will be required to bring ^{68}Ga-labelled peptides into routine clinical use?Nucl Med Commun.2011 Dec;32:1109–12.

Chapter 4: Preparation and Quality control of ^{68}Ga-citrate

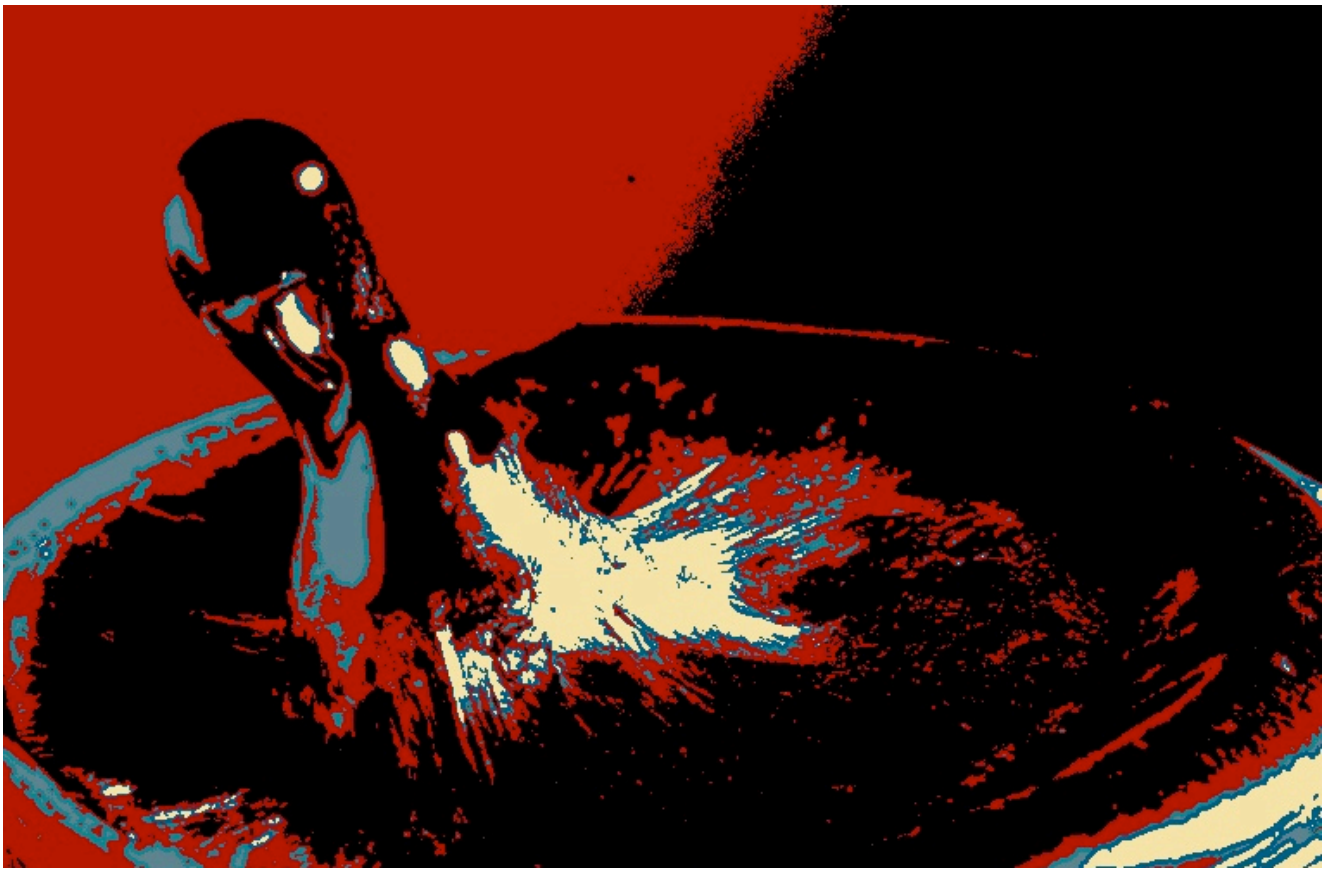

*An amended version of this chapter has been published in the Hellenic Journal of Nuclear Medicine:

A modified technique for efficient radiolabeling of 68Ga-citrate from a SnO2-based ^{68}Ge/^{68}Ga generator for better infection imaging.

Vorster, Mariza, Mokaleng Brenda, Sathekge Mike, Ebenhan Thomas.
Hell J Nucl Med 2013.

Abstract

Introduction

Imaging opportunities exist for ^{68}Ga-tracer applications outside of oncological practice, most of which remains greatly underutilized. The field of infection and inflammation imaging is rapidly growing using generator-based PET radiopharmaceuticals. We sought to develop a practical method to prepare ^{68}Ga-citrate using a SnO_2-based ^{68}Ge/^{68}Ga generator and evaluate its use in infection imaging.

Methods

^{68}Ga-citrate synthesis was performed in a straightforward, quantitative, one-step-aseptic procedure; an amended labeling method was applied using ACD-A buffered citrate as a precursor. Study participants were imaged on a Siemens Biograph 40 PET/CT scanner 60 minutes post IV injection.

Results

90-95% ^{68}Ga-yield was obtained and subsequently used at 324-527 MBq to perform three to four parallel ^{68}Ga-citrate syntheses. 96-99% ^{68}Ga-citrate was yielded after 10 min incubation. The radiochemical purity was > 99% with a pH value of 4.0-4.5. All other quality control requirements were met. The ^{68}Ga-citrate stability was > 96%. The final product was sterile, pyrogen- and solvent-free, with very low ^{68}Ge-levels, with 191±33MBq in 6.6±2.8 ml. High quality images were obtained at 60 minutes post-injection of 185 MBq of ^{68}Ga-citrate.

Conclusion

A fast, direct and cheap method with a quantitative preparation of ^{68}Ga-citrate is described. We report on the adaptations needed when using a SnO_2-based ^{68}Ge/^{68}Ga generator and ACD-A buffered citrate as a precursor. This method allows for multiple patient productions from one generator elution, with 300 MBq/patient of ^{68}Ga-citrate produced in less than 30 minutes and excellent labeling reproducibility for routine infection imaging.

Keywords: SnO_2-based ^{68}Ga/^{68}Ge generator, ^{68}Ga-ACD-A; ^{68}Ga-citrate; PET/CT infection imaging

Introduction

The field of infection and inflammation imaging is an interesting and rapidly growing one and the increase in the availability and accessibility of PET/CT facilities has sparked renewed interest in generator-based PET radiopharmaceuticals. ^{68}Gallium in particular, has received a lot of attention as an alternative positron emitter since it offers several important advantages when compared to ^{18}F-FDG. Many exciting imaging opportunities also exist for ^{68}Ga-tracer applications outside of oncological practice, most of which remains greatly underutilized (Vorster, NMC 2013). ^{67}Ga-citrate has long provided nuclear physicians with a versatile tool for use in both oncological and infective settings. With regards to infection imaging it has been widely used in the diagnosis and management of skeletal and lung infections (especially in immune-compromised individuals) and in those presenting with fever of unknown origin. The mechanism of action, although incompletely explained, is generally accepted to be the result of various specific and non-specific factors, which play a role in infective / inflammatory and malignant processes. Non-specific factors include the increased vascular permeability found in areas of inflammation or increased vascularity, whereas specific factors comprise both transferrin-dependent and transferrin-independent mechanism. Gallium acts as an iron analogue, the majority of which is bound to transferrin in plasma and then internalized as a gallium-transferrin complex in to cells with expression of transferrin receptors. Other localization mechanisms include binding to lactoferrin, siderophores and leukocytes.[1-3] Therefore, it stands to reason, that ^{68}Ga would be as useful as ^{67}Ga with the added advantages of improved image resolution, quantification possibilities, improved dosimetry and imaging logistics gained from PET/CT technology. Compared to ^{18}F-FDG, ^{68}Ga offers shorter imaging times, no special patient preparation, and on-demand year-round tracer availability that negates the need for an onsite or nearby cyclotron-based infrastructure. This could have significant financial implications, which may lead to a more cost-effective way of imaging. Several authors have investigated the use of ^{68}Ga-citrate in the evaluation of various infectious and inflammatory conditions. So far, the most promising results have been found with the imaging of musculoskeletal infections.[4]

Our study demonstrates a straightforward, optimized method for using the more acidic eluate from a SnO_2-based $^{68}Ge/^{68}Ga$ generator to produce ^{68}Ga-citrate. This is done by means of labeling it with Anti-coagulant Citrate Dextrose Solution, USP formula A (ACD-A), which allows solvent free radiolabeling. To our knowledge this is the first report of ^{68}Ga-citrate labeling making use of the eluate from a SnO_2-based generator and making use of ACD-A. In addition, ours is the first study to evaluate the use of ^{68}Ga-citrate in the novel setting of respiratory infections.

Materials & Methods

All solvents used were of a pharmacological grade. For labeling with ^{68}Ga, Anti-coagulant Citrate Dextrose Solution, USP formula A (ACD-A) was purchased as sterile and non-pyrogenic solution from Fenwal Inc. (Lake Zurich, Illinois, USA). The aqueous solution of ACD-A contains 2.20% sodium citrate dehydrate, 0.73% citric acid anhydrous and 2.45% glucose monohydrate. A 30% solution of suprapure grade Hydrochloric acid (HCl) was purchased from Merck Sharp & Dohme (Readington, New Jersey, USA). Glacial acetic acid and methanol (for quality control purposes) were obtained from Waters (Milford, Massachusetts, USA). Instant thin-layer chromatography-silica gel paper (ITLC-SG) was purchased from PALL Life Science (New York, USA). Sterile filters MILLEX GV 0.22 μm were obtained from Millipore (Millipore, New York, USA). High-performance liquid chromatography (HPLC) grade water (resistivity=18.2MOcm) was produced in-house by a Simplicity 185 Millipore system (Cambridge, Massachusetts, USA).

General information

A SnO_2-based $^{68}Ge/^{68}Ga$ generator with a 1.85 GBq loading activity (iThemba LABS, Somerset West, South Africa) was used for radiolabeling ($T_{1/2}$ of ^{68}Ge and ^{68}Ga are 270.8 days and 67.6 min, respectively).[5] ^{68}Ga-citrate synthesis was performed in a simple, straightforward, one-step-aseptic procedure using published knowledge by Kumar et al. [6]and Rizzello et al.[7]It allows for elution from the latter $^{68}Ge/^{68}Ga$ generator (a higher acidity of 0.6 N HCl is mandatory for generator elution) and substituted the labeling of sodium citrate with a sterile, pyrogen-free ACD-A (the radiolabeled product will further be referred as ^{68}Ga-citrate).

Evaluation of labeling parameters

In order to achieve the highest labeling efficiency in optimal time, the following labeling parameters were optimized: ACD-A/$^{68}GaCl_3$ ratio (i.e. pH correlation) and incubation time (with or without applying vortex stirring action of the sample). Therefore 0.5 ml of the ^{68}Ga eluate was mixed with 1.5, 4.5, 6.5 or 8.5 ml of ACD-A buffer; each mixture was subsequently divided in two equal aliquots, respectively. The samples were incubated at room temperature up to 45 min; however one set of samples underwent vortex stirring action every 5 min for 20-30 sec. At 5, 15, 25, and 45 min, 4-6 µL per sample were obtained for ITLC analysis. The labeling efficiency for all samples was determined by ITLC as described.

Standard ^{68}Ga-citrate labeling procedure

The ACD-A solution was distributed sterile in aliquots of 6.5 ml (half scale) or 13 ml (full scale) using certified sterile pyrogen-free sealed borosilicate glass vials provided by NTP Radioisotopes (Pelindaba, South Africa). In order to withdraw contents from the reaction vial, the top of its septum was punctured by a Jelco 22G x 1'' polymer catheter (Smiths Medical, Croydon, South Africa) to allow non-metallic transfer of the $^{68}Ge/^{68}Ga$ generator eluate. Thereafter, the generator was fractionally eluted with 10 ml of 0.6 N HCl using a three-way valve connecting the generators outlet to a waste vial as well as the reaction vial (containing the ACD-A solution). The first 1.0 ml fraction was collected in a waste vial, the second fraction of 0.5 ml (half scale) or 1.0 ml (full scale) was transferred directly to the reaction vial and the third fraction of the residual volume was subsequently collected in the waste vial. The reaction vial was allowed to incubate at room temperature for a minimum of 10 but no longer than 20 min and vortexed gently for at least 20 seconds in five minutes intervals. Before dispensing of ^{68}Ga-citrate, the solution was sterile-filtered through a 0.22 µm membrane using a low protein-binding filter (Millex GV, Millipore, New York, USA). An aliquot of 1-2 ml was retained for quality control purposes.

^{68}Ga-identity and pH

Radionuclide identity was measured by 10 minutes decay analysis for determination of ^{68}Ga half-life using a CRC 25 ionization chamber (Capintec Inc., Ramsey, NJ, USA). The pH value was assessed using narrow range pH paper method. Therefore the pH strip (pH Fix 0-6,

Macherey-Nagel, Düren, Germany) was spiked with 5-8 µL of the product solution, allowed to dry, compared with the color scale and read off the corresponding pH-value in 0.5 increments.

Instant thin layer chromatography (ITLC) analysis

The radiochemical purity of ^{68}Ga-citrate was determined by ITLC following the guidelines for ^{67}Ga citrate [^{8} ITLC impregnated silica gel paper (ITLC-SG) was used as stationary phase. The paper stripes were spiked at the bottom with 3-6 µL of the ^{68}Ga-citrate solution, using a insulin needle (Hamilton, Milano, Italy) following exposure to a solvent mixture (methanol/glacial acetic acid 9:1 v/v) for 4-5 min. Stripes were dried and analyzed on an ITLC scanner (VSC-201, Veenstra Ind., Oldenzaal, Netherlands) using a gamma radiation detector (Scionix 25B25/1.5-E2, Bunnik, Netherlands) obtaining chromatograms which allowed identifying the peaks and performing "area under the curve" analysis for percentage quantification (Genie2000 software, Veenstra Ind., Oldenzaal, Netherlands).

^{68}Ge breakthrough

The levels of co-eluted ^{68}Ge were routinely surveyed in the total generator eluate and compared with the retained ^{68}Ga-citrate solution. ^{68}Ge was measured indirectly in CRC 25 ionization chamber (Capintec Inc., Ramsey, NJ, USA) waiting 48 h (at 12 h, only ca. 0.01 % of the original ^{68}Ga activity will be present), then detecting the ^{68}Ga, which was generated by ^{68}Ge impurities from the decayed sample. A ^{68}Ge sample of known activity was used as positive control.

Quantification of ^{68}Ge impurities

Decayed ^{68}Ga-citrate aliquots were mixed with water to achieve a total sample volume of 10 ml. Quantification was performed on a high purity germanium detector with a relative efficiency of 10% using a digital signal analyzer (Canberra DSA 1000) converting the pulses produced by detected gamma-rays to be recorded by the gamma analysis software (Canberra, Genie-2000). For calibration samples were positioned at selected distances from the detector by a movable rig on a rail. Energy, peak shape and efficiency calibrations were performed by a traceable standard containing ^{152}Eu, ^{133}Ba and ^{241}Am. Energy range of the calibration was

set 60 keV to 1408 keV. The 1077 keV gamma ray signal was used for all quantifications. A nuclide library was compiled accordingly and compared with half-life of ^{68}Ge for decay correction by the gamma analysis software. Acquisition times (counting times) was set-up so that the peak area and counts (cps) > 5000 were obtained for the 1077 gamma line within 8 hours. If this was not attainable, the sample counting was extended overnight (16 hours). Raw values were expressed in Bq. The percentage ^{68}Ge was calculated by this equation: ^{68}Ge $_{\text{impurity}}$ (%) = 100 / ^{68}Ga-citrate activity (Bq) x ^{68}Ge-citrate activity (Bq).

Sterility

A decayed product fraction was sent for sterility testing for aerobe, anaerobe and fungal growth to NHLS microbiological laboratory at Steve Biko Academic Hospital. For aerobe growth, samples were inoculated on a nutrient broth and incubated for 24 h at 35-37 ˚C, followed by incubation at room temperature for 6 days. In contrast, for anaerobe growth, the samples were inoculated on thioglycolate broth and incubated for 7 days at 35-37 ˚C. If turbid within 7 days, samples were plated onto nutrient agar plates and organisms were identified. For fungal growth, samples were inoculated onto Sabarond's dextrose agar and incubated for 14 days at 30 ˚C and any fungal growth that was isolated was identified by conventional methods.

Radiochemical ^{68}Ga-citrate stability

For tracer stability determination under the clinical environment, ^{68}Ga-citrate was incubated at room temperature for additional four hours post tracer production and analyzed by ITLC-SG for potential appearance of non-bound ^{68}Ga percentage.

Image acquisition & analysis

Approval was granted by the University of Pretoria's research Ethics committee and informed consent was obtained from all study participants prior to injection and imaging. No particular patient preparation was required (such as fasting or restriction of physical activities). Study participants were imaged on a Siemens Biograph 40 PET/CT scanner 60 minutes post IV ^{68}Ga-citrate administration. Both oral (Barium in water) and IV contrast (100 ml Ultravist, at a rate of 2 ml/s) was administered, except where a contra-indication existed, such as

inadequate kidney function or known iodine allergy. Images were acquired in a three-dimensional mode with a 4 min emission scan for each of 7-9 bed positions (Matrix size 512x512) from the skull base to the pelvis. Reconstruction of images with and without attenuation correction (CT based) was done using OSEM (ordered subset expectation maximization) to yield axial, sagittal and coronal slices. All images were first evaluated qualitatively for abnormal uptake, which if present, was then followed by semi-quantification analysis. This was done in the following way: a region of interest was manually drawn around any lung lesions and the size selected to correspond to the pathology on CT. This resulted in a standard uptake value (SUV), which is representative of the relative concentration of radiotracer in a lesion of interest, normalized to the patient's weight and the dose of radiotracer administered. (SUV=radiotracer activity x patient weight/injected dose). We used the maximum SUV (SUV_{max}) in this study, which represents the pixel with the highest tracer uptake in the lesion.

Statistical analysis

If systematic errors were non-existent, outliers were determined by the Grubbs Test. If not stated otherwise, analytical data were expressed as mean and standard deviation (SD) using Microsoft Excel Software. Significance of two mean values was calculated by *Student-t-test* (paired and unpaired comparison). The level of significance was set at $p < 0.05$.

Results

Generator elution

A new 1.85 GBq $^{68}Ge/^{68}Ga$ generator was used over a 7 months period. A consistent yield of 90-96 % ^{68}Ga-activity was eluted in 1.5- 3 ml 0.6 N HCl. Contains of co-eluted metals (Fe, Al, Cu, Sn, Zn) > 10 ppm were found in citrate samples produced with ^{68}Ga from the 7 months old generator. 324-527 MBq (n=18) were added to the ACD-A for labeling using 0.5 or 1 ml generator eluate. Thus, three to four parallel ^{68}Ga-citrate syntheses were performed from one generator elution for individual use, if multi-patient administration was required.

Evaluation of labeling parameters

Several parameters were evaluated to optimize the radiolabeling efficiency and to achieve an applicable procedure for routine production (Table 1). A volume of 7 ml ACD-A buffer (containing 0.5 ml ^{68}Ga eluate) should be incubated at least 10 min (including vortex stirring action) to reach quantitative labeling (96-99% bound activity of ^{68}Ga-citrate). Higher incubation temperatures didn't show significantly higher or faster labeling (data not shown).

Ratio (v/v) $^{68}Ga^{3+}$/ ACD-A	Sample volume (ml)	pH	Vortex stirring action[#]	Incubation time			
				3 min	10 min	20 min	45 min
1 : 4	2 x 1.0	1.5-2	+	73 ± 3.4	77 ± 4.6	85 ± 4.2	87 ± 2.9
			-	71 ± 2.8	73 ± 2.1	79 ± 4.3	84 ± 4.3
1 : 8	2 x 2.0	3-3.5	+	76 ± 3.3	81 ± 1.1	88 ± 0.7	90 ± 1.2
			-	75 ± 3.0	78 ± 2.6	82 ± 5.8	88 ± 3.6
1 : 14	2 x 3.5	4.5-5	+	82 ± 4.9	96 ± 1.2*	99 ± 0.3*	99 ± 0.1*
			-	81 ± 3.8	84 ± 3.5	86 ± 3.0	91 ± 3.5
1 : 20	2 x 5.0	5.5-6	+	82 ± 2.9	91 ± 3.1*	93 ± 1.7*	95 ± 0.5
			-	81 ± 2.0	82 ± 1.9	85 ± 3.1	89 ± 4.2

Table 1: Parameter evaluation for high yield ^{68}Ga-citrate labeling. Data is displayed as mean (± SD) of three independent experiments (n=3).

Standard radiolabeling with ^{68}Ga

In total 24 identical radiosyntheses were considered for the study. The pH value of the product for injection was 4.0-4.5. Optical inspection showed a product solution, clear, colorless and free of particulate matter. The average duration from generator elution to sterile dispensing of ^{68}Ga-citrate was 29±17 min (n=17). 302±69 MBq/patient of labeled product was obtained for dispensing and for quality control purposes. The final product was supplied in 6.6±2.8 ml with an activity of 191±33 MBq (155-255 MBq) for imaging purposes. The experimental results of three subsequent productions of ^{68}Ga-citrate showed that all quality control tests applied met the GMP release criteria (Table 2). There was no noticeable decline in the ^{68}Ga-citrate labeling efficiency observed over the 7 months duration.

Quality control test[#)]	GMP release criteria	Run 1	Run 2	Run 3
Yield	≥ 250 MBq in 1 mL eluate	389	448	426
Visual inspection	Clear, colorless, particle-free	Pass	Pass	Pass
Radiochemical identity (ITLC-SG)	Rf ^{68}Ga-ACD-A = 0.90±0.10	0.95	0.98	0.95
Internal control	$\frac{Rf\ ^{68}\text{Ga-ACD-A}}{Rf\ ^{68}\text{Ga-citrate}}$ = 0.90±0.10	0.97	0.99	0.95
Chemical amount	Na-citrate dehydrate ≤3 mg/dose	0.075	0.072	0.080
	Citric acid $_{anhydrous}$ ≤1 mg/dose	0.023	0.026	0.023
Radiochemical purity	≥ 95 %	99.4	99.8	99.2
pH	4.5±0.5	4.5	4.5	4.5
Sterile filter integrity	≥ 3.5 bar	5.8	6.8	6.2
Residual ^{68}Ge	≤ 0.005%	0.0007	0.0004	0.0008
Radionuclide identity	67.7±1.5 min	67.5	68.0	68.1
Sterility testing	Sterile	Pass	Pass	Pass

[#] The following tests were not considered: residual solvent analysis and LAL bacterial endotoxin analysis

Table 2: Quality control tests for ^{68}Ga-citrate labeling. Release criteria and experimental results from three subsequent ^{68}Ga-citrate productions (n=3).

ITLC analysis and radionuclide identity

The average radiochemical purity determined by ITLC-SG was 99±0.9% (n=18). The retention factors (R*f*) for free ^{68}Ga and ^{68}Ga-citrate are 0.0 and 0.95, respectively. Radiolabeled ACD-A showed the same retention factor as the internal control (1.0 % citrate), thus, the ratio was calculated 0.98. Radionuclide identity was positively tested for ^{68}Ga with a $T_{1/2}$ calculated 67.4-68.1 min (n=10).

Sterility

The tested sterile filters showed integrity >62 psi (ca 4.1 bar) by bubble burst point test. The mean value for filter burst pressure was 86±13 psi. Samples were tested further free of aerobe, anaerobe bacteria as well as fungal growth.

Detection of ^{68}Ge impurities

Decayed ^{68}Ga-citrate samples were routinely measured in a Capintec CRC 25 ionization chamber and were further quantified by gamma spectrometry. The maximum value comparing the sample ^{68}Ge relative to total ^{68}Ge in the total eluate amounted to 0.037%. The average amounted to 0.0015±0.0009% (n=15). This falls well within the limits for ^{68}Ge-breakthrough (0.05%) as set out by de Blois et al.[5]

Stability of ^{68}Ga-citrate

The radiochemical ^{68}Ga-citrate integrity was found to be > 96% over the 240 min duration observed (n=4). The percentage of released ^{68}Ga was 1.1±0.62%, 1.7±0.65%, 3.1±1.5%, 3.1±0.85% and 3.4±1.1% for 30, 60, 120, 180 and 240 min, respectively.

Patient preparation, injection and image acquisition

The average injected dose of ^{68}Ga-citrate was 192 MBq (155-255MBq), with the most frequently given dose being 185 MBq (n=20). Five patients did not receive IV contrast due to one of the following reasons: sub-optimal kidney functions, iodine allergy or a recent contrasted CT. All study participants received oral contrast no and no additional patient preparation was required. Quality control was performed prior to injection and no serious side effects were reported (two patients reported a slight burning sensation upon injection). The average blood glucose of the study participants was 5.2 mmol/l (3.5-9.1 mmol/l). Images obtained at 60 min post-injection of ^{68}Ga-citrate, resulted in good quality images. The quality of images deteriorated significantly after 150 min, causing the target to background ratio to become unfavorable for interpretation. ^{68}Ga-citrate images demonstrated high vascular activity. In addition, normal biodistribution demonstrated noticeable tracer uptake in the

salivary glands, liver, spleen and bone marrow (Fig 1). The respective SUV_{max} values in the areas of normal ^{68}Ga-citrate organ/tissue biodistribution were as follows: Bone marrow: 4.3, liver: 5.5, mediastinal blood pool: 6.8 and spleen: 3.7. Furthermore, ^{68}Ga-citrate showed successful diagnostic imaging of pulmonary infection (Fig 2 A) as well as lymph node involvement in a HIV/TB compromised male patient (Fig. 2 B).

Fig.1 A maximum intensity projection (MIP) image that demonstrates the expected biodistribution of ^{68}Ga-citrate. This was acquired on a Siemens Biograph 40 PET/CT scanner at 60 min post-injection of 185 MBq of ^{68}Ga-citrate. The normal bio-distribution includes high vascular activity (as has been demonstrated before) and activity in the salivary glands, liver, spleen and bone marrow.

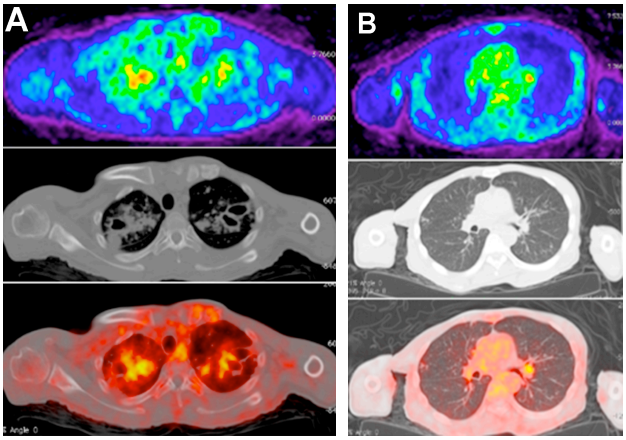

Fig. 2 A 44 yr old man with HIV and TB demonstrated increased ^{68}Ga-citrate accumulation in the apices of both lungs **(A)** which corresponded to the areas of cavitations noted on CT together with **(B)** mediastinal lymph node involvement indicative of active tuberculosis. These transverse mages were acquired on a Siemens Biograph 40 PET/CT scanner at 60 minutes post-injection of 185 MBq of ^{68}Ga-citrate.

Discussion

This is the first report on the labeling of ACD-A (a buffered citrate solution) with Gallium-68 using a novel SnO_2-based $^{68}Ge/^{68}Ga$ generator. This generator is produced by iThemba LABS in South Africa, and recently became commercially available (IDB Holland, Netherlands). We have described a direct and rapid procedure using fractionation of the generator eluate to provide up to four parallel ^{68}Ga-citrate radiosyntheses for individualized patient injection. Moreover, it is a safe and simplified, one-step aseptic procedure which shows robust and nearly quantitative labeling efficiencies of greater than 96% following a 10 min incubation period. The SnO_2-based generator can be very efficiently milked by fractionating the eluate[9], as described by de Blois et al. [5] This group demonstrated that the ^{68}Ga activity yield varies depending on the applied concentration of HCl, while ^{68}Ge activity remained virtually constant. The authors further reported that the generator elutes 100% of the ^{68}Ga activity at calibration time and ±75% after 300 days with the use of 0.6 N HCl. We could provide a 90-96% yield of ^{68}Ga activity within the 220 days use by milking the instrument daily to three times weekly. There was no correlation observed between the age of the generator and the ^{68}Ga-citrate labeling efficiency. This direct ^{68}Ga-citrate labeling, making use of ACD-A, resulted in nearly quantitative radiochemical yields and can facilitate individualized PET/CT imaging of multiple patients from one generator elution. A few efficient methods of ^{68}Ga-citrate production have been published recently[1,3,4,10] as well as high yield labeling using TiO_2-based $^{68}Ge/^{68}Ga$ generators, eluate post procession and semi-atomization. However, only Jensen and coworkers have considered a solvent free labeling approach.[11] We have used a very cheap, safe and direct method for ^{68}Ga-citrate production with a one-vial solution and without the need for post-processing of the ^{68}Ga-eluate. In theory, the total radiochemical yield for injection is 764±132 MBq. Our ^{68}Ga-citrate labeling method also offers the advantage of easy adaptation to another ^{68}Ga labeling procedure, e.g. DOTA-TATE, since a maximum eluate fraction of only one milliliter is required per patient. For quality control of ^{68}Ga-citrate, the ITLC method, which is a well-established analytical method in nuclear medicine departments, was used routinely. Products were proven to be pure, sterile, clear and within a moderate pH range. Moreover, all quality control methods applied were reproducible and variation in the total activity yield was only determined by the age of the generator, hence the starting activity must be sufficiently high and not compromised by impurities. We observed traces of co-eluted metals <10 ppm and very low levels of ^{68}Ge towards the 7

months use. Productions utilizing a generator older than nine months would require a pre-purification step of the eluate. We are currently implementing a recently published method that warrants an overall solvent-free procedure to void elaborate testing e.g. gas chromatographic analysis.[12]

Our recent review [13] yielded very few results on the use of ^{68}Ga-citrate in infection imaging, and none on its application in respiratory infections, despite the excellent track record of ^{67}Ga-citrate in this setting. The advantages of ^{68}Ga-citrate over ^{67}Ga-citrate and white blood cell imaging include its improved imaging resolution, its generator-dependence, shorter imaging times and improved dosimetry, amongst others. We have included a representative example of a patient with infective lung lesions imaged with ^{68}Ga-citrate PET/CT (Fig 2), which is part of a larger (as yet) unpublished patient series. To our best knowledge, this is the first report on this novel application of ^{68}Ga-citrate labeled from a SnO_2-based ^{68}Ge/^{68}Ga generator.

Conclusion

We have described here a simple, rapid, one-step, aseptic method for the quantitative preparation of ^{68}Ga-citrate (via labeling of ACD-A) on a moderate scale. This has been successfully adapted to the more acidic conditions that are needed for the elution of ^{68}Ga from a SnO_2-based ^{68}Ge/^{68}Ga generator. Our method also allows for the production of more than 300 MBq/patient in less than 30 min. We trust that the herein published data will facilitate the routine use of ^{68}Ga-citrate in general infection imaging, which should also include applications other than musculoskeletal infections.

Acknowledgements

The authors acknowledge the Department of Nuclear Medicine for technical assistance with PET/CT imaging as well as the Nuclear Energy Corporation of South Africa for providing the infrastructure for the in-depth quality control measurements.

References

1. Chen DC, Newman B, Turkall RM, Tsan MF. Transferrin receptors and gallium-67 uptake in vitro. Eur J Nucl Med.1982;7(12):536–40.

2. Tsuchiya Y. Relationship between gallium 67 citrate scanning and transferrin receptor expression in lung diseases. Chest. American College of Chest Physicians; 1992 Aug 1;102(2):530–4.

3. Tsan MF. Mechanism of gallium-67 accumulation in inflammatory lesions. J Nucl Med.1985 Jan;26(1):88–92.

4. Nanni C, Errani C, Boriani L, Fantini L, Ambrosini V, Boschi S, et al. 68Ga-Citrate PET/CT for Evaluating Patients with Infections of the Bone: Preliminary Results. J Nucl Med.2010 Dec 1;51(12):1932–6.

5. de Blois E, Sze Chan H, Naidoo C, Prince D, Krenning EP, Breeman WAP. Characteristics of SnO2-based 68Ge/68Ga generator and aspects of radiolabelling DOTA-peptides. Appl Radiat Isot. 2011 Feb;69(2):308–15.

6. Kumar V, DK B, SG E, S A. (68)Ga-Citrate-PET for diagnostic imaging of infection in rats and for intra-abdominal infection in a patient. Curr Radiopharm. 2012 Jan 1;5(1):71–5.

7. Rizzello A, Di Pierro D, Lodi F, Trespidi S, Cicoria G, Pancaldi D, et al. Synthesis and quality control of 68Ga citrate for routine clinical PET. Nucl Med Commun. 2009 Jul;30(7):542–5.

8. Bombardieri E, Aktolun C, Baum RP, Bishof-Delaloye A, Buscombe J, Chatal JFO, et al. 67 Ga scintigraphy: procedure guidelines for tumour imaging. Eur J Nucl Med Mol Imaging. 2003 Dec 1;30(12):1–1.

9. Rossouw, Breeman. Scaled-up radiolabelling of DOTATATE with ^6^8Ga eluted from a SnO"2-based ^6^8Ge/^6^8Ga generator. Applied Radiation and Isotopes. 2011 Dec 31;70(1):5–5.

10. Al-Nahhas A, Win Z, Szyszko T, Singh A, Nanni C, Fanti S, et al. Gallium-68 PET: a new frontier in receptor cancer imaging. Anticancer Res. 2007 Nov;27(6B):4087–94.

11. Jensen SB, Nielsen KM, Mewis D, Kaufmann J. Fast and simple one-step preparation of ^{68}Ga citrate for routine clinical PET. Nucl Med Commun. 2013 Jul 31;34(8):806–12.

12. Mueller DD, Klette II, Baum RPR, Gottschaldt MM, Schultz MKM, Breeman WAPW. Simplified NaCl based (68)Ga concentration and labeling procedure for rapid synthesis of (68)Ga radiopharmaceuticals in high radiochemical purity. Bioconjugate Chem. 2012 Aug 14;23(8):1712–7.

13. Vorster M, Maes A, Van de Wiele C, Sathekge M. Gallium-68: a systematic review of its nononcological applications. Nucl Med Commun. 2013 Sep;34(9):834–54.

Chapter 5: Distinguishing benign from malignant lung lesions with a novel tracer

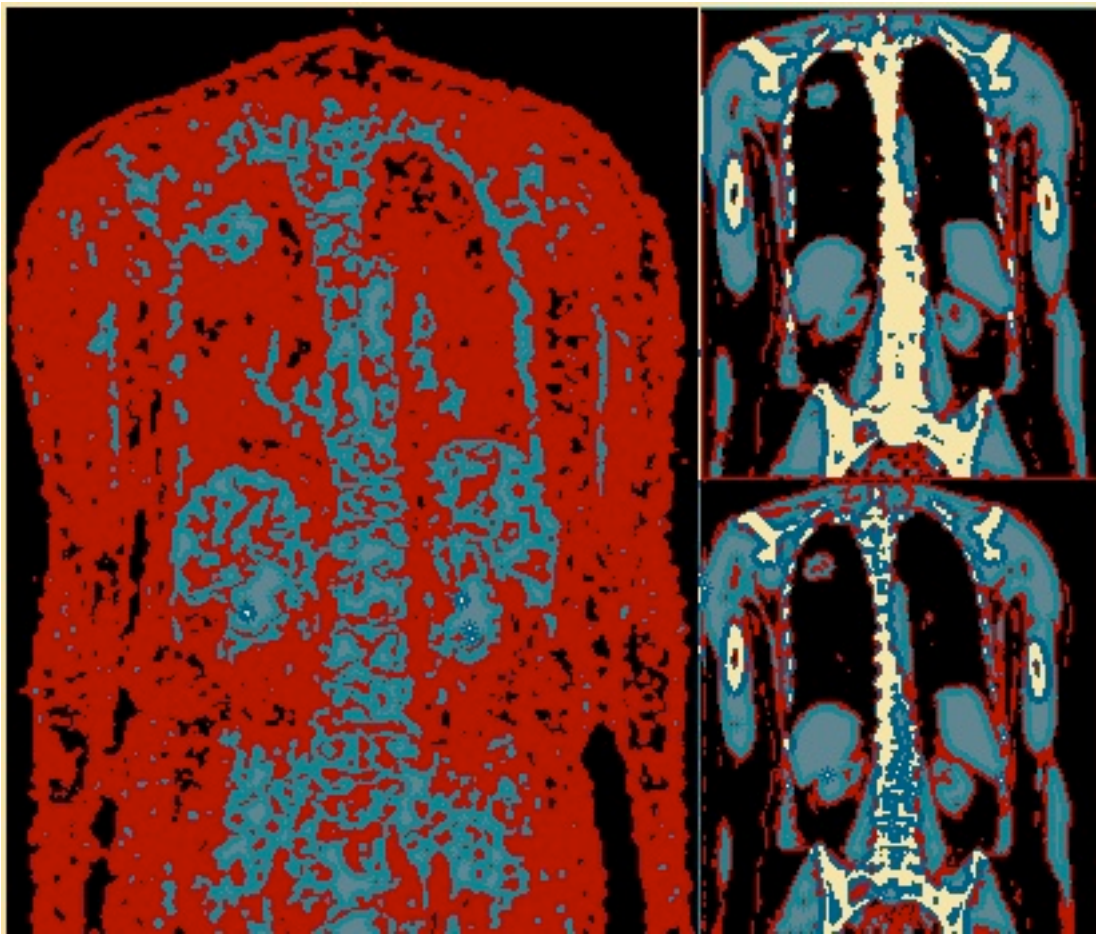

*An adapted version of this chapter has been accepted for publication in the Annals of Nuclear Medicine:

Evaluating the possible role of ^{68}Ga-citrate PET/CT in the characterization of indeterminate lung lesions

Vorster M_1, Maes A_2 , Jacobs AG_4, Malefahlo S_4, Pottel H, Van de Wiele C_3, Sathekge MM_1
University of Pretoria, Department of Nuclear Medicine, Steve Biko Academic Hospital$_1$
Department of Nuclear Medicine AZ Groeninge, Reepkaai, Kortrijk, Belgium $_2$
Department of Nuclear Medicine, University hospital Ghent, Ghent, Belgium $_3$
University of Pretoria, Department of Cardiothoracic Surgery, Steve Biko Academic Hospital $_4$

Abstract

Background

The ability to accurately distinguish benign from malignant lesions in the chest is important in the correct and timeous management of patients presenting with such pathology. Imaging with PET/CT provides a non-invasive tool that could potentially reduce the amount of futile biopsies performed We sought to determine whether PET/CT imaging with ^{68}Ga-citrate could be of value in distinguishing benign from malignant lung pathology in a setting with a high prevalence of granulomatous diseases.

Methods

Patients with indeterminate lung lesions underwent a PET/CT study with ^{68}Ga-citrate prior to lung biopsy. Qualitative and semi-quantitative measures of tracer uptake in the lung lesions (SUV_{max}) were compared to the histopathology in order to establish an imaging pattern to distinguish benign from malignant lesions.

Results

Thirty-six consecutive patients with lung lesions of an indeterminate nature were prospectively recruited and imaged with ^{68}Ga-citrate PET/CT. Fourteen patients (38.9%) were diagnosed with a malignant lesion, twelve (33.3%) with Tuberculosis, and ten participants (27.8%) with other benign lung lesions (fibrosis, infective- or inflammatory lesions and sarcoidosis). Low SUVmax values were demonstrated in benign lesions with higher values noted in malignant- and tuberculous lung lesions, although considerable overlap existed in values

Conclusion

This study, as the first human study making use of ^{68}Ga-citrate for the *in vivo* imaging of lung pathology, demonstrated that ^{68}Ga-citrate PET has potential for the detection of malignancy and tuberculosis. However, it seems unable to provide a clear distinction between malignant and benign lung lesions in a setting with a high prevalence of Tuberculosis.

Introduction

PET/CT imaging plays an important role in the characterization of Solitary Pulmonary Nodules (SPN) and has been one of the first indications for which medical aids have agreed to reimburse. However, in the South African setting, SPN and other lung lesions of an indeterminate nature, continues to present physicians with a diagnostic challenge. This is mainly due to the high prevalence of granulomatous diseases such as Tuberculosis (TB), which is frequently associated with Human Immunodeficiency Virus (HIV).

Various studies have indicated the inability of ^{18}F-FDG-PET/CT, despite the use of dual phase imaging, to distinguish accurately between benign- and malignant causes of SPN in the setting of a high TB prevalence.[1,2,3] This is due to the (as yet unexplained) similar behavior over time of malignant and granulomatous lesions in terms of FDG uptake and this has also been confirmed in our setting.[4,5]

Reaching a diagnosis in patients presenting with suspected *Pneumocystis jiroveci* pneumonia (PJP) or non-tuberculous mycobacteria and determining the etiology in those presenting with pleural disease, also remains challenging. ^{18}F-FDG PET/CT appears to be of limited value in reaching the above-mentioned diagnoses as well as differentiating benign from malignant diseases of the pleura.[6] Therefore multiple tests are often required which still often ultimately require biopsy for histological confirmation.[7]

An increase in the availability and accessibility of PET/CT facilities has sparked renewed interest in generator-based PET radiopharmaceuticals. Gallium-68 in particular, has received a lot of attention as an alternative positron emitter since it offers several important advantages when compared to FDG and could overcome some of the well-known limitations of FDG-PET (non-specificity and the need for a nearby cyclotron) and may be especially valuable in the imaging of infection/inflammation. Gallium (in the form of ^{67}Ga-citrate) has long provided nuclear physicians with a versatile tool for use in both oncological and infective settings. With regards to infection imaging it has been widely used in the diagnosis and management of skeletal and lung infections as well as in immuno-compromised individuals and those presenting with fever of unknown origin.[8,9]

The mechanism of action, although incompletely explained, is generally accepted to be the result of various specific and non-specific factors, which play a role in both infective/inflammatory and malignant processes. Non-specific factors include the increased vascular permeability found in areas of inflammation or increased vascularity, whereas specific factors comprise both transferrin-dependent and transferrin-independent mechanism. Gallium acts as an iron analogue, the majority of which is bound to transferrin in plasma and then internalized as a gallium-transferrin complex in to cells with expression of transferrin receptors. Other localization mechanisms include binding to lactoferrin, siderophores and leukocytes.[8,10,11]

It therefore stands to reason, that Ga-68 would be as useful as Ga-67 with the added advantages of improved image resolution, quantification possibilities, improved dosimetry and imaging logistics gained from PET/CT technology. Compared to ^{18}F-FDG, ^{68}Ga offers shorter imaging times and on-demand, year-round tracer availability that negates the need for an onsite or nearby cyclotron. This could have significant financial implications, which may lead to a more cost-effective way of imaging. In addition, the short half-life of 68 minutes provides attractive peptide labeling options for novel diagnostic and therapeutic applications.[12]
Several authors have investigated the use of ^{68}Ga-citrate in the evaluation of various infectious and inflammatory conditions. Sofar, the most promising results have been found with the imaging of musculoskeletal infections.[13,14]

With this study, we aimed to evaluate whether ^{68}Ga-citrate could potentially be of value in distinguishing benign from malignant lesions in the lung.
To our knowledge, ^{68}Ga-citrate has been used mainly in the setting of musculoskeletal imaging and lung imaging is a novel application of this tracer.

Materials and Methods

Approval was granted by the University of Pretoria's research Ethics committee and informed consent was obtained from all study participants prior to injection and imaging.

Patient population

Patients with lung pathology of an uncertain nature (eg lung mass, nodules/infiltrates) and who were being considered for lung biopsy were recruited for this study.

^{68}Ga-citrate Preparation and QC

A SnO_2-based ^{68}Ge/^{68}Ga generator (iThemba LABS, Somerset West, South Africa)[15] was fractionally eluted with 10 ml of 0.6N HCl for ^{68}Ga-citrate synthesis. This was performed manually in a one-step-aseptic procedure, which was based on a combination of the protocols used by Kumar [16] and Rizzello [17] and made use of ACD-A. All solvents used were of a pharmacological grade. For labeling with ^{68}Ga, Anticoagulant Citrate Dextrose Solution, USP formula A (ACD-A) was purchased as sterile and non-pyrogenic solution from Fenwal Inc. (Lake Zurich, Illinois, USA).
The aqueous solution of ACD-A contains 2.20% sodium citrate dehydrate, 0.73% citric acid anhydrous and 2.45% glucose monohydrate. A 30% solution of supra-pure grade Hydrochloric acid (HCl) was purchased from Merck Sharp & Dohme (Readington, New Jersey, USA).

PET/CT Imaging Protocol

Study participants were imaged on a Siemens Biograph 40 PET/CT scanner 60 minutes post IV ^{68}Ga-citrate administration. Both oral (Barium in water) and IV contrast (100 ml Ultravist, at a rate of 2ml/s) was administered, except where a contra-indication, such as inadequate kidney function or an allergy to iodine existed. Images were acquired in a three-dimensional mode with a 4-minute emission scan for each of on average 7-9 bed positions (Matrix size 512x512) from the skull base to the pelvis. Reconstruction of images with and without

attenuation correction (CT based) was done using OSEM (ordered subset expectation maximization) to yield axial, sagittal and coronal slices.

Image Analysis

All images were first evaluated qualitatively for abnormal uptake,which if present, was then followed by semi-quantification analysis. ^{68}Ga-citrate demonstrates almost no uptake in the lungs in the absence of pathology and therefore any tracer accumulation in the thorax outside of the mediastinal blood pool was considered abnormal.
We made use of the following scale with the liver intensity* as reference point in order to grade Gallium uptake:
0=no uptake
1=uptake less intense than the liver
2=uptake equal in intensity to the liver
3=uptake more intense than the liver

* The liver was chosen as the reference point based on similar scales used with ^{67}Gallium-citrate in other studies.[18]Also, the liver did not demonstrate any statistically significant difference in SUVmax between patients with benign or malignant lesions. (p=0.9292)

Semi-quantitative analysis was done in the following way: a region of interest was manually drawn around any lung lesions and the size selected to correspond to the pathology on CT. This results in a standard uptake value (SUV), which is representitive of the relative concentration of radiotracer in a lesion of interest, normalized to the patient's weight and the dose of radiotracer administered. (SUV=radiotracer activity x patient weight/injected dose). We used the maximum SUV (SUV_{max}) in this study, which represents the voxel with the highest tracer uptake in the lesion.The SUVmax was then recorded and compared to the SUVmax of various reference points, such as the mediastinal blood pool, the liver, spleen and bone marrow in order to calculate various ratios. Where dual time point imaging was performed (n=20), a second SUVmax was recorded. The 60 min value was labeled $SUVmax_1$ and the 120 min image $SUVmax_2$.The change in SUVmax was calculated as follows (and expressed as a percentage change): Difference between $SUVmax_1$ and $SUVmax_2$/$SUVmax_1$

Results Validation

Image findings were validated by comparing the PET/CT results to the results of biopsy, tracheal aspirates, sputum microscopy and cultures, biochemistry and results of other conventional imaging modalities (CXR, CT, MRI & Ultrasound). Where tissue could not be obtained for histological confirmation (patient refusal or clinically deemed unnecessary by referring physician) a combination of the afore-mentioned special investigations and clinical data was used to reach a diagnosis.

In order to compare the accuracy of PET to that of CT using histology as the gold standard, the following criteria for expected uptake of ^{68}Ga-citrate were set:
Making use of the qualitative assessment or visual score, the following patterns of uptake was used provide clinically useful distinctions between various types of lung pathology:
-Benign lesions:no or very little ^{68}Ga-citrate uptake (grade 0 or 1);
-Malignant lesions: similar to or more intense than the liver (grade 2 or 3)
PET was therefore considered correct whenever these patterns were present. CT was considered correct whenever the final diagnosis was included in the diagnosis.

Statistical Methods

Descriptive statistics were used to report patient characteristics and procedural details. Summary statistics is presented as mean (SD, standard deviation) or as median (IQR, interquartile range) in case of non-normality of the data. Numbers or percentages are reported otherwise. Statistical analysis was performed with SAS version 9.3.Differences in the SUVmax (and various lesion to background ratios) between benign and malignant lung lesions were assessed using unpaired t-test to find means that are significantly different from each other.Statistical significance was defined as $p<0.05$.

Results

Procedural details

The average injected dose of ^{68}Ga-citrate was 196 MBq (155-255MBq). The average radiochemical purity determined by ITLC-SG was 98.9% ± 0.94% which was confirmed by HPLC. The pH value of the product for injection was 4.0-4.5. All other requirements for QC were met.

Intravenous contrast was administered to 19 patients (omitted in patients with sub-optimal kidney functions, iodine allergy or a recent contrasted CT) and all study participants received oral contrast. Quality control was performed prior to injection with both ITLC- and pH strips and no serious side effects were reported. (Three patients reported a burning sensation upon injection, which resolved upon dilution with normal saline).
Images were acquired at 60 minutes post-injection and no particular patient preparation was required. In 20 ptients an additional scan was performed at 120 mins post-injection and the change in SUV calculated.The average blood glucose of the study participants was 5.2 mmol/l (3.5-9.1mmol/l).High quality images were obtained at 60 minutes post-injection without the need for any patient preparation.

Patient population

Thirty-six consecutive patients with lung lesions of an indeterminate nature were prospectively recruited and imaged at the department of nuclear medicine, at the Steve Biko Academic Hospital, Pretoria, South Africa. Study participants included 20 males and 16 females with a median age of 52.5 years. The demographics were as follows: Black (56%), Caucasian (36%) and a smaller group consisting of Asian and Coloured participants (8%). Five of the 36 patients were confirmed to be HIV positive (14%) and 47.2% were smokers.

Patients most commonly presented with a lung lesion localized to the upper lobe of the right lung (39%). Histological or tissue confirmation could be obtained in 27/36 (75%) and the remaining 25% of diagnoses were reached based on combination of clinical, biochemical and other imaging findings. The final diagnoses were distributed as follows: Fourteen patients

(38.9%) were diagnosed with a malignant lesion, twelve patients (33.34%) with Tuberculosis and the remaining ten participants (27.8%) were diagnosed with other benign lung lesions (fibrosis, infective- or inflammatory lesions and sarcoidosis). See Table 1 for individual patient details.

No	Lung lesion	Diagnosis	Diagnostic modality and detail	^{68}Ga-uptake
1	RUL mass	Benign	Bronchial washings, Sputum MCS, CXR &CT Pneumoconiosis & previous PTB	Absent
2	RML	Likely Malignant (Refused bronchoscopy)	CT findings: Consistent with bronchogenic CA with multiple brain and adrenal metastases	Low
3	RUL	Malignant	Histology: Moderately differentiated, infiltrating adenocarcinoma	Low
4	RUL	Benign	Histology: Interstitial lung disease and hypersensitivity pneumonitis Recent sputum + *Mycobacterium gordonae*	Low
5	RUL	Benign	Histology: chronic inflammation, no malignant cells	Low
6	RML	Likely Malignant (Refused bronchoscopy	CT findings consistent with bronchogenic carcinoma and bilateral adrenal metastases	High
7	LUL	Benign	Clinically TB & treated as such	Low
8	RML	Likely Malignant (Biopsy deemed unnecessary)	CT findings consistent with lung malignancy and brain metastases	High
9	RUL	Malignant	Histology: Moderately differentiated adenocarcinoma	High
10	L empyema	Likely Malignant (Refused bronchoscopy)	CT hilar mass with obstruction of left main stem bronchus. Sputum negative.	High
11	Lingula nodule	Malignant	Histology: low-grade epithelioid tumour with neuro-endocrine differentiation consistent with carcinoid tumour	Moderate
12	RUL	Benign	Histology & pleural fluid cytology: moderately differentiated squamous cell carcinoma	Low
13	RUL	Likely benign	Confirmed esophageal carcinoma with aspiration pneumonitis on chest CT	Low
14	SPN RUL	No Malignant/ infective cells	Histology	Low
15	LUL	TB	PCR	High
16	SPN LUL	Likely malignant based on CT	No histology	Low
17	Left paratracheal mass	Likely benign	No histology	Low
18	LL mass	Malignant	Moderately differentiated adenocarcinoma	Moderate
19	LL mass	More in favour of infective process	No histology	Low

20	RL mass	TB	Liver biopsy	Low
21	RL mass	Squamous cell carcinoma	Squamous cell carcinoma	High
22	R hemi-thorax	TB and AML	Pleural fluid analysis & BM biopsy	High
23	RUL mass	Squamous cell carcinoma	Biopsy	Moderate
24	RML mass	Metastatic adenocarcinoma	Biopsy	Moderate
25	L pleural effusion	Metastatic neuro-endocrine bronchus tumour	Biopsy	Low
26	L posterior lung mass	TB	Combination clinical & imaging	Low
27	L lung changes	TB	Sputum MCS	Moderate
28	Mediastinal lymph nodes	TB	Combination clinical & imaging	Absent
29	Bilateral lung changes	Sarcoidosis	Combination clinical & imaging	Low
30	RUL changes	TB	PCR, sensitive for INR & Rifampicin	Low
31	Bilateral apical changes	TB	Combination clinical & imaging	High
32	LUL cavities	TB	PCR, sensitive for INR & Rifampicin	High
33	Mediastinal mass	TB	Combination clinical & imaging	Low
34	R Lung apex	TB	AFB+ on aspirates	High
35	RUL SPN	Fibrosis	Intra-operative frozen section	Absent
36	Bilateral lung changes	Sarcoidosis	Combination clinical & imaging	Moderate

Table 1: Individual patient diagnostic details

We found no difference in gender distribution between patients with benign (n=22) and malignant lung lesions (n=14) using Fischer's exact Test (p=1). There was, however a statistically significant difference (p=0.0080) in the mean age distribution between these two groups: patients with a benign lesion had a mean age of 47.2 (13.1) compared to 58.9 (10.7)

The proportion of smokers in the benign group (44%) vs. those with a malignancy (75%) was not statistically significant (p=0.1414). The localization of the primary lung lesion was also not significantly different with the majority of lesions in both groups presenting in the right upper lobe (p=0.3011).

Image Analysis

Image acquisition performed at 60 minutes post-injection of (on average) 185 MBq of ^{68}Ga-citrate resulted in good quality images. The quality of the images deteriorated significantly after 150 minutes, causing the target to background ratio to became unfavorable for interpretation.

The normal bio-distribution of ^{68}Ga-citrate is represented in Figure 1 and involves the following: lacrimal- and salivary glands, the heart, liver, spleen, bone marrow, large vasculature and dural venous sinuses. The pronounced vascular activity was similar to the findings published by Nanni et al.[14] and Rizzello et al.[17]

Typical SUV (max) in the areas of normal ^{68}Ga-citrate bio-distribution were as follows: Bone marrow: 4.0 (3.0-4.4), Liver: 4.8 (3.84-5.8), Mediastinal Blood pool: 5.6 (4.3-7.2), Spleen:3.4 (2.9-4.2) These values were obtained by adding the SUVmax for the particular organ of every patient and calculating the median value. Values in brackets represent the 25th percentile to the 75th percentile.

Fig 1: ^{68}Ga-citrate bio-distribution

SUV_{max} at 60 min post-injection:

- Patients who were diagnosed with a **malignant lesion** (n=14) demonstrated a mean SUVmax of **3.36** +/-1.14, with a median value of 3.04 (min=1.56, max=4.65)
- Those with **tuberculosis** (n=12) demonstrated a SUVmax of **3.99** +/-2.28, a median value of 3.71 (pct_{25}=2.19, pct_{75}=4.95)
- In patients with **other benign lesions** (n=10) , the following values were observed: a SUVmax of **2.70** +/-1.31, a median value of 2.50 (pct_{25}=1.76, pct_{75}=3.59)
  The means of these three types of pathology were not statistically significant (p=0.1919), and therefore the $SUVmax_1$ could not be used to accurately distinguish between these lesions (See figure 2a).

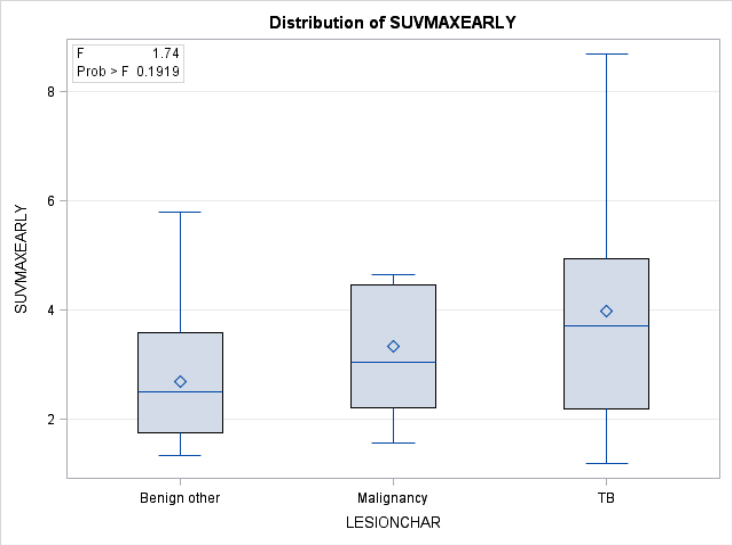

Fig 2a: Boxplot demonstrating inability to distinguish between TB, malignant lesions and other benign lesions based on early SUVmax alone (p=0.19)

- Combining the last two groups mentioned into one benign group (n=22) resulted in a mean Suvmax of **3.3** (+/-2), a minimum value of 1.19 and a maximum of 8.69). Again, no distinction could be made between benign (n=22) and malignant (n=14) lesions based on $SUVmax_1$. (p=0.9374)

SUV_{max} at 120 min post-injection:

- Imaging at this time point did also not reveal any difference in the mean SUVmax between benign (n=11) and malignant (n=9) lung lesions. (p=0.4024)
- Benign lesions demonstrated a mean SUVmax of 2.7 (1.65) compared to a mean SUVmax of 3.4 (1.9) in malignant lesions.

Dual-time point imaging (SUV_{max} at 60 minand 120 min post-injection):

- Benign lesions demonstrated a mean change between these values of 0.19 (0.15),ranging from 0.02-0.49
- Malignant lesions demonstrated a mean value of 0.29 (0.2), which ranged from 0-0.59 These differences were not statistically significant (p=0.2299) (See Fig 2b).

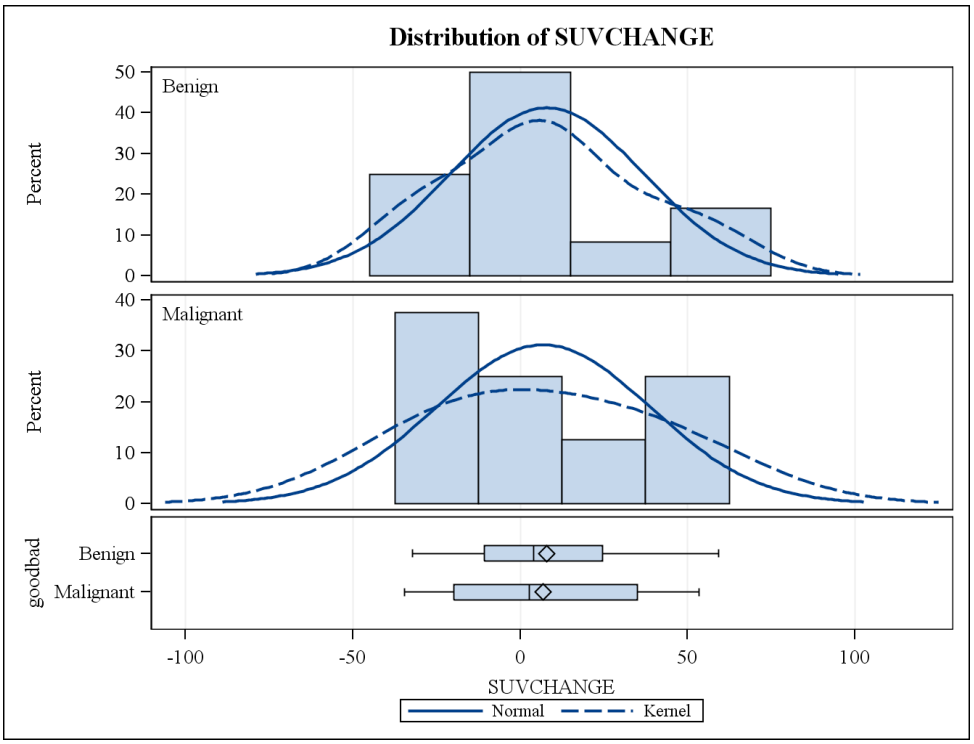

Fig 2b: Diagram representing the change between SUVmax early (60 min) and SUVmax delayed (120 min) and the inability to distinguish lesions based on a change in SUV.

Differences in various lesion: background/reference ratios were also considered in order to distinguish benign from malignant lesions. These consisted of the SUVmax in the primary lesion relative to the SUVmax of the liver, spleen, bone marrow and mediastinal blood pool, none of which were statistically significant.

Also,when considering the study participants as three groups: Benign (n=10), Tuberculosis (n=12) and Malignant (n=14) and repeating the same calculations as above, no statistically significant differences could be elicited.
All of the malignant lesions (14/14) in this study (including two tumours of neuro-endocrine origin) demonstrated increased tracer accumulation (See fig 3).

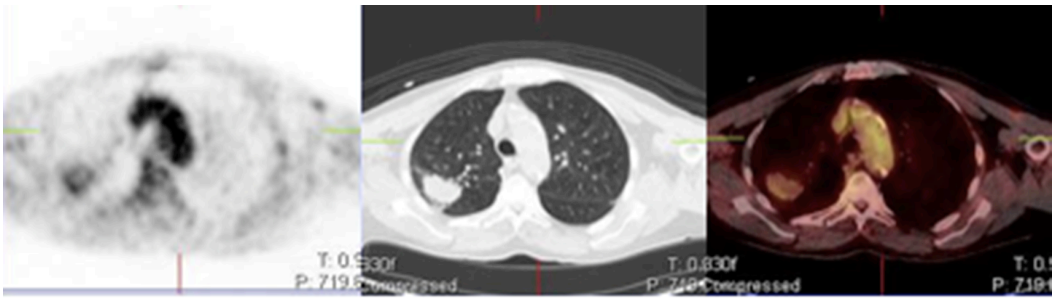

Figure 3 A 74 yr old male smoker who presented with a right upper lobe mass on CXR. a) Coronal and b) transverse PET, CT and fused PET/CT images demonstrate increased tracer accumulation (similar to the liver intensity) in the lung mass (SUVmax: 2.99) and histology revealed a moderately differentiated adenocarcinoma

In addition, malignant lung lesions (almost without exeption) were associated with diffusely increased bone marrow uptake when compared to patients with benign lesions. However,this was not found to be statistically significant and may require a larger patient population for validation.

Tuberculous lesions demonstrated variable tracer uptake which ranged widely from only mildly increased to very intense uptake. (Median SUVmax of 3.71 25th percentile=2.l9; 75th percentile=4.95). Areas of increased ^{68}Ga-citrate often indicated far less extensive involvement than that noted on CT, and could therefore indicate only areas of active disease (See fig 4).

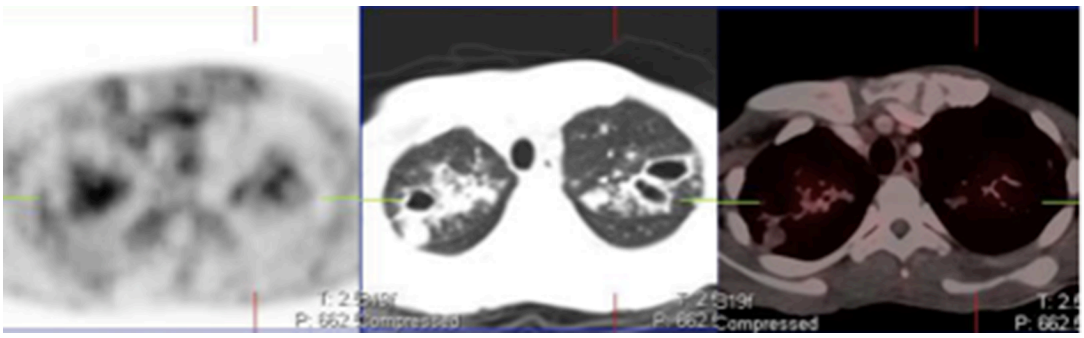

Figure 4 A 44 yr old male smoker with RVD who presented with bilateral apical lung changes. Transverse PET, CT and fused PET/CT images demonstrate increased tracer uptake in both apical lobes. Sputum cultures confirmed Mycobacterium Tuberculosis.

Five patients demonstrated no tracer accumulation in the lesions noted on CT and were found on histology not to have any malignant, infective- or inflammatory changes (See Fig 5).

Figure 5 A 71 yr old female smoker with a right upper lobe mass and pleural effusion. Transverse PET/CT images demonstrate no uptake in the afore-mentioned lesions. Histology did not reveal any malignant or inflammatory cells. These findings suggest a good negative predictive value for lesions without uptake.

Finally, a comparison was made between PET and CT to determine which was more accurate at predicting the nature of a lesion. Making use of the above described qualitative assessment or visual score, PET was considered correct, whenever these patterns were present. CT was considered correct whenever the final diagnosis was included in the diagnosis.

The following observations were made:

Using the above-mentioned expected patterns of uptake, **^{68}Ga-citrate PET (considered in isolation)** performed as follows:

- For benign lesions a **100% sensitivity** and a **100% negative predictive value** was calculated. Specificity and PPV was 57.7% and 47.6% respectively.
- For malignant lesions the following: **Specificity: 77.3%, NPV: 77.3%,** Sensitivity: 64.3%, PPV: 64.3%
- Distinguishing benign (n=22) from malignant lesions (n=14): **Sensitivity: 77.3%, NPV: 77.3%,** Specificity: 36%, PPV: 65.4%
- PET correctly predicted the nature of the lesion in 26/36 cases (72%), compared to CT's correct prediction in 28/36 (77.78%). However, if we exclude the cases (n=7) where CT was correct only because an extensive differential diagnosis was provided, its performance falls to 21/36 (58.335)
- It would be safe to say that PET is at least as accurate in the predicition of the nature of indeterminate lesions as CT and possibly more accurate.

Discussion

Distinguishing benign from malignant lesions in the lung continues to present a major problem, with no clear set of distinguishing features on conventional imaging to guide further patient management.

Although dual-phase imaging with ^{18}F-FDG has been shown to be useful in certain settings[19], it has not been helpful in settings with a high prevalence of granulomatous lung diseases. These diseases often go hand in hand with a high prevalence of immunocompromised individuals, which complicates reaching a diagnosis even further. More often than not, a multitude of investigations are undertaken, which still often result in the need for bronchoscopy with biopsy for histological confirmation. Even then, histology may still not provide a clear answer.

The limitations of PET/CT imaging with F-18-FDG are well known and especially in settings where limited access to cyclotrons exist, there is a need for a reliable, simple to label, generator-based PET tracer, such as Gallium-68. There is renewed interest in ^{68}Ga-labeled compounds due to the many imaging advantages,which includes round-the-clock availability, the short half-life, labeling possibilities and anticipated higher cost-effectiveness, amongst many others.Considering the fact that ^{67}Ga-citrate has served nuclear physicians well in the past with the diagnosis of various lung conditions (especially in the setting of immune compromised individuals), it would make sense to also evaluate the use of ^{68}Ga-citrate in these settings. Especially in light of ^{68}Ga-citrate's superior imaging qualities, half-life and dosimetry when compared to ^{67}Ga-citrate.

Several authors have investigated the use of ^{68}Ga-citrate in the evaluation of various infectious and inflammatory conditions. Sofar, the most promising results have been found with the imaging of musculoskeletal infections.[13,14]
Vijay Kumar et al. demonstrated the potential use of ^{68}Ga-apo-transferrin (^{68}Ga-TF) in the detection of *Staphylococcus aureus* infection and Gram-negative *Proteus mirabilis* with very promising results.[20]

In the setting of respiratory disease the use of other ^{68}Ga-tracers , such as ^{68}Ga-labeled siderophore desferri-triacetylfusarinine C has been used to display highly selective accumulation by *Aspergillus fumigatus in vivo*. This could potentially be useful to image invasive pulmonary aspergillosis, which may benefit patients who are immunosuppressed.[21]
In addition, Ambrosini and co-workers have found ^{68}Ga-DOTANOC PET imaging to be useful in the evaluation of idiopathic pulmonary fibrosis (IPF) and non-specific interstitial pneumonia (NSIP).[22]

With this study we proposed the novel use of ^{68}Ga-citrate for imaging of lung lesions of an indeterminate nature.From our initial experience, the labeling method is relatively simple, the image quality is good and dual-point imaging up to 2 hrs post-injection is possible. Also, the dosimetry compares favourably to that of ^{18}F-FDG[17] and normal bio-distribution does not include any lung uptake, which would provide good lesion to background ratios.

Our hypothesis therefore was that imaging with ^{68}Ga-citrate could be used to distinguish benign from malignant lesions in the lung. We postulated that the SUVmax could be used to determine a clear cutoff value between malignant, tuberculous and other benign lesions in the lung. In addition, we hypothesized that ^{68}Ga-citrate would not suffer from the same limitations as ^{18}F-FDG in that it would also be abe to distinguish these lesions even in a setting with a high prevalence of granulomatous disease (which is known to imitate malignant behaviour with ^{18}F-FDG).

Our results demonstrated very low or absent tracer accumulation in lesions where no malignant or inflammatory cells could be demonstrated on histology. Other benign lesions, such as infective changes or sarcoidosis demonstrated slightly higher uptake, which was still relatively low to the uptake of malignant lesions. Malignant and tuberculous lesions, demonstrated higher ^{68}Ga-citrate uptake with considerable overlap in the SUV_{max}, which made accurate differentiation between these two processes impossible.

Making use of various lesion to background/ reference ratios, similarly could not accurately differentiate between malignant and tuberculous lesions, despite being able to accurately differentiate tuberculous lesions from other benign lung lesions.

Taking into consideration that the study may be underpowered to compare three groups of pathology, the following **observations** or **trends** seem worth highlighting, (despite the lack of ststistical significance in this study):

- All of the malignant lesions in this study (including two tumours of neuro-endocrine origin) demonstrated increased tracer accumulation, which may be indicative of few false negatives.

- Malignant lung lesions were often associated with diffusely increased bone marrow uptake, which was more intense than that seen in patients with benign lesions. One possible explanation could be that malignant lesions are often accompanied by anemia of chronic disease, which may cause diffusely increased bone marrow and splenic uptake of ^{68}Ga-citrate. Another factor may be increased transferrin expression[23]. This could potentially bring about significant differences in ratios when using the RES as

reference in trying to distinguish malignant from granulomatous lesions. This would require further investigation and validation in a larger sample.

- Tuberculous lesions demonstrated variable tracer uptake. Areas of increased ^{68}Ga-citrate often indicated less extensive involvement than what was noted on CT and could be indicative of areas of of active disease. It may therefore prove helpful in the follow-up evaluation of treatment response. PET images with ^{68}Ga-citrate also revealed additional areas of extra-pulmonary involvement in some patients.

- Importantly,five patients in our study demonstrated no tracer accumulation in the lesions noted on CT and were found on histology not to have any malignant, infective- or inflammatory changes. This indicates a possible role for ^{68}Ga-citrate as a tracer with a good negative predictive value. Patients who present with these photopenic lesions corresponding to suspicious lesions noted on morphological imaging, could therefore be followed up instead of having to undergo invasive diagnostic procedures, such as lung biopsy. All of the patients who had histology which did not reveal any malignant, inflammatory or infective cells, demonstrated no uptake of ^{68}Ga-citrate in these lesions (100% NPV).

Future considerations should include a large number of participants and comparing the findings to 18F-FDG. Furthermore improvements on the present study would be the addition of dynamic imaging with kinetic modeling and more imaging time points in order to evaluate different washout rates of ^{68}Ga-citrate in benign, malignant and tuberculous lesions. Quantification of lung lesions on PET could also be optimized.

Conclusion

This study, as the first human study using ^{68}Ga-citrate for *in vivo* lung pathology imaging, demonstrated that 68Ga-Citrate PET has a potential for detection of malignancy. Although it has higher ability to detect Tuberculosis lesions than CT, 68Ga-Citrate seems unable to provide a clear distinction between malignant and benign lung lesions in a setting with a high prevalence of granulomatous diseases such as Tuberculosis. Larger trials are needed in order to better evaluate this novel application as well as the role of dual time point imaging.

References

1. Jones YM, Irion KL, Holemans JA. A review of the imaging and clinical management of solitary pulmonary nodules. Imaging. 2008 Nov 30;20(4):303–11.

2. Kim SKS, Allen-Auerbach MM, Goldin JJ, Fueger BJB, Dahlbom MM, Brown MM, et al. Accuracy of PET/CT in characterization of solitary pulmonary lesions. J Nucl Med. 2007 Jan 31;48(2):214–20.

3. Tsushima YY, Tateishi UU, Uno HH, Takeuchi MM, Terauchi TT, Goya TT, et al. Diagnostic performance of PET/CT in differentiation of malignant and benign non-solid solitary pulmonary nodules. Ann Nucl Med. 2008 Jul 31;22(7):571–7.

4. Sathekge MM, Maes AA, Kgomo MM, Stoltz AA, Pottel HH, Van de Wiele CC. Impact of FDG PET on the management of TBC treatment. A pilot study. Nuklearmedizin. 2009 Dec 31;49(1):35–40.

5. Sathekge MMM, Maes AA, Pottel HH, Stoltz AA, van de Wiele CC. Dual time-point FDG PET-CT for differentiating benign from malignant solitary pulmonary nodules in a TB endemic area. S Afr Med J. 2010 Aug 31;100(9):598–601.

6. Alavi AA, Gupta NN, Alberini J-LJ, Hickeson MM, Adam L-EL, Bhargava PP, et al. Positron emission tomography imaging in nonmalignant thoracic disorders. YSNUC. 2002 Sep 30;32(4):293–321.

7. Mavi AA, Lakhani PP, Zhuang HH, Gupta NCN, Alavi AA. Fluorodeoxyglucose-PET in characterizing solitary pulmonary nodules, assessing pleural diseases, and the initial staging, restaging, therapy planning, and monitoring response of lung cancer. Radiol Clin North Am. 2004 Dec 31;43(1):1–ix.

8. Tsan MF. Mechanism of gallium-67 accumulation in inflammatory lesions. J Nucl Med. 1985 Jan;26(1):88–92.

9. Weiner RE. The mechanism of 67Ga localization in malignant disease. Nuclear Medicine and Biology. 1996 Aug;23(6):745–51.

10. Chen DC, Newman B, Turkall RM, Tsan MF. Transferrin receptors and gallium-67 uptake in vitro. Eur J Nucl Med. 1982;7(12):536–40.

11. Tsuchiya Y. Relationship between gallium 67 citrate scanning and transferrin receptor expression in lung diseases. Chest. American College of Chest Physicians; 1992 Aug 1;102(2):530–4.

12. AL-Nahhas A, Win Z, Szyszko T, Singh A, Khan S, Rubello D. What can gallium-68 PET add to receptor and molecular imaging? Eur J Nucl Med Mol Imaging. 2007 Aug 23;34(12):1897–901.

13. Mäkinen TJ, Lankinen P, Pöyhönen T, Jalava J, Aro HT, Roivainen A. Comparison of 18F-FDG and 68Ga PET imaging in the assessment of experimental osteomyelitis due to Staphylococcus aureus. Eur J Nucl Med Mol Imaging. 2005 Nov 9;32(11):1259–68.

14. Nanni C, Errani C, Boriani L, Fantini L, Ambrosini V, Boschi S, et al. 68Ga-Citrate PET/CT for Evaluating Patients with Infections of the Bone: Preliminary Results. J Nucl Med. 2010 Dec 1;51(12):1932–6.

15. de Blois E, Sze Chan H, Naidoo C, Prince D, Krenning EP, Breeman WAP. Characteristics of SnO2-based 68Ge/68Ga generator and aspects of radiolabelling DOTA-peptides. Appl Radiat Isot. 2011 Feb;69(2):308–15.

16. Kumar V, DK B, SG E, S A. (68)Ga-Citrate-PET for diagnostic imaging of infection in rats and for intra-abdominal infection in a patient. Curr Radiopharm. 2012 Jan 1;5(1):71–5.

17. Rizzello A, Di Pierro D, Lodi F, Trespidi S, Cicoria G, Pancaldi D, et al. Synthesis and quality control of 68Ga citrate for routine clinical PET. Nucl Med Commun. 2009 Jul;30(7):542–5.

18. Miller RF. Nuclear medicine and AIDS. Eur J Nucl Med. 1990;16(2):103–18.

19. Lin Y-Y, Chen J-H, Ding H-J, Liang J-A, Yeh J-J, Kao C-H. Potential value of dual-time-point ^{18}F-FDG PET compared with initial single-time-point imaging in differentiating malignant from benign pulmonary nodules: a systematic review and meta-analysis. Nucl Med Commun. 2012 Oct;33(10):1011–8.

20. Kumar V, Boddeti DK, Evans SG, Roesch F, Howman-Giles R. Potential use of 68Ga-apo-transferrin as a PET imaging agent for detecting Staphylococcus aureus infection. Nucl Med Biol. 2011 Apr 1;38(3):393–8.

21. Petrik MM, Franssen GMG, Haas HH, Laverman PP, Hörtnagl CC, Schrettl MM, et al. Preclinical evaluation of two (68)Ga-siderophores as potential radiopharmaceuticals for Aspergillus fumigatus infection imaging. Eur J Nucl Med Mol Imaging. 2012 Jun 30;39(7):1175–83.

22. Ambrosini V, Zompatori M, De Luca F, Antonia D, Allegri V, Nanni C, et al. 68Ga-DOTANOC PET/CT Allows Somatostatin Receptor Imaging in Idiopathic Pulmonary Fibrosis: Preliminary Results. J Nucl Med. 2010 Nov 23;51(12):1950–5.

23. Wang S-J, Gao C, Chen B-A. Advancement of the study on iron metabolism and regulation in tumor cells. Chin J Cancer. 2010 Apr;29(4):451–5.

Chapter 6: ^{68}Ga-citrate imaging in TB: a pilot study

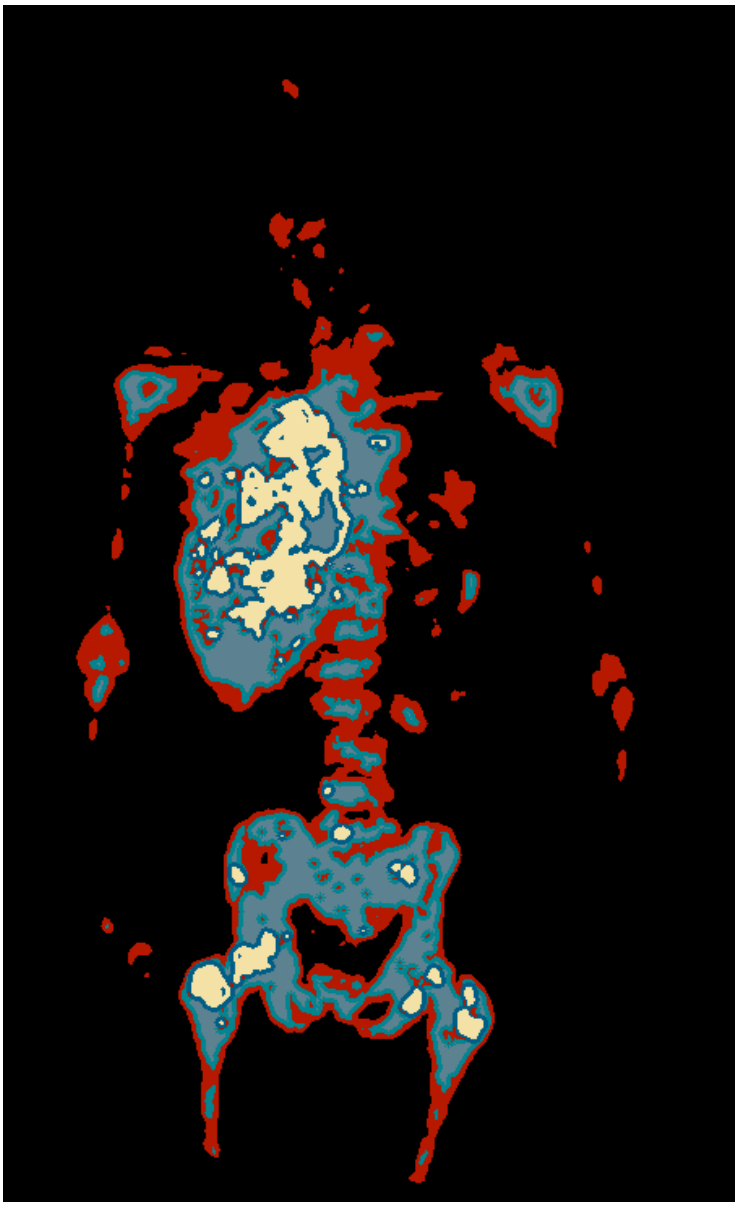

*An adapted version of this chapter has been accepted for publication in the Quarterly Journal of Nuclear Medicine.

^{68}Ga-citrate PET/CT in Tuberculosis: A pilot study

Vorster M_1, Maes A_2, Van de Wiele C_3, Sathekge MM_1

University of Pretoria, Department of Nuclear Medicine, Steve Biko Academic Hospital$_1$

Department of Nuclear Medicine AZ Groeninge, Reepkaai, Kortrijk, Belgium $_2$

Department of Nuclear Medicine, University hospital Ghent, Ghent, Belgium $_3$

Abstract

Purpose

To describe image findings on ^{68}Ga-citrate PET/CT in patients with Tuberculosis

Methods

Thirteen patients with tuberculosis underwent PET/CT imaging with ^{68}Ga-citrate. Tuberculosis was diagnosed with bacteriological or histopathology studies (n=8) or based on a combination of clinical data, biochemistry and imaging (n=5). Study participants were imaged at 60 minutes following IV administration of 185 MBq of ^{68}Ga-citrate. Seven patients underwent additional delayed imaging at 120 minutes post-injection. PET images were analyzed both qualitatively (relative to liver uptake) and semi-quantitatively (making use of SUVmax) and compared to CT findings. Clinical data, other imaging- and biochemistry results were also reviewed.

Results

Five patients (38.5%) had confirmed concomitant HIV infection. All 13 patients demonstrated abnormal tracer accumulation in the lungs or extra-pulmonary or both. (Median SUVmax of 3.71 25th percentile=2.l9; 75th percentile=4.95). ^{68}Ga-citrate accumulated in every lung lesion noted on CT in six cases (46%). In the other seven cases (54%) some of the lung lesions noted on CT were not ^{68}Ga-citrate avid, which is consistent with non-active tuberculous lesions. Ten patients (77%) demonstrated extra-pulmonary involvement, which included various lymph node groups, skeletal lesions, and involvement of the pleura, spleen and gastro-intestinal tract. Detection of extra-pulmonary involvement was higher on PET compared to CT (more lesions detected) in eight cases (80%). The remaining two cases (20%) demonstrated equal detection on both modalities and none of these patients demonstrated central nervous involvement on either study.

Conclusion

^{68}Ga-citrate PET accumulates in both pulmonary and extra-pulmonary tuberculous lesions and may provide a way of distinguishing active from inactive lesions for treatment response evaluation. In addition, ^{68}Ga-citrate PET appears superior to CT in the detection of extra-pulmonary involvement.

Introduction

Tuberculosis is a major contributor to mortality and morbidity in developing countries and continues to present physicians with diagnostic challenges. In the South African setting, these problems are compounded by the frequent co-infection with HIV, subsequent re-activation associated disease and the relatively high prevalence of drug-resistant Tuberculosis.[1-3]

Imaging with PET/CT provides clinicians with a non-invasive tool, which is capable of early detection, assessment of the extent of pulmonary and extra-pulmonary involvement as well as evaluation of treatment response. As such, investigation with PET/CT is potentially invaluable in the management of patients infected with Mycobacterium Tuberculosis.

The most frequently used PET tracer in this setting to date is ^{18}F-FDG. However, several studies have demonstrated its limitations in distinguishing TB from malignant lesions. In addition, the normal bio-distribution of ^{18}F-FDG impedes interpretation of possible tuberculous involvement in the CNS, CVS, genito-urinary- and gastro-intestinal tracts.

^{67}Gallium-citrate SPECT imaging has been widely used in the setting of immunosuppression with suspected lung involvement. Imaging with the PET tracer ^{68}Gallium-citrate should theoretically provide the same clinically useful information with the added advantages of PET/CT imaging. These include better resolution, improved logistics with shorter imaging time and less radiation exposure. In addition, this generator-produced tracer provides round-the clock, yearlong availability.[4,5] However, to the best of the author's knowledge, ^{68}Ga-citrate has not yet been evaluated in this setting.

The aim of this pilot study was to describe ^{68}Ga-citrate PET/CT findings in patients with tuberculosis.

Materials and methods

Study population

Thirteen patients with a diagnosis of tuberculosis were included prospectively in this study following written informed consent. Approval to conduct this study was granted by the Ethics Committee of the University Hospital of Pretoria.
Tuberculosis was diagnosed with bacteriological or histopathology studies (n=8) or based on a combination of clinical data, biochemistry and imaging (n=5).

Labeling protocol for ^{68}Ga-citrate

A SnO_2-based ^{68}Ge/^{68}Ga generator with a 1.85 GBq loading activity (iThemba LABS, Somerset West, South Africa) was used for radiolabeling.[6]
^{68}Ga-citrate synthesis was performed manually in a straightforward, one-step-aseptic procedure, which was based on a combination of the protocols used by Kumar [7] and Rizzello [8] All routine quality control requirements were met.

Image acquisition

Study participants were imaged at 60 minutes following IV administration of 185 MBq of ^{68}Ga-citrate. Seven patients underwent additional delayed imaging at 120 minutes post-injection. Both oral (Barium in water) and IV contrast (100 ml Ultravist, at a rate of 2ml/s) was administered, except where a contra-indication, such as inadequate kidney function or an allergy to Iodine existed. Images were acquired in a three-dimensional mode with a 4-minute emission scan for each of on average 7-9 bed positions (Matrix size 512x512) from the skull base to the pelvis. Reconstruction of images with and without attenuation correction (CT based) was done using OSEM (ordered subset expectation maximization) to yield axial, sagittal and coronal slices. For diagnostic CT scanning, the following parameters were used: collimation of 24 x 1.2 mm; gantry rotation time of 500ms; tube voltage of 120kV; effective tube current of 100 mAs with online tube current modulation and a table feed of 18mm/rotation.

Image interpretation

Qualitative

All images were initially evaluated qualitatively. Any tracer accumulation outside of the normal bio-distribution was considered abnormal. The intensity of the uptake was compared visually to that of the liver, according to the following scale: 1/low=less intense than the liver, 2/moderate= equal to the liver, 3/high=more intense than the liver. Other authors in the interpretation of ^{67}Ga-citrate imaging have also used a similar scale.[9]

Quantitative

A region of interest was drawn manually around any abnormal tracer accumulation in such a way as to correspond to the size of the lesion on CT. The SUVmax was recorded for each lesion. This value is obtained from the following calculation: SUV=radiotracer activity x patient weight/injected dose. We used the maximum SUV (SUV_{max}) in this study, which represents the pixel with the highest tracer uptake in the lesion.The SUVmax was then recorded and compared to the SUVmax of various reference points, such as the mediastinal blood pool, the liver, spleen and bone marrow in order to calculate various ratios.

Where dual time point imaging was performed (n=7), a second SUVmax was recorded. The 60 min value was labeled $SUVmax_1$ and the 120 min image $SUVmax_2$. The change in SUVmax was calculated as follows (and expressed as a percentage change up or down):
The difference between $SUVmax_1$ and $SUVmax_2$/ $SUVmax_1$ x 100

Results

Demographics

The study participants consisted of five males (38.5%) and eight females (61.5%) with a median age of 40 years. Four patients (31%)were Caucasian and nine (69%) were Black.

Clinical presentation

The most frequent clinical presentation was one or a combination of the following: a productive or non-productive, intermittent cough (hemoptysis rarely reported), dyspnea, chest pain and loss of weight. None of these patients reported a history of previous TB. Five patients (38.5%) had confirmed concomitant HIV infection and were presumed to have reactivation TB. (Seven patients had already started with anti-tuberculous treatment regimes).

Procedural

The average injected dose of ^{68}Ga-citrate was 196 MBq (155-255MBq), with 185 MBq the most frequently given dose. The average radiochemical purity determined by ITLC-SG was 98.9% ± 0.94% which was confirmed by HPLC. The pH value of the product for injection was 4.0-4.5. All other requirements for QC were met. IV contrast was administered in ten patients (77%).

PET/CT Findings

Images obtained at 60 minutes post-injection of (on average) 185 MBq of ^{68}Ga-citrate, resulted in good quality images. ^{68}Ga-citrate images demonstrated high vascular activity, as has been demonstrated before. In addition, normal bio-distribution demonstrated increased tracer accumulation in the salivary glands, liver, spleen and bone marrow. Mean SUVmax values in areas of normal tracer bio-distribution, were as follows: Liver 0.94 +/- 0.44; Mediastinal blood pool 0.77+/-0.44; spleen 1.44 +/- 0.89; Bone marrow 1.29+/-0.71. Qualitative evaluation (relative to the liver intensity) demonstrated low ^{68}Ga-citrate uptake in 5 patients (38.5%) moderate to high uptake in five (38.5%) and high tracer accumulation in three (23%). (See Table 1 for individual patient details.)

No	Lung lesion	Other areas of involvement	Diagnostic modality and detail	^{68}Ga-uptake*
1	Right upper lobe nodule	None	Sputum	Low
2	Left upper lobe nodule	None	Combination clinical & imaging	Low
3	Left upper lobe mass	Cervical-& Mediastinal lymph nodes	PCR, sensitive to INR & Rifampicin	Moderate
4	Right upper lobe nodules	Multiple lymph nodes, spleen, GIT	Liver biopsy: Large numbers of AFBs on Ziehl-Neelsen stain	Low
5	Right pleural effusion	Right hemi-thorax, mediastinal lymph nodes, skeletal, soft tissue	Pleural fluid analysis	High
6	Left lung nodule	None	Combination clinical & imaging	Moderate
7	Left lung changes	Mediastinal, axillary & inguinal lymph nodes	Sputum MCS	Moderate
8	Mediastinal lymph nodes	Skeletal, spleen, kidneys lymph nodes, soft tissue	Combination clinical & imaging	High
9	Right upper lobe changes	Mid-thoracic spine (T6-T8)	PCR, sensitive to INR & Rifampicin	Low
10	Bilateral apical thick-walled cavitations	Skeletal, soft tissues, lymph nodes	Combination clinical & imaging	High
11	Left upper lobe cavities	Mediastinal lymph nodes	PCR, sensitive to INR & Rifampicin	Moderate to high
12	Mediastinal mass	Widespread lymph nodes, spleen, mycotic aneurysm	Combination clinical & imaging	Low
13	Right lung apex	Lymph nodes (supra-clavicular, porta hepatis)	AFB+ on aspirates	Moderate to high

Table 1: Individual patient diagnostic details

- Low=less than the liver, Moderate=equal to liver, High=more than the liver

Dual time point imaging demonstrated a decrease in SUVmax from 60 min to 120 min in five patients (71.43%) ranging from 2%-34%, and an increase in two patients (28.57%) of 24% and 32%.

All 13 patients demonstrated abnormal tracer accumulation in the lungs or extra-pulmonary or both. (Median SUVmax of 3.71 25th percentile=2.l9; 75th percentile=4.95).

^{68}Ga-citrate accumulated in every lung lesion noted on CT in six cases (46%). In the other seven cases (54%) some of the lung lesions noted on CT were not ^{68}Ga-citrate avid, which is consistent with non-active tuberculous lesions (See Fig 1 for an example of active pulmonary

TB). Ten patients (77%) demonstrated extra-pulmonary involvement, which included the pleura (see Fig 2), various lymph node groups (see Fig 3), skeletal lesions (see Fig 4) and involvement of various soft tissues (see Fig 5), the spleen and gastro-intestinal tract. Detection of extra-pulmonary involvement was higher on PET compared to CT (more lesions detected) in eight cases (80%). The remaining two cases (20%) demonstrated equal detection on both modalities and none of these patients demonstrated central nervous involvement on either study.

Fig 1a) A 57 yr old HIV negative female presented with a mass in the left upper lobe (3.5 cmx 3 cm) on CXR. PCR demonstrated Mycobacterium tuberculosis complex, sensitive to INH and Rifampicin.

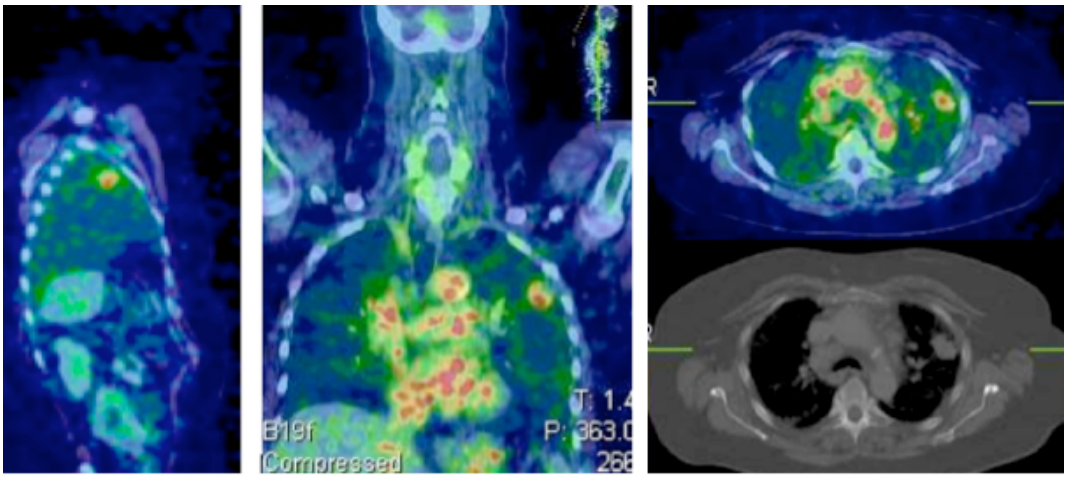

1b)

Fig 1 b) PET/CT images were acquired 60 min following IV injection of 166.5 MBq of ^{68}Ga-citrate. IV contrast was given. Moderately increased tracer uptake was noted in the LUL mass (SUVmax: 5.24, Liver: 6.10)

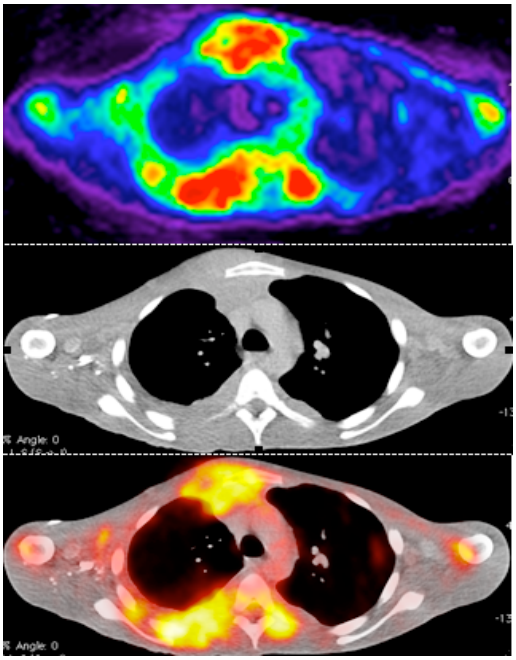

Fig 2 A 28 yr old man with a large right-sided pleural effusion and Mycobacterium Tuberculosis on pleural fluid analysis. Dual-time point imaging was performed at 60 min and 120 min following IV administration of 224.59 MBq (6.07 mCi) of ^{68}Ga-citrate and IV contrast. Intense tracer accumulation was noted in the anterior chest wall and posterior thickened pleura on the right. ($SUVmax_1$ 7.42; $SUVmax_2$ 7.17; decrease of 3.4 %) Liver SUVmax: 3.90

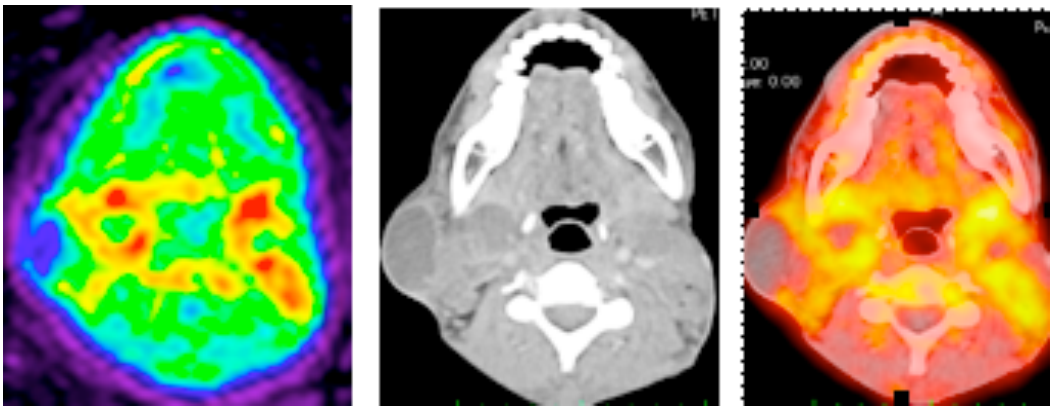

Fig 3 40 yr old man with TB and HIV-co-infection demonstrating enlarged lymph nodes with necrotic centers and peripheral rim tracer accumulation, similar to what has been demonstrated with 18F-FDG PET/CT. 232MBq (6.3 mCi) of ^{68}Ga-citrate was injected IV, uptake time 60 min, IV contrast given.

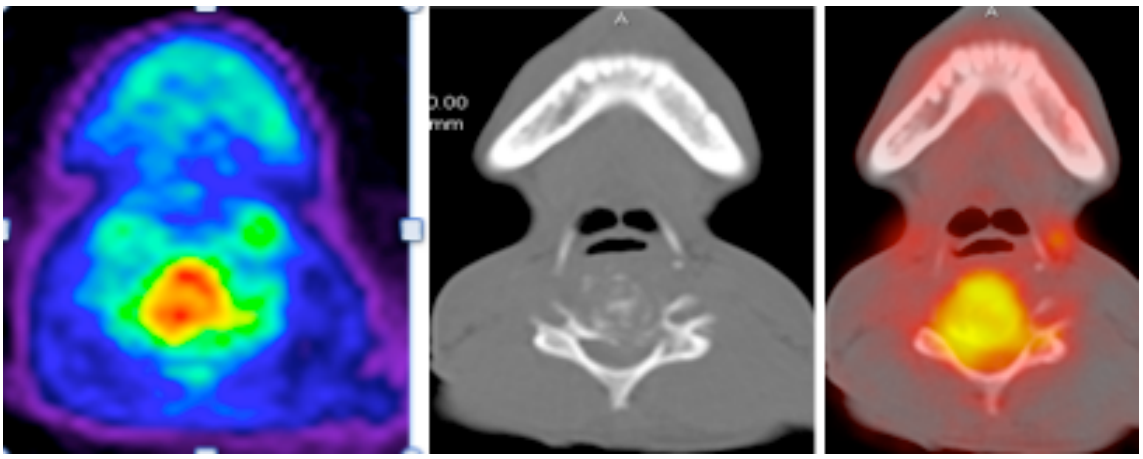

Fig 4 A 44 yr old male with HIV and TB (Absolute CD4 196 x106/l) who presented with quadriparesis. CT demonstrates destruction of the vertebral bodies of C4/C5 and the intervertebral disc with intense tracer accumulation in this region. Dual-time point imaging was performed following IV injection of 257.5 MBq (6.96mCi) of ^{68}Ga-citrate and IV contrast. $SUVmax_1$ of 3.83 decreased by 2% to a $SUVmax_2$ of 3.75. (Liver SUVmax: 3.24).

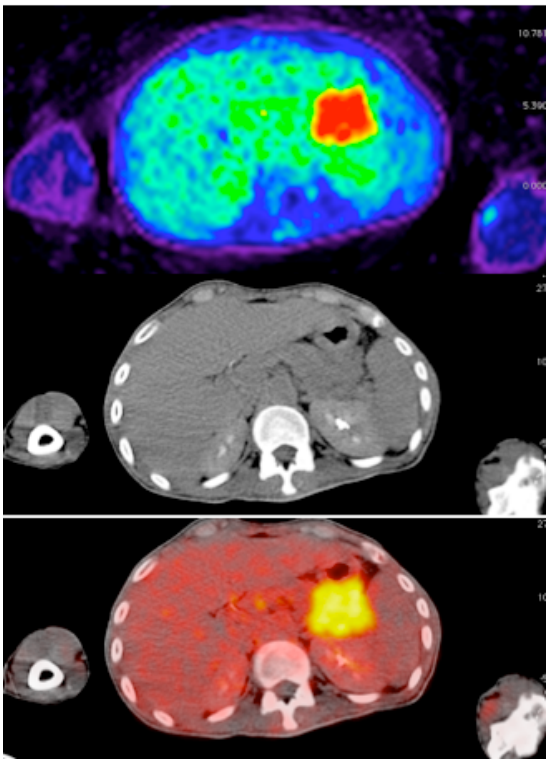

Fig 5 PET/CT images demonstrate intense ^{68}Ga-citrate uptake in this left-sided psoas abscess in a 44 yr old male patient with concomitant HIV infection. (SUVmax: 6.89;Liver SUVmax: 3.24) 257.5 MBq (6.96 mCi) of ^{68}Ga-citrate and IV contrast was administered.

CT Findings

On CT, the upper lobes were the most frequently involved areas (consisting of nodules and cavitations), followed by mediastinal- and other lymph node involvement as well as pleural involvement.

Additional special investigations

All patients also had a chest radiograph prior to PET/CT imaging, which was abnormal in only four cases (31%).

Hyponatremia as a result of inappropriate ADH secretion has been reported in patients with pulmonary disease and more specifically, in tuberculosis.[10] We have noticed the same trend; where recent sodium results were available (n=8), six patients (75%) demonstrated low sodium values (ranging from 127 to 134 mmol/l). The other two patients had values that were on the very low limit of normal.

Another frequent biochemistry abnormality is an abnormal full blood count (FBC), which in our study was present in all of the patients who had a recent FBC (n=10). The most frequently observed abnormality was anemia (with hemoglobin values ranging from 7.4-13.7 g/dl) and the presence of pancytopenia in two patients. Albumin levels were low in all, ranging from 24-30 g/l. In the patients with confirmed HIV infection, CD4 and viral counts were not readily available.

Statistical Analysis

Descriptive statistics were used to report patient characteristics and procedural details. Summary statistics is presented as mean (SD, standard deviation) or as median (IQR, interquartile range) in case of non-normality of the data. Numbers or percentages are reported otherwise. Statistical analysis was performed with STATA version 10.

Discussion

The importance of tuberculosis (TB) and its impact on mortality and morbidity is indisputable worldwide and even more so in countries with a high prevalence of Human Immunodeficiency Virus (HIV) co-infection and increasing multi-drug resistance. Development of a non-invasive diagnostic tool capable of early and accurate detection, staging and follow-up evaluation of tuberculosis is therefore of the utmost importance in minimizing the devastating effects of TB.

The pathophysiology of Tuberculosis is still incompletely understood, but involves both protective and immune-pathogenic mechanisms. According to surveys done with Tuberculin skin tests (TST) more than 2 billion people have a latent *Mycobacterium tuberculosis* infection.[11] Reactivation may occur with any compromise to the host's immunity, as is seen with (amongst others) HIV co-infection, other viral- and bacterial infections, diabetes and treatment with TNF/ interleukin blockers. Although the host immune response is dominated by several specialized T-cells ($CD4^+$ Th_1, Th17, $CD8^+$, Treg) and phagosomes, B-cells and NK cells also play a role, supported by various cytokines and interleukins.[11]

Airborne tuberculosis bacilli reach the alveolar space where macrophages, local dendritic cells and epithelial cells that line the bronchi and alveoli rapidly take it up. *Mycobacterium tuberculosis* then delays onset of the host's adaptive immune response for 2-3 weeks, presumably in order to establish a critical bacilli mass. This is probably achieved most by bringing about a delay in the migration of infected dendritic cells to the draining lymph nodes, thereby interfering with the "homing" process. *Mycobacterium tuberculosis* persists in the infected host cells where it evades the host immune response by inhibiting the maturation of bacterial phagosomes, apoptosis, antigen processing and IFN-γ receptor-mediated signaling. Triggering of the host's protective immune response eventually leads to granuloma formation, which consists of centrally located M Tuberculosis and macrophages and peripheral T-cells. Experimentation with a zebra fish model[12] has demonstrated that granulomas are actually dynamic structures that host cells can move in and out of quickly. Uncontrolled local infection and inflammation finally results in caseous necrosis, which greatly promotes further bacterial growth and airborne spread of large numbers of bacilli.[11]

The acquired immunodeficiency syndrome epidemic has lead to a higher incidence of tuberculosis with changed disease patterns and increases in disseminated and extra-pulmonary involvement. Extra-pulmonary tuberculosis can occur with or without pulmonary involvement and may affect any organ. The most frequently reported affected sites include lymph nodes, the pleurae, musculoskeletal, gastro-intestinal and genito-urinary tract involvement.[13] Despite recent advances; the diagnosis of extra-pulmonary involvement remains problematic, since obtaining tissue or fluid for analysis from these sites is not always possible and is invasive. The correct assessment of the disease extent is important when deciding on the correct treatment regimen, since it involves prolonged treatment and, in some cases, the addition of corticosteroids.

In our study, all of the patients with HIV co-infection had pulmonary and extra-pulmonary involvement. Despite neurological symptoms in two patients, no central nervous system involvement was be demonstrated on ^{68}Ga-citrate PET/CT. This is consistent with the findings reported by Lin and Hsieh.[14]

Current diagnostic modalities include a variety of tests ranging from clinical evaluation, imaging and skin tests to advanced serological-, immunological and histopathological analysis. Unfortunately, all of these suffer from various limitations in sensitivity and specificity and may only be useful in particular clinical situations. It seems that the gold standard remains bacteriological cultures for now, which is not always possible and causes a significant delay in reaching the diagnosis.[15,16]

Imaging in the form of PET/CT provides a non-invasive diagnostic tool, which combines the high-resolution morphological information of CT with the molecular information on disease activity gained from PET. In addition, PET/CT is able to assess the extent of whole body involvement in one investigation and evaluate treatment response early on. While radiological features may remain unchanged during early treatment, evaluation with PET provides an early indication of response to treatment.

Several authors have now investigated the use of ^{18}F-FDG PET/CT in settings with a high prevalence of granulomatous disease**.** ^{18}F-FDG PET/CT is essentially based on the detection of increased glucose metabolism, which in TB is mainly due to increased macrophage and neutrophil activity.

Sathekge et al. made the following contributions with regards to ^{18}F-FDG PET/CT imaging in tuberculosis:

- ^{18}F-FDG detects more tuberculous lesions, especially extra-pulmonary, when compared to CT
- The number of lymph node bastions can be used to predict treatment response in patients with TB and HIV co-infection. Five bastions provide the cut-off between treatment responsive and non-responsive TB patients (sensitivity 88%, specificity 81%, NPV 93%)[17]
- A higher SUVmax was also noted in the lymph nodes of non-responders. A cut-off of 4.5 can be used to discriminate between responders and non-responders with a sensitivity of 95% and specificity of 85%.[17]
- Lymph nodes with central attenuation and peripheral enhancement were also associated with non-response to tuberculostatics.[18]

Several authors have also demonstrated the value of 18F-FDG PET/CT in follow-up and treatment response evaluation of TB, especially with extra-pulmonary involvement and where drug-resistance is prevalent.[19-21]

Soussan et al. identified two different patterns of tuberculosis on FDG-PET; a pulmonary type with a more localized type of infection and a lymphatic pattern of involvement associated with a more intense, systemic infection.[22]

Despite the above-mentioned advances made, several limitations remain, such as the inability to differentiate between malignant lesions and TB.[23,24]
Other disadvantages include the need for a nearby cyclotron as well as the inability to accurately detect lesions in the areas of normal tracer bio-distribution.

The uptake mechanism of Gallium is complex, incompletely understood and involves several direct as well as indirect mechanisms. Local inflammation and vasodilation results in increased tracer accumulation due to higher tracer delivery (indirect), while direct mechanisms are the result of Gallium's similarity to iron. Its accumulation in tuberculous

lesions is believed to be the result of transcapillary exudation of transferrin-bound gallium and subsequent binding to leucocytes and bacteria. Gallium accumulation is therefore unaffected by the impaired cellular immunity found in patients with HIV.[25]

Gallium scintigraphy (in the form of ^{67}Ga-citrate) has played an important role in the diagnosis and management of patients with TB and HIV as early as the 1970s. Sarkar et al. evaluated the use of ^{67}Ga-citrate imaging in eleven patients with suspected extra-pulmonary involvement and found that it could correctly predict the absence or presence of active disease. They also suggested that ^{67}Ga-citrate should be routinely used in patients with suspected extrapulmonary involvement and that it would probably be valuable in the follow-up evaluation since scan findings correlated well with clinical improvement.[26] Several other authors have evaluated the use of Gallium imaging in patients with immuno-suppression and lung diseases such as tuberculosis with similar conclusions reached.[9,27-29]

In summary, PET/CT imaging provides clinicians with a one-stop non-invasive tool for the assessment and response evaluation of active pulmonary-, and especially extra-pulmonary, tuberculosis. ^{68}Ga-citrate is an alternative generator-produced PET tracer, which could potentially be more cost-effective and may suffer from fewer limitations when compared to ^{18}F-FDG. Larger trials with ^{68}Ga-citrate are needed to evaluate the value of dual-time point imaging in distinguishing tuberculosis from malignant lesions.

Conclusion

^{68}Ga-citrate PET accumulates in both pulmonary and extra-pulmonary tuberculous lesions and may provide a way of distinguishing active from inactive lesions for treatment response evaluation. In addition, ^{68}Ga-citrate PET appears superior to CT in the detection of extra-pulmonary involvement.

References

1. Karim SSA, Churchyard GJ, Karim QA, Lawn SD. HIV infection and tuberculosis in South Africa: an urgent need to escalate the public health response. The Lancet. 2009 Sep;374(9693):921–33.

2. Gandhi NR, Moll A, Sturm AW, Pawinski R, Govender T, Lalloo U, et al. Extensively drug-resistant tuberculosis as a cause of death in patients co-infected with tuberculosis and HIV in a rural area of South Africa. The Lancet.2006 Nov 4;368(9547):1575–80.

3. Dheda K, Shean K, Zumla A, Badri M, Streicher EM, Page-Shipp L, et al. Early treatment outcomes and HIV status of patients with extensively drug-resistant tuberculosis in South Africa: a retrospective cohort study. The Lancet.2010 May 22;375(9728):1798–807.

4. Roesch F, Riss PJ. The renaissance of the ^{68}Ge/^{68}Ga radionuclide generator initiates new developments in ^{68}Ga radiopharmaceutical chemistry. Curr Top Med Chem. 2009 Dec 31;10(16):1633–68.

5. Rosch F. Past, present and future of (68)Ge/(68)Ga generators. Appl Radiat Isot. 2012 Nov 21.

6. de Blois E, Sze Chan H, Naidoo C, Prince D, Krenning EP, Breeman WAP. Characteristics of SnO2-based 68Ge/68Ga generator and aspects of radiolabelling DOTA-peptides. Appl Radiat Isot. 2011 Feb;69(2):308–15.

7. Kumar V, Boddeti DK, Evans SG, Angelides S. (68)Ga-Citrate-PET for diagnostic imaging of infection in rats and for intra-abdominal infection in a patient. Curr Radiopharm. 2012 Jan;5(1):71–5.

8. Rizzello A, Di Pierro D, Lodi F, Trespidi S, Cicoria G, Pancaldi D, et al. Synthesis and quality control of 68Ga citrate for routine clinical PET. Nucl Med Commun. 2009 Jul;30(7):542–5.

9. Miller RF. Nuclear medicine and AIDS. Eur J Nucl Med. 1990;16(2):103–18.

10. Lee P. Hyponatremia in Pulmonary TBEvidence of Ectopic Antidiuretic Hormone Production. Chest. American College of Chest Physicians; 2010 Jan 1;137(1):207–8.

11. Ottenhoff THM. The knowns and unknowns of the immunopathogenesis of tuberculosis [State of the art]. int j tuberc lung dis. 2012 Nov 1;16(11):1424–32.

12. Ramakrishnan L. Revisiting the role of the granuloma in tuberculosis. Nature Reviews Immunology. Nature Publishing Group; 2012 Apr 20;12(5):352–66.

13. Golden MP, Vikram HR. Extrapulmonary tuberculosis: an overview. American family physician. 2005 Nov;72(9):1761–8.

14. Lin WY, Hsieh JF. Gallium-67 citrate scan in extrapulmonary tuberculosis. Nuklearmedizin.1999;38(6):199–202.

15. Steingart KR, Flores LL, Dendukuri N, Schiller I, Laal S, Ramsay A, et al. Commercial serological tests for the diagnosis of active pulmonary and extrapulmonary tuberculosis: an updated systematic review and meta-analysis. PLoS Med. 2011 Aug;8(8):e1001062.

16. Zhou Q, Chen Y-Q, Qin S-M, Tao X-N, Xin J-B, Shi H-Z. Diagnostic accuracy of T-cell interferon-γ release assays in tuberculous pleurisy: A meta-analysis. Respirology. 2011 Mar 30;16(3):473–80.

17. Sathekge M, Maes A, Kgomo M, Stoltz A, Van de Wiele C. Use of 18F-FDG PET to Predict Response to First-Line Tuberculostatics in HIV-Associated Tuberculosis. J Nucl Med. 2011 May 27;52(6):880–5.

18. Sathekge M, Maes A, D'Asseler Y, Vorster M, Gongxeka H, Van de Wiele C. Tuberculous lymphadenitis: FDG PET and CT findings in responsive and nonresponsive disease. Eur J Nucl Med Mol Imaging. 2012 Jul;39(7):1184–90.

19. Martinez V, Castilla-Lievre MA, Guillet-Caruba C, Grenier G, Fior R, Desarnaud S, et al. 18F-FDG PET/CT in tuberculosis: an early non-invasive marker of therapeutic response. Int J Tuberc Lung Dis. 2012 Sep 1;16(9):1180–5.

20. Park YH, Yu CM, Kim ES, Jung JO, Seo HS, Lee JH, et al. Monitoring Therapeutic Response in a Case of Extrapulmonary Tuberculosis by Serial F-18 FDG PET/CT. Nucl Med Mol Imaging. 2011 Nov 10;46(1):69–72.

21. Heysell SK, Thomas TA, Sifri CD, Rehm PK, Houpt ER. 18-fluorodeoxyglucose positron emission tomography for tuberculosis diagnosis and management: a case series. BMC Pulm Med. 2013 Mar 21;13(1):1–1.

22. Soussan M, Brillet P-Y, Mekinian A, Khafagy A, Nicolas P, Vessieres A, et al. European Journal of Radiology. Eur J of Radiol.2012 Oct 1;81(10):2872–6.

23. Sathekge MMM, Maes AA, Pottel HH, Stoltz AA, van de Wiele CC. Dual time-point FDG PET-CT for differentiating benign from malignant solitary pulmonary nodules in a TB endemic area. S Afr Med J. 2010 Aug 31;100(9):598–601.

24. Goo JMJ, Im JGJ, Do KHK, Yeo JSJ, Seo JBJ, Kim HYH, et al. Pulmonary tuberculoma evaluated by means of FDG PET: findings in 10 cases. Radiology. 2000 Jun 30;216(1):117–21.

25. Tsan MF. Mechanism of gallium-67 accumulation in inflammatory lesions. J Nucl Med. 1985 Jan;26(1):88–92.

26. Sarkar SD, Ravikrishnan KP, Woodbury DH, Carson JJ, Daley K. Gallium-67 citrate scanning--a new adjunct in the detection and follow-up of extrapulmonary tuberculosis: concise communication. J Nucl Med.1979 Jul 31;20(8):833–6.

27. Rubin RHR, Fischman AJA. Radionuclide imaging of infection in the immunocompromised host. Clin Infect Dis. 1996 Feb 29;22(3):414–23.

28. Bekerman C, Hoffer PB, Bitran JD, Gupta RG. Gallium-67 citrate imaging studies of the lung. Semin Nucl Med.1980 Jul;10(3):286–301.

29. Santin M, Podzamczer D, Ricart I, Mascaro J, Ramon JM, Dominguez A, et al. Utility of the Gallium-67 Citrate Scan for the Early Diagnosis of Tuberculosis in Patients Infected with the Human Immunodeficiency Virus. Clin Infect Dis. 1995 Mar 1;20(3):652–6.

Chapter 7: Pulmonary Fibrosis Case Series: A possible niche for ^{68}Ga-citrate PET?

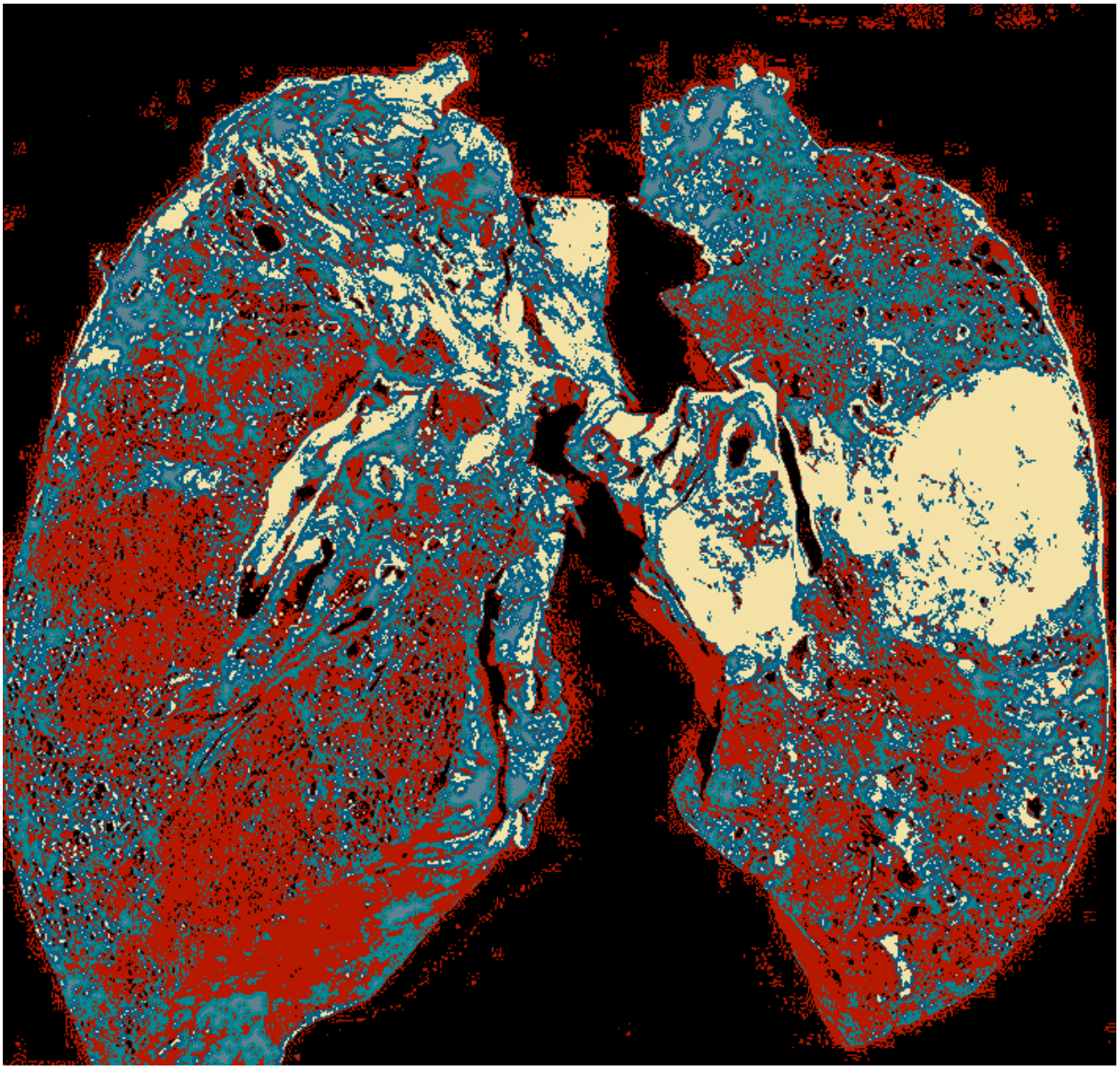

*An amended version of this chapter has been submitted for publication to Molecular Imaging and Biology

Introduction

Idiopathic Pulmonary Fibrosis (IPF) has recently been redefined as a progressive interstitial pneumonia of unknown cause, which occurs in adults. It is limited to the lungs and associated with the histological and/or radiological pattern of usual interstitial pneumonia (UIP).[1]

The diagnosis is based on the exclusion of other known causes and the presence of specific combinations of radiological- and histopathological patterns. The diagnostic criteria for radiology and histopathology include three radiological categories (on HRCT) and four histological categories. Until recently, surgical lung biopsy (SLB) has been regarded as the gold standard in the diagnosis of idiopathic pulmonary fibrosis, but revised international statements on the diagnosis and management of these conditions now recommend a multi-disciplinary approach.[2] SLB is also associated with significant increases in morbidity, mortality and costs.[3]

Imaging could potentially play an important role in the reduction of unnecessary lung biopsies, with an associated improvement in costs and outcomes. High resolution CT has played an important role in the morphological imaging of pulmonary fibrosis. However, this provides only a part of the information needed and typical patterns have reportedly been present in around 60% of cases only.[4-6] Most reports on the role of functional imaging in the diagnosis of IPF, have involved SPECT imaging with ^{67}Ga-citrate [7-9] or PET imaging with ^{18}F-FDG. [10-12] Again, all of these modalities suffer from certain limitations. Combined PET/CT should ideally play an important role in the non-invasive diagnosis and treatment response evaluation of IPF.

We report here the ^{68}Ga-citrate PET/CT image findings of three patients with IPF who were discovered as part of a larger study done on patients with indeterminate lung lesions. In our series, we found that five patients had histopathology that did not reveal any malignant or infective/inflammatory cells, and was consistent with a final diagnosis of fibrosis. We have considered three of these patients in more detail here.
None of these five patients demonstrated any significant Gallium-68-citrate accumulation. In the last patient discussed here, ^{68}Ga-citrate findings were compared to ^{18}F-FDG PET/CT, which demonstrated significant tracer accumulation in the lesion.

This suggests a possible niche area for imaging with ^{68}Ga-citrate. (In the remainder of the complete study, which involved 36 subjects, there were no other lesions that demonstrated absence of tracer accumulation).

Case 1

Clinical details

A 48 yr old asymptomatic male mineworker was referred with an ill-defined density in the superior segment of the right upper lobe. The lesion was an incidental finding detected following a routine CXR investigation. The patient was subsequently referred for PET/CT in other to stage the patient for a suspected malignancy.

Fig 1: MIP of ^{68}Ga-citrate PET 60 minutes after IV injection of 207.2 MBq (5.6 mCi) ^{68}Ga-citrate. Normal tracer-biodistribution, with high vascular activity was noted.

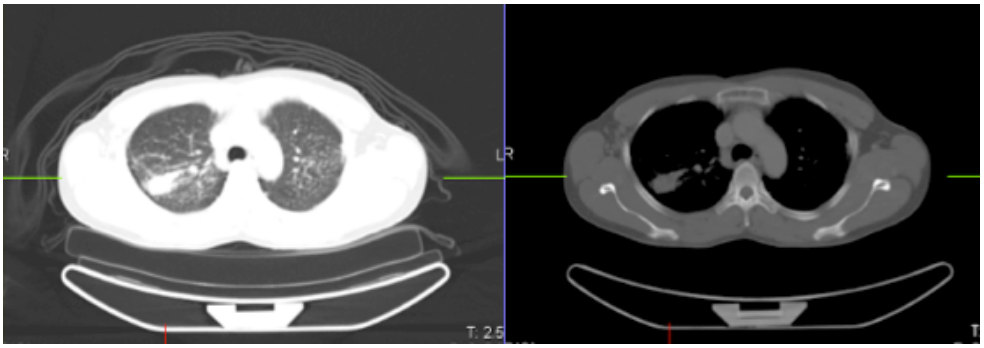

Fig 2: A contrasted CT was performed, which demonstrated a dense opacity in the posterior segment of the Right Upper Lobe (RUL). A spiculated border and contrast enhancement (70→110 HU) of the lesion, lead to the conclusion that a malignant process could not be excluded. Para-tracheal lymph nodes were also noted.

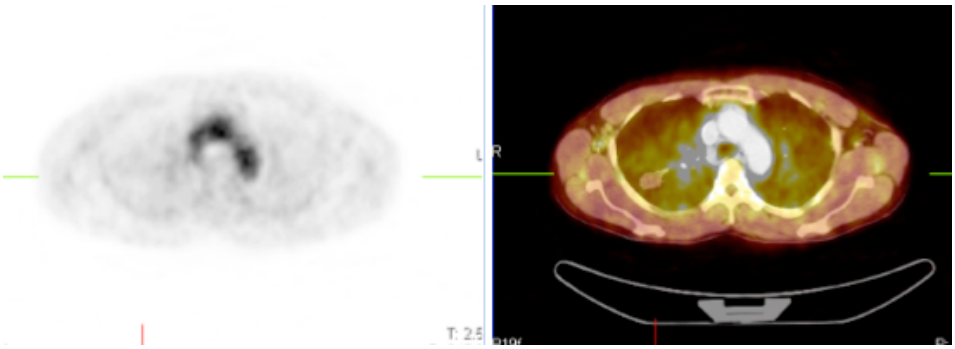

Fig 3: ^{68}Ga-citrate PET and fused PET/CT images revealed a photopenic area, which corresponded to the RUL opacity noted on CT. No areas of abnormal tracer accumulation were noted on PET. Subsequent histopathological investigations failed to demonstrate any malignant, infective- or inflammatory involvement, and were consistent with a final diagnosis of pulmonary fibrosis

Case 2

Clinical details

A 60 yr old female with a long-standing smoking history (35yrs) presented with hemoptysis and a solitary pulmonary nodule in the RUL on Chest CT (26mm x14 mm).

Fig 1: MIP image of ^{68}Ga-citrate PET, 60 minutes post-injection of 185 MBq (5mCi) of ^{68}Ga-citrate IV. No abnormal tracer bio-distribution was noted.

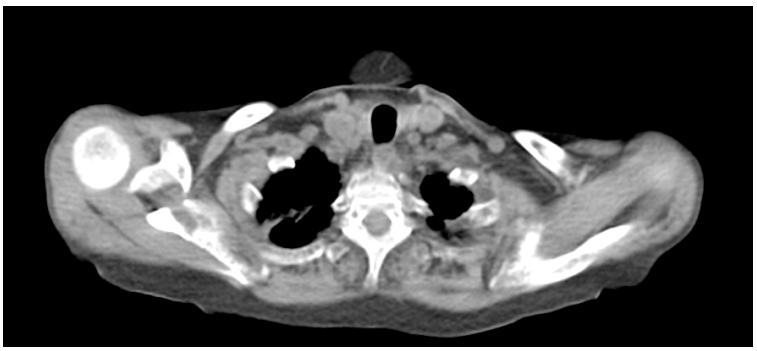

Fig 2: CT (non-contrasted) demonstrated a right-sided apical, pleural-based nodule with the following measurements: 32 x 11 mm. No definite diagnosis could be made.

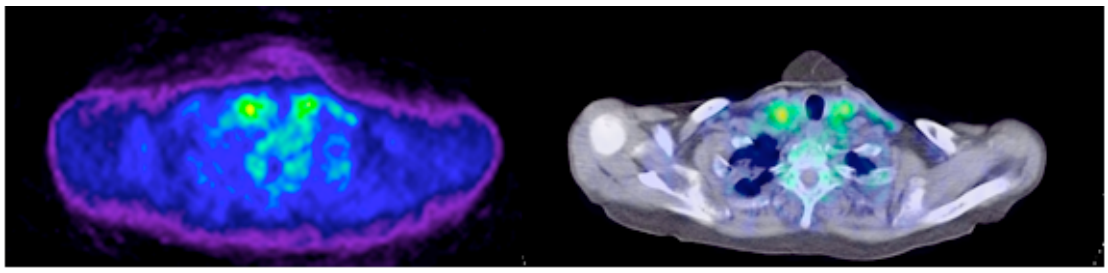

Fig 3: ^{68}Ga-citrate PET/CT did not demonstrate any significant tracer accumulation in the RUL lesion. Subsequent histopathological investigations failed to demonstrate any malignant-, infective- or inflammatory cells. A final diagnosis of fibrosis was made.

Case 3

Clinical details

A 49-year-old male presented with a right upper lobe mass, which was discovered incidentally following a routine CXR. He had a long-standing smoking history (greater than 20 years) and worked in a coal mine for 17 years. He was completely asymptomatic and had no other co-morbidities. Two PET/CT scans were performed within a week of one another- one with ^{68}Ga-citrate and the other with ^{18}F-FDG for comparison.

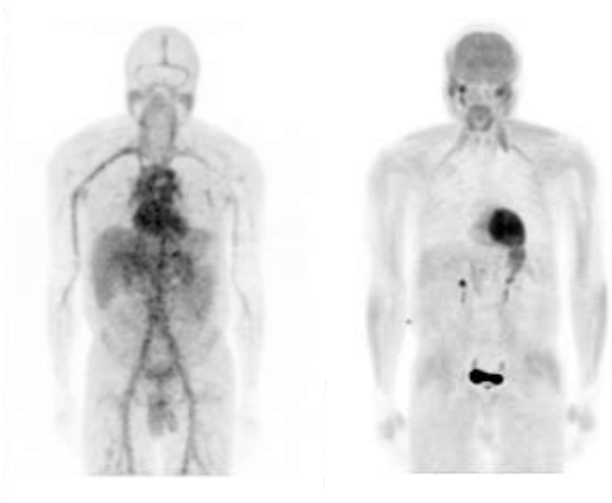

a) **b)**

Fig 1a) MIP image of ^{68}Ga-citrate PET, 60 minutes post-injection of 123 MBq (3.33mCi) of ^{68}Ga-citrate IV. No abnormal tracer bio-distribution was noted.**1b)** MIP image 90 minutes post-injection of 333 MBq (9mCi) ^{18}F-FDG.

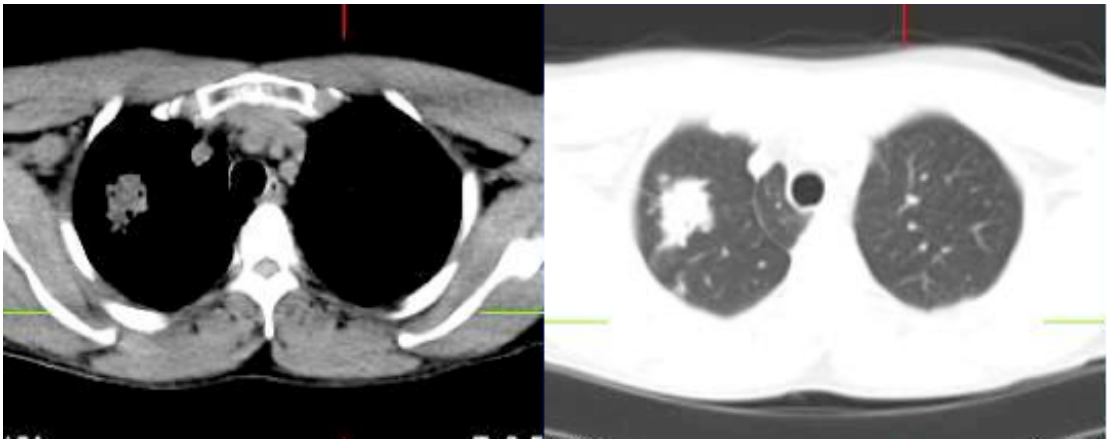

Fig 2: CT (contrasted) demonstrated a right-sided spiculated mass in the right apex with the following measurements: 25 x 29 mm. Morphological features were considered highly suggestive of a malignancy, such as bronchogenic carcinoma.

a)

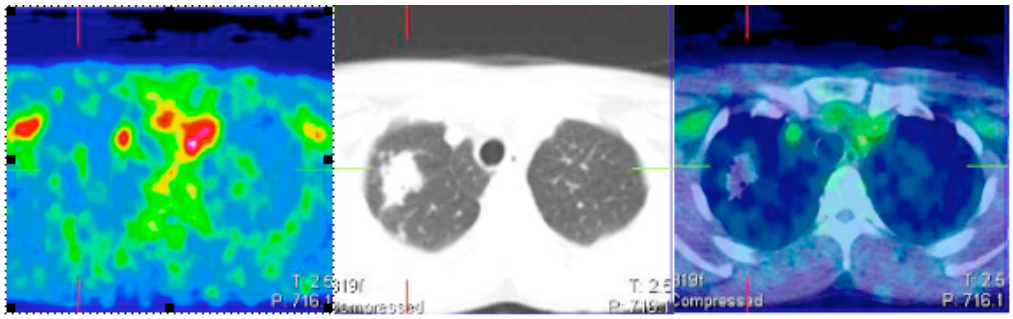

b)

Fig 3: a) Transverse images demonstrate significant ^{18}F-FDG accumulation in the right apical lesion (SUVmax: 2.63), with **b)** no significant ^{68}Ga-citrate accumulation noted in the same region.

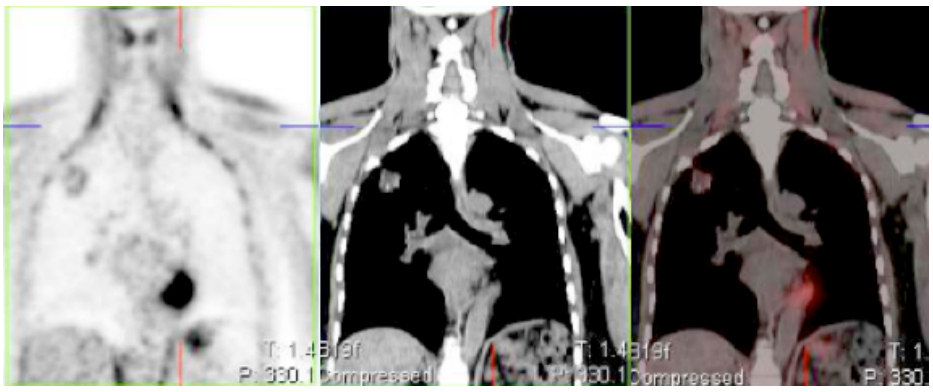

a)

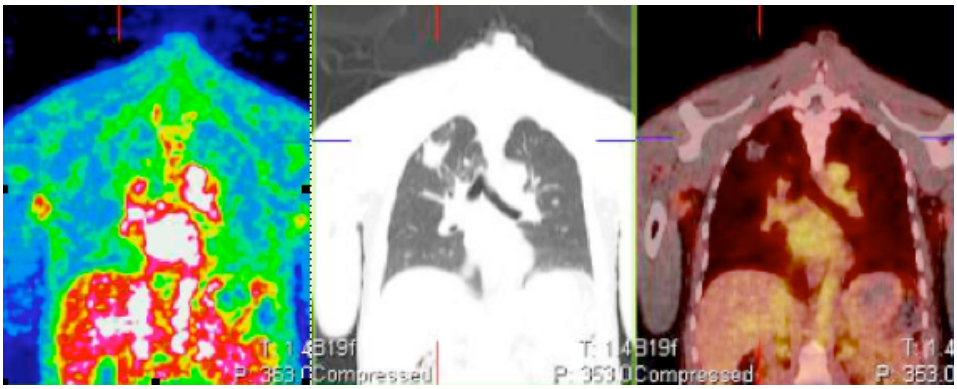

b) Fig 4: a) Coronal PET, CT and fused PET/CT images demonstrate significant ^{18}F-FDG accumulation in the right apical lesion with **b)** no significant ^{68}Ga-citrate accumulation in the same region. Intra-operative frozen section histology revealed fibrosis.

Discussion

Background

Accurate non-invasive diagnosis of Idiopathic Pulmonary fibrosis (IPF) remains difficult and is important in reducing futile biopsies. The diagnosis is based on combinations of radiological, clinical- and histopathological criteria with the pathophysiologic hallmark of fibroblast foci.[1,13]

Surgical lung biopsy (SLB) is associated with significant risks, which increase in patients with IPF, many of whom tend to be older, with various co-morbidities and reduced lung function. The most common complication of SLB is a prolonged air-leak, which occurs in about 6– 12% of the cases. Other common complications include the need for mechanical ventilation, pneumonia, pneumothorax, hemothorax, pleural effusion, empyema and prolonged ventilation.[3,14] The most serious complication is mortality within one month of the procedure, which is commonly caused by an acute exacerbation of IPF.[15,16]

There is clearly a need for an accurate, non-invasive diagnostic tool in this setting. Imaging investigations in patients with pulmonary fibrosis have involved mostly CT, ^{67}Ga-SPECT and ^{18}F-FDG PET until now and are briefly discussed below. Considering the value of Gallium-67 in evaluating a wide spectrum of lung pathology in the past, it would be reasonable to expect at least a similar performance with ^{68}Ga-citrate.

Imaging in the diagnosis of pulmonary fibrosis

In the past, high resolution CT has played an important part in reaching a diagnosis.[7,17] Raghu et al. (2011) reported that IPF could be diagnosed based on clinical and radiological criteria in about two thirds of all cases.[2] This has been confirmed by subsequent studies, which demonstrated that the characteristic HRCT features are absent in around 30% to 40% of IPF patients and that lung biopsy was still needed in around a third of IPF patients to reach a diagnosis.[4-6]

False positive findings on imaging (where a fibrotic lesion is mistaken for a malignancy), causes an unacceptable increase in morbidity, mortality and costs. On the other hand, a malignancy is less likely to be mistaken for fibrosis (false negative). This may occur, though with tumours which are not tracer-avid, such as neuro-endocrine tumours, broncho-alveolar- and other slow-growing or mucinous tumours in the case of imaging with ^{18}F-FDG PET. Several groups have investigated the role of ^{18}F-FDG PET in diffuse pulmonary lung diseases, including idiopathic pulmonary fibrosis and massive pulmonary fibrosis.[10,11]

Meissner et al. (2006) compared ^{18}F-FDG PET in patients with and without interstitial pulmonary fibrosis and found no differences in uptake values.[18] Groves and co-workers (2009) described findings with ^{18}F-FDG PET in 36 patients with diffuse pulmonary lung disease. They found that increased glucose metabolism was associated with both ground glass- and reticulation or honeycombing changes noted on HRCT and that higher uptake was noted in areas with honeycombing. They reported a SUVmax of 2.8 (1.4-5.4), a mean Target-to-background ratio of 4.1 (2.2-8.2) and a mean SUVmax in normal lung of 0.7.[11] Chung et al. (2010) evaluated the ^{18}F-FDG PET features of massive pulmonary fibrosis and found that this condition could be identified even in the absence of concomitant TB or malignancy. They imaged 14 masses in 9 patients (all located in the upper lobes) and reported SUVmax values ranging from 3.1-14.6 with a mean SUVmax of 6.5 (+/- 3.1).[10]

False positive findings with ^{18}F-FDG PET are well documented and have been attributed to leucocyte- and macrophage infiltration, fibroblast activity and the presence of various cytokines and growth factors.[19,20]

^{67}Ga-SPECT imaging has been used for many decades in the assessment of a variety of lung pathologies.[8,21,22] Clinically important non-oncologic applications of gallium in lung imaging include the early detection of opportunistic infections, distinguishing pulmonary infection from infarction, staging idiopathic pulmonary fibrosis, and the evaluation of treatment response in sarcoidosis.

Niden and colleagues (1976) have demonstrated that inflammatory lesions of the lung are almost invariably positive on gallium scan, whereas uncomplicated pulmonary infarcts do not show increased uptake. They have suggested the use of Gallium scintigraphy to distinguish infarction from infection in cases where clinical and radiographic findings are indeterminate. Line and co-workers (1978) found that pulmonary uptake of Gallium-67 correlates well with the active phase of idiopathic pulmonary fibrosis. They also developed a quantification method for Gallium-67, which takes into account the pattern, intensity and extent of lung involvement, which could be useful in the evaluation of treatment response.[23]

Several groups have reported on the use of ^{67}Ga-citrate SPECT imaging in early, late, and even asymptomatic diffuse parenchymal lung disease (DPLD). It has also been reported to be valuable in the prediction of lung function, but appears to be of limited value in the prediction of treatment response. This may have been due (in part) to difficulties in quantification with gamma camera imaging.

Other novel tracers for functional imaging of IPF

Ambrosini et al. (2010) have investigated the novel use of **^{68}Ga-DOTANOC** PET/CT in the imaging of Idiopathic Pulmonary Fibrosis (IPF). The pathophysiological hallmark of fibroblast foci, express somatostatin receptors that can be imaged with ^{68}Ga-DOTANOC due to the tracer's affinity for somatostatin receptors 2,3 and 5. Due to the fact that healthy lungs demonstrate no ^{68}Ga-DOTANOC, any tracer accumulation may be regarded as abnormal. The authors concluded that somatostatin over-expression in IPF could be imaged with Ga-68-DOTANOC with the potential for future treatment response evaluation.[24]

Pre-clinical and pilot studies have demonstrated that increased uptake of **^{18}F-Fluoro-Proline** can be used to monitor fibrosis. It is hypothesized that increased uptake reflects up-regulation of proline transport into fibroblasts, rather than collagen synthesis. PET imaging of 18F-FP

clearly has considerable potential in monitoring the fundamental processes involved in the development of scarring of the lung.[25,26]

Concluding remarks

In light of the above-mentioned (and other) studies with ^{67}Ga-citrate SPECT, it would make sense to also investigate the use of ^{68}Ga-citrate in these settings and to anticipate similar or better results due to the inherent improvements in resolution and quantification provided by PET/CT.

We have briefly described here the clinical- and imaging findings of three patients with a final diagnosis of pulmonary fibrosis. All of them had a smoking history and-or occupational exposure, presented around the fifth decade (as expected) and had a relatively high pre-test probability for a malignant process. None of them were known with HIV or TB and sputum cultures and tracheal aspirates were negative for various infective agents (including TB). Morphological imaging was consistent with a malignant process in all three patients and resulted in these patients being referred for surgical lung biopsies. In the one patient who also underwent a PET scan with ^{18}F-FDG, findings were also suggestive of a malignant process (SUVmax 2.63). However, none of the five patients in this series demonstrated any significant accumulation of ^{68}Ga-citrate in the presenting lung lesions. This may prove valuable in selected patients who pose a high risk for increased morbidity and mortality during invasive procedures. In cases with absence of ^{68}Ga-citrate accumulation in the lung lesions, such patients may benefit from careful follow-up evaluation instead.

We hypothesize that imaging with ^{68}Ga-citrate PET could be used to exclude a possible malignant process in a selected patient population and that validation of this finding in a larger study population is needed.

References

1. Kaarteenaho R. The current position of surgical lung biopsy in the diagnosis of idiopathic pulmonary fibrosis. Respir. Res. 2013 Apr 15;14(1):43–3.

2. Raghu G, Collard HR, Egan JJ, Martinez FJ, Behr J, Brown KK, et al. An official ATS/ERS/JRS/ALAT statement: idiopathic pulmonary fibrosis: evidence-based guidelines for diagnosis and management. Am J Respir Crit Care Med. 2011:788–824.

3. Park, Joo Hun, et al. Mortality and risk factors for surgical lung biopsy in patients with idiopathic interstitial pneumonia.Eur J Cardio-thor Surg.2007; 31(6): 1115-9.

4. Flaherty KRK, Thwaite ELE, Kazerooni EAE, Gross BHB, Toews GBG, Colby TVT, et al. Radiological versus histological diagnosis in UIP and NSIP: survival implications. Thorax. 2003 Jan 31;58(2):143–8.

5. Lynch DAD, Godwin JDJ, Safrin SS, Starko KMK, Hormel PP, Brown KKK, et al. High-resolution computed tomography in idiopathic pulmonary fibrosis: diagnosis and prognosis. Am J Respir Crit Care Med. 2005 Aug 14;172(4):488–93.

6. Lynch DAD. Fibrotic idiopathic interstitial pneumonia: high-resolution computed tomography considerations. Semin Respir Crit Care Med. 2003 Jul 31;24(4):365–76.

7. Gross TJT, Hunninghake GWG. Idiopathic pulmonary fibrosis. N Engl J Med. 2001 Aug 15;345(7):517–25.

8. Niden AHA, Mishkin FSF, Khurana MMM. 67Gallium citrate lung scans in interstitial lung disease. Chest. 1976 Jan 31;69(2 Suppl):266–8.

9. Tsan MF. Mechanism of gallium-67 accumulation in inflammatory lesions. J Nucl Med. 1985 Jan;26(1):88–92.

10. Chung SY, Lee JH, Kim TH, Kim SJ, Kim HJ, Ryu YH. 18F-FDG PET imaging of progressive massive fibrosis. Ann Nucl Med. 2010 Jan 24;24(1):21–7.

11. Groves AM, Win T, Screaton NJ, Berovic M, Endozo R, Booth H, et al. Idiopathic Pulmonary Fibrosis and Diffuse Parenchymal Lung Disease: Implications from Initial Experience with 18F-FDG PET/CT. J Nucl Med. 2009 Mar 15;50(4):538–45.

12. Win TT, Lambrou TT, Hutton BFB, Kayani II, Screaton NJN, Porter JCJ, et al. 18F-Fluorodeoxyglucose positron emission tomography pulmonary imaging in idiopathic pulmonary fibrosis is reproducible: implications for future clinical trials. Eur J Nucl Med Mol Imaging. 2012 Feb 29;39(3):521–8.

13. Reynolds HY, Fulmer JD, Kazmierowski JA, Roberts WC, Frank MM, Crystal RG. Analysis of cellular and protein content of broncho-alveolar lavage fluid from patients with idiopathic pulmonary fibrosis and chronic hypersensitivity pneumonitis. J. Clin. Invest. 1977 Jan;59(1):165–75.

14. Sigurdsson MI, Isaksson HJ, Gudmundsson G. Diagnostic surgical lung biopsies for suspected interstitial lung diseases: a retrospective study. Ann Thorac Surg. 2009;88(1), 227-32.

15. Kaarteenaho RR, Kinnula VLV. Diffuse alveolar damage: a common phenomenon in progressive interstitial lung disorders. Pulm Med. 2010 Dec 31;2011:531302–2.

16. Fibla JJ, Brunelli A, Cassivi SD, Deschamps C. Aggregate risk score for predicting mortality after surgical biopsy for interstitial lung disease. Interact Cardiovasc Thorac Surg. 2012 Aug;15(2):276–9.

17. Kondoh Y, Taniguchi H, Kawabata Y, Yokoi T, Suzuki K, Takagi K. Acute exacerbation in idiopathic pulmonary fibrosis. Analysis of clinical and pathologic findings in three cases. Chest. American College of Chest Physicians; 1993;103(6):1808–12.

18. Meissner H-H, Soo Hoo GW, Khonsary SA, Mandelkern M, Brown CV, Santiago SM. Idiopathic pulmonary fibrosis: evaluation with positron emission tomography. Respiration. 2006;73(2):197–202.

19. Kavanagh PVP, Stevenson AWA, Chen MYM, Clark PBP. Nonneoplastic diseases in the chest showing increased activity on FDG PET. American Journal of Roentgenology. 2004 Sep 30;183(4):1133–41.

20. Alavi AA, Gupta NN, Alberini J-LJ, Hickeson MM, Adam L-EL, Bhargava PP, et al. Positron emission tomography imaging in nonmalignant thoracic disorders. YSNUC. 2002 Sep 30;32(4):293–321.

21. Lin WY, Hsieh JF. Gallium-67 citrate scan in extrapulmonary tuberculosis. Nuklearmedizin.1999;38(6):199–202.

22. Bekerman C, Hoffer PB, Bitran JD, Gupta RG. Gallium-67 citrate imaging studies of the lung. Seminars in Nuclear Medicine. 1980 Jul;10(3):286–301.

23. Line BR, Fulmer JD, Reynolds HY. Gallium-67 citrate scanning in the staging of idiopathic pulmonary fibrosis: Correlation and physiologic and morphologic features and bronchoalveolar lavage. The Am Rev Resp Dis.1978;118(2):355

24. Ambrosini V, Zompatori M, De Luca F, Antonia D, Allegri V, Nanni C, et al. 68Ga-DOTANOC PET/CT Allows Somatostatin Receptor Imaging in Idiopathic Pulmonary Fibrosis: Preliminary Results. J Nucl Med. 2010 Nov 23;51(12):1950–5.

25. Wallace WEW, Gupta NCN, Hubbs AFA, Mazza SMS, Bishop HAH, Keane MJM, et al. Cis-4-[(18)F]fluoro-L-proline PET imaging of pulmonary fibrosis in a rabbit model. J Nucl Med. 2002 Feb 28;43(3):413–20.

26. Lavalaye J, Grutters JC, Garde EMW, Buul MMC, Bosch JMM, Windhorst AD, et al. Imaging of fibrogenesis in patients with idiopathic pulmonary fibrosis with cis-4-[(18)F]-Fluoro-L: -proline PET. Mol Imaging Biol. 2009 Feb 28;11(2):123–7.

Chapter 8: Alternative tracers: a case study with ^{18}F-FDG and ^{18}F-choline

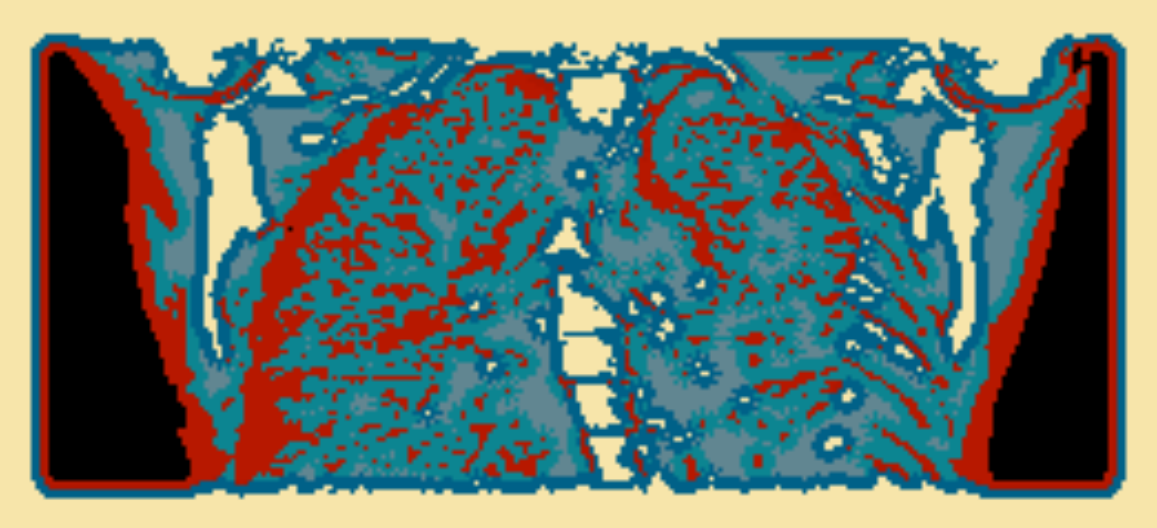

*An amended version of this chapter was submitted to and accepted by the Open Journal of Nuclear Medicine

Title: Imaging of Pulmonary Tuberculosis with ^{18}F-FDG and ^{18}F-Choline

Authors: M Vorster MD [1]AG Jacobs MD[2] A Stoltz PhD[3] MM Sathekge PhD[1]

University of Pretoria, Department of Nuclear Medicine, Steve Biko Academic Hospital$_1$

University of Pretoria, Department of Cardiothoracic Surgery, Steve Biko Academic Hospital$_2$

University of Pretoria, Department of Infectious Diseases, Steve Biko Academic Hospital$_3$

Abstract

Purpose

A 37 year old man was referred for PET/CT with the following diagnostic challenge: a longstanding smoking history, histologically confirmed TB and sarcoidosis with worsening chest-related symptoms and a non-responsive right upper lobe lung lesion.

Materials and Methods

PET/CT imaging was performed with both ^{18}F-FDG and ^{18}F-Choline in an attempt to better characterize the lung lesion. This was followed by biopsies of the right upper lobe nodule, the pleura and a brain lesion.

Results

Both tracers demonstrated increased uptake in the lung lesion and multiple widespread lymph nodes.
Histology revealed granulomatous disease in the lung lesion, the pleura and the brain. Follow-up evaluation with ^{18}F-choline demonstrated response to treatment, which correlated to clinical improvement.

Conclusion

Tuberculous lesions demonstrate increased accumulation of ^{11}C-choline on PET/CT, which may be useful in the evaluation of treatment response. When used in combination with ^{18}F-FDG,it could be of value in distinguishing malignant lesions from tuberculosis.

Keywords: Tuberculosis; PET ^{18}F-Choline ^{18}F-FDG

Clinical history

A 37 yr old man with a long-standing smoking history presented with worsening chest-related symptoms whilst receiving anti-Tuberculosis treatment. Treatment with Rifafour was re-started empirically three months prior to the initial PET/CT, following an earlier histological diagnosis of TB from pleural and liver tissue. At the time of investigation, sarcoidosis was also diagnosed on histology from enlarged abdominal lymph nodes which were discovered on CT. Treatment with steroids was subsequently commenced, but had to be discontinued after six months, following the occurrence of unacceptable side-effects.

A subsequent CT revealed a collapsed right lung with a large pleural effusion, for which an intercostal drain was inserted and a lesion in the right upper lung that had not responded to treatment.

We were therefore faced with the diagnostic challenge of a patient with histologically proven TB (pleura & liver) and sarcoidosis (abdominal lymph nodes) with worsening chest-related symptoms (after three months of Rifafour treatment) and a non-responsive lung lesion. Mycobacterial culture and sensitivity studies demonstrated sensitivity of acid-fast bacilli to Rifampicin and patient compliance to treatment was good.

It is well known that imaging with ^{18}F-FDG PET/CT (including dual-phase imaging) is unable to distinguish malignant lesions from granulomatous disease in countries where these diseases are highly prevalent.[1] We subsequently decided to image the patient with both ^{18}F-FDG and ^{18}F-Choline (which was done 5 days apart) in order to try and better characterize the right upper lung lesion.

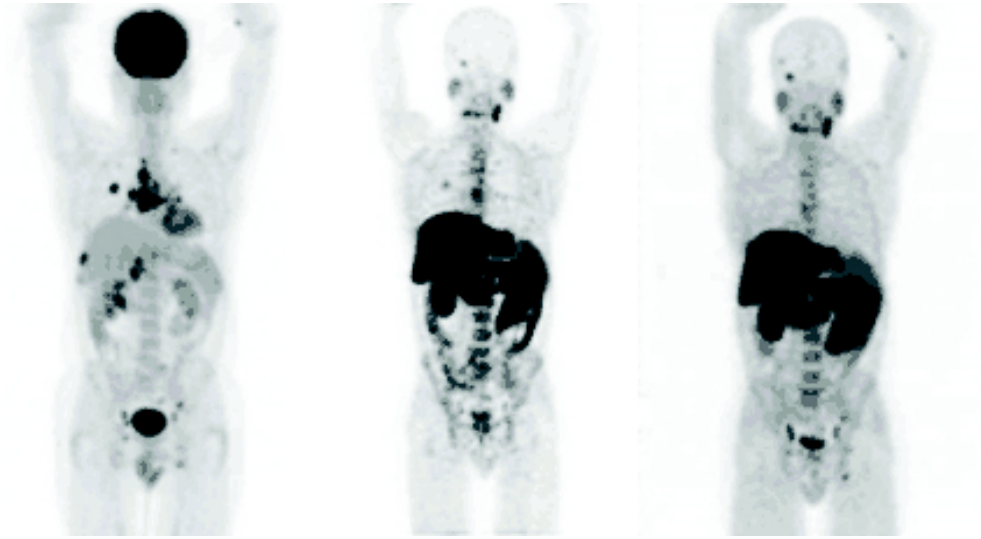

Fig 1a) **b)** **c)**

Fig 1a) F-18-FDG MIP 305 MBq (8.2 mCi) of ^{18}F-FDG was administered IV. Uptake time: 60 min, IV contrast given. **F-18-FDG** demonstrates intense uptake in the right upper lobe nodule (SUVmax 9.48), which corresponded to a spiculated pleural-based right upper lobe nodule (14.3x15.3 mm) on CT. Imaging with ^{18}F-FDG PET/CT (including dual-phase imaging) is unable to distinguish malignant lesions from granulomatous disease in countries where these diseases are highly prevalent [1-3].Hence additional imaging with F-18-choline was performed. **Fig 1 b) F-18-Choline MIP** 104 MBq (2.8 mCi) of ^{18}F-Choline was administered IV. Uptake time 90 min, no IV contrast given. **Fig 1c)** Anti-tuberculosis treatment was re-started and follow-up imaging with ^{18}F-Choline-PET/CT was performed 8 months after the initial scan to assess treatment response. Image findings indicated a good response to therapy, which corresponded to clinical improvement. **F-18-Choline MIP** the nodule in the right upper lobe is no longer clearly visualized and lymph node involvement appeared less intense.

F-18-Choline-PET demonstrated a similar pattern of abnormal tracer accumulation, although **less extensive and much less intense**. Uptake in the right upper lobe nodule demonstrated a SUVmax of 3.25.A repeat biopsy of the lung lesion and pleura revealed granulomatous inflammation with caseous necrosis. Langerhans giant cells were present and special stains for AFBs were strongly positive. No evidence of an underlying neoplastic process could be found. The combined findings of high ^{18}F-FDG uptake and relatively low ^{18}F-choline uptake may indicate granulomatous disease rather than malignancy (in which case high uptake would be expected with both tracers.) Choline can be labeled to either ^{11}C- or ^{18}F- and is biochemically indistinguishable from the natural form of choline as a component of cell membranes. In tumor cells, the increased metabolism results in an increase in the uptake of choline to maintain the increased membrane synthesis.

The use of ^{18}F-Choline in the setting of prostate cancer is well known, however, several authors have also evaluated its use in other malignancies.[4-6]

Choline can be labeled to either ^{11}C- or ^{18}F- and is biochemically indistinguishable from the natural form of choline as a component of cell membranes. In tumor cells, the increased metabolism results in an increase in the uptake of choline to maintain the increasing demand for synthesis of phospholipids in cellular membranes. The use of ^{18}F-Choline in the setting of prostate cancer is well known, however, several authors have also evaluated its use in other malignancies.[4] In the setting of chest pathology, *Liu et al. (2006)* investigated the role of ^{11}C-Choline in the evaluation of middle mediastinal pathology and found an accuracy of 75% in distinguishing benign from malignant lesions[7], whereas *Hara et al. (2000)* found a 100% diagnostic accuracy of ^{11}C-choline in detecting mediastinal lymph node metastases from non-small cell lung cancer.[8]

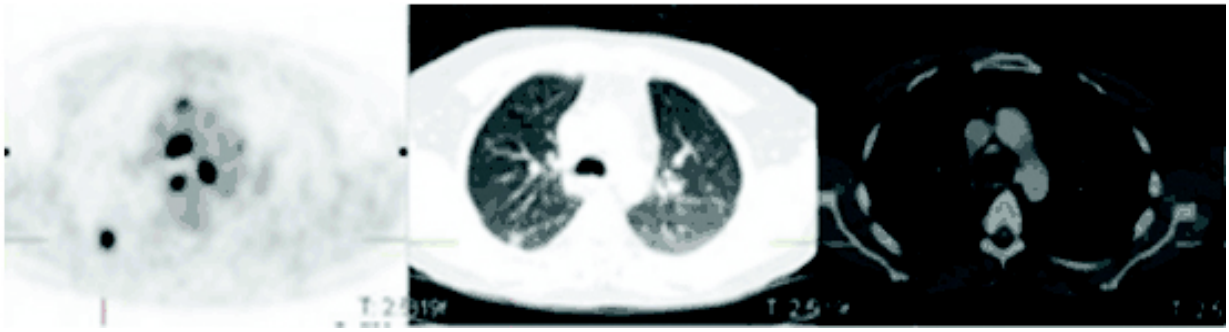

Fig 2a) F-18-FDG Mediastinal LNs: Anterior SUVmax 8.44, Middle SUVmax 14.47, and Posterior SUVmax 16.0

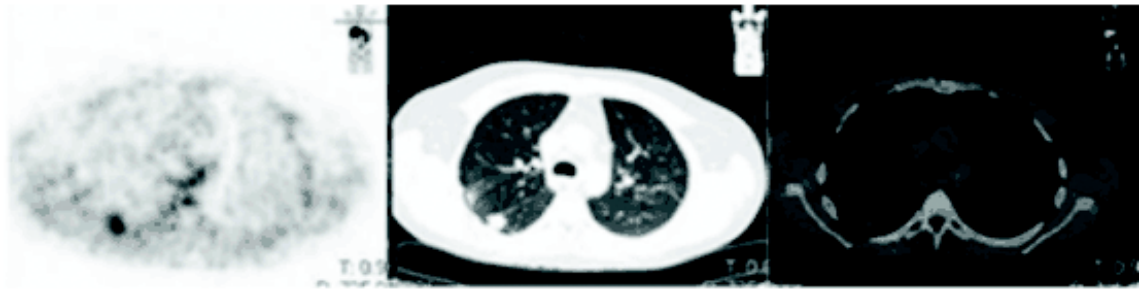

Fig 2b) F-18-Choline Mediastinal Lymph nodes: Anterior SUVmax 3.40, Pre-tracheal SUVmax 3.89.

Compared to the FDG images, the lymph node involvement (both in extent and intensity) appears less pronounced. In the setting of chest pathology, *Liu et al. (2006)* investigated the role of ^{11}C-Choline in the evaluation of middle mediastinal pathology and found an accuracy of 75% in distinguishing benign from malignant lesions[7], whereas *Hara et al. (2000)* found a 100% diagnostic accuracy of ^{11}C-choline in detecting mediastinal lymph node metastases from non-small cell lung cancer.[8]

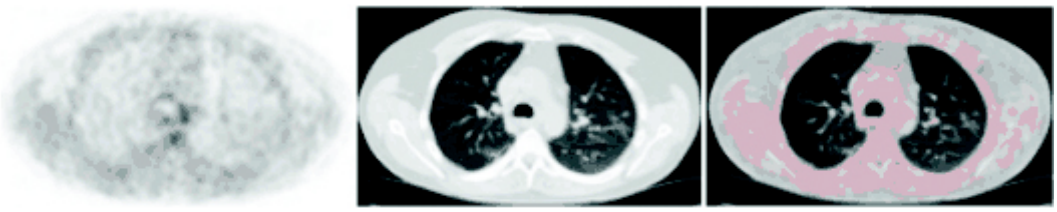

Fig 2c) Follow-up F-18-Choline

Fig 3a) F-18-FDG Sub-carinal lymph nodes: Several markedly enlarged nodes (17x8mm, 28.5x22.5 & 12.6x9mm) were noted in this region (SUVmax 15)

Fig 3b) ^{18}F-Choline Sub-carinal lymph nodes: These were the most intense lymph nodes noted (SUVmax 4.91)

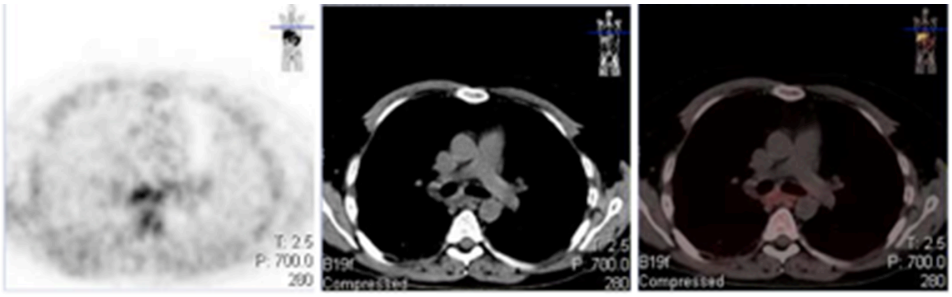

Fig 3c) Follow-up ^{18}F-Choline still demonstrates activity in the sub-carinal lymph nodes

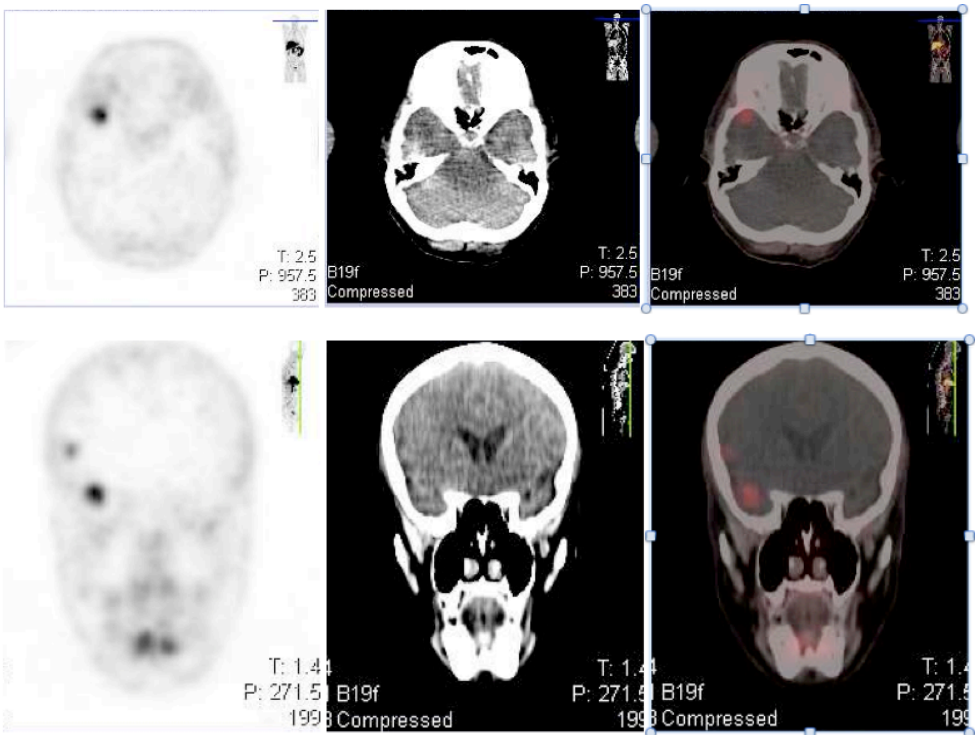

Fig 4 F-18-Choline allows for better detection of tuberculous brain involvement compared to F-18-FDG.

^{18}F-FDG-PET images demonstrated an intensely FDG-avid pulmonary nodule with left supraclavicular as well as multiple mediastinal-, abdominal- and pelvic lymph node involvement. Hyper-metabolic liver lesions were also noted. The initial **^{18}F-Choline-PET images** demonstrated a similar pattern of abnormal tracer accumulation, although **less extensive and much less intense**.

A repeat biopsy of the lung lesion and pleura revealed the presence of granulomatous inflammation with caseous necrosis. Langerhans giant cells were also present and special

stains done for AFBs were strongly positive. No evidence of an underlying neoplastic process could be found.

Treatment with anti-tuberculous drugs was subsequently started and follow-up imaging with **^{18}F-Choline-PET/CT** was performed 8 months after the initial scan to assess treatment response. Image findings suggested a good response to therapy, which corresponded to clinical improvement.

Conclusion

This patient with histologically confirmed granulomatous disease demonstrated increased tracer accumulation with both ^{18}F-FDG and ^{18}F-choline, which differed in terms of the extent and intensity of the involvement. Our findings suggest that ^{18}F-Choline may be used in the evaluation of treatment response. Furthermore, that the combined findings of high ^{18}F-FDG uptake and relatively low ^{18}F-choline uptake may indicate granulomatous disease rather than malignancy (in which case high uptake would be expected with both tracers.) Further investigations are needed in order to establish a possible SUV cut-off.

References

1. Sathekge MMM, Maes AA, Pottel HH, Stoltz AA, van de Wiele CC. Dual time-point FDG PET-CT for differentiating benign from malignant solitary pulmonary nodules in a TB endemic area. S Afr Med J. 2010 Aug 31;100(9):598–601.

2. Ito K, Morooka M, Minamimoto R, Miyata Y, Okasaki M, Kubota K. Imaging spectrum and pitfalls of 18F-fluorodeoxyglucose positron emission tomography/computed tomography in patients with tuberculosis. Jpn J Radiol.2013 May 30:1–10.

3. Cheng G, Torigian DA, Zhuang H, Alavi A. When should we recommend use of dual time-point and delayed time-point imaging techniques in FDG PET? Eur J Nucl Med Mol Imaging. 2013 May;40(5):779–87.

4. Treglia G, Giovannini E, Di Franco D, Calcagni ML, Rufini V, Picchio M, et al. The role of positron emission tomography using carbon-11 and fluorine-18 choline in tumors other than prostate cancer: a systematic review. Bulletin du Cancer.2012 May 8;26(6):451–61.

5. Peng ZZ, Liu QQ, Li MM, Han MM, Yao SS, Liu QQ. Comparison of (11)C-choline PET/CT and enhanced CT in the evaluation of patients with pulmonary abnormalities and locoregional lymph node involvement in lung cancer. Clin Lung Cancer. 2012 Jun 30;13(4):312–20.

6. Pieterman RM, Que TH, Elsinga PH, Pruim J, van Putten JWG, Willemsen ATM, et al. Comparison of 11C-Choline and 18F-FDG PET in Primary Diagnosis and Staging of Patients with Thoracic Cancer. J Nucl Med.2002;43(2):167-72.

7. Liu Q, Peng Z-M, Liu Q-W, Yao S-Z, Zhang L, Meng L, et al. The role of 11C-choline positron emission tomography-computed tomography and videomediastinoscopy in the evaluation of diseases of middle mediastinum. Chin. Med. J. 2006 Apr 20;119(8):634–9.

8. Hara T, Inagaki K, Kosaka N, Morita T. Sensitive detection of mediastinal lymph node metastasis of lung cancer with 11C-choline PET. J Nucl Med. 2000 Sep;41(9):1507–13.

Chapter 9: Concluding remarks & Future considerations

The distinction between benign and malignant lesions in the lung is a commonly encountered clinical problem with important patient management- and prognosis implications. For reasons that are still incompletely understood, tuberculous lesions demonstrate similar metabolic behaviour to that of malignant lesions. We hypothesized that imaging with ^{68}Ga-citrate would overcome some of the well-known limitations of imaging with ^{18}F-FDG to enable a clear distinction between these lesions.

The main findings of this study are the following: ^{68}Ga-citrate PET demonstrates uptake in both granulomatous- and malignant lesions with significant overlap noted in the Standardized uptake Values (SUV). However, this study is likely insufficiently powered to demonstrate possible underlying differences, which may well emerge with larger studies. Dual-time point imaging was only possible in 20 patients and did not demonstrate any statistically significant discriminating powers.

In patients with TB, ^{68}Ga-citrate PET demonstrated extra-pulmonary involvement which was more extensive than that predicted by CT. It could potentially play an important role in the detection of extra-pulmonary involvement and the evaluation of treatment response as a cost-effective alternative to ^{18}F-FDG.

When considering the afore-mentioned findings, the behaviour of ^{68}Ga-citrate PET appears similar to that of ^{18}F-FDG. In contrast to ^{18}F-FDG however, ^{68}Ga-citrate demonstrated increased uptake even in patients with neuro-endocrine tumours of the lung. In patients with lung malignancies, a trend was noted towards diffusely increased bone marrow uptake. This may be related to increased transferrin receptor expression by the reticulo-endothelial system, but requires further exploration. Importantly, imaging with ^{68}Ga-citrate demonstrated absent or very low tracer accumulation in patients with lung fibrosis. It is anticipated that this may lead to a reduction of futile biopsies in patients with idiopathic pulmonary fibrosis and provide a possible niche area for ^{68}Ga-citrate.

When comparing the performance of ^{68}Ga-citrate and CT individually to the histopathological diagnosis, ^{68}Ga-citrate PET outperformed CT in the characterization of indeterminate lung lesions.

Limitations of this study include the small, diverse study population, the absence of comparison to ^{18}F-FDG PET and the inability (due to ethical-and other reasons) to biopsy every lesion noted on PET. The comparison to ^{18}F-FDG PET was initially considered, but abandoned in light of the cost and radiation exposure considerations. In addition, previous studies performed in our setting have provided us with valuable knowledge on the expected uptake patterns seen when imaging patients with TB and malignant lung lesions with^{18}F-FDG PET. Histological confirmation was possible in 75% of study participants and its absence in the remaining 25% was due to either patient refusal or loss to follow-up. In these cases, a combination of clinical- and other special investigations was used to reach a final diagnosis. Regarding the diagnosis of TB, there is no single, universally accepted gold standard that can be applied to every clinical situation. This often necessitates combining the results of various clinical- and special investigations in order to reach a diagnosis. Various clinical scenarios may also prompt the institution of empirical treatment with anti-tuberculous drugs with subsequent monitoring of the patient's condition. These variations in reaching the diagnosis of TB may limit comparisons and generalizability.

The ideal uptake time for imaging with ^{68}Ga-citrate has not yet clearly been established. Good image quality was obtained at 60 minutes and 120 minutes, with significant deterioration in quality after 150 minutes. Dynamic imaging has improved knowledge on the behaviour and characterization of various lesions to some degree and could have added interesting additional

information in this setting. However, the logistics of these imaging protocols precludes its use as part of routine imaging in a busy nuclear medicine department. Therefore, evaluating these techniques (combined with kinetic modeling) in a pre-clinical research setting with validated TB, HIV- and lymphoma animal models may prove more feasible.

PET/CT imaging of lung lesions present a number of unique technical- and quantification issues. These include problems with misregistration of images due to breathing, changes in lung volumes due to patient posture or position and pathology that cannot easily be measured, such as areas of honeycombing, patchy infiltrates, reticulo-nodular involvement, etc. Overlap with highly vascular structures may occur and lesions less than one centimeter in diameter are subject to the partial volume effect. Standardized quantification measures may also be needed in order to overcome some of the inherent problems related to the SUVmax and to facilitate comparisons between various centers.

Potential solutions to these problems include the use of respiratory gating and the application of various corrections, such as tissue fraction correction and partial volume correction. New quantification techniques and software packages are also emerging, some of which will be used in future projects involving quantification of lung lesions. Due to several cost- and logistic considerations, the application of these measures was unfortunately not possible in our setting.

Imaging of lung pathology with PET/CT provides unlimited possibilities, which are as yet incompletely utilized. ^{68}Ga-citrate imaging appears promising in the setting of lung pathology and offers potentially important advantages compared to ^{18}F-FDG. A generator-dependent positron emitter such as Gallium-68 would be ideal in providing round-the clock, cost-effective tracer availability for imaging of both infectious- and malignant processes. Future projects include quantification of ^{68}Ga-citrate lung lesions making use of PERCIST and the following quantification parameters: SUL, TLG and MTV as well as the evaluation of various other novel tracers, such as anti-tuberculous drugs and peptides labeled to Gallium-68 in the setting of TB and HIV.

This is (to our best knowledge), the first reported use of ^{68}Ga-citrate in the setting of indeterminate lung lesions and larger clinical trials are required to validate our study findings.

Chapter 10: Thesis Summary

The distinction between benign and malignant lesions in the lung is a commonly encountered clinical problem with important patient management, cost- and outcome implications. In the South African setting, this problem is complicated even further by the high prevalence of Tuberculosis (TB) and Human Immuno-deficiency Virus (HIV) co-infection. This often results in diagnostic challenges in which various combinations of infective and malignant processes may occur simultaneously.

The present study follows on previous work done in our center by *Sathekge et al.* and is aimed at trying to improve on some of the limitations experienced with ^{18}F-FDG-PET/CT imaging. Various studies have indicated the inability of ^{18}F-FDG-PET/CT, even with the use of dual phase imaging, to distinguish accurately between benign- and malignant lung lesions in settings with a high TB prevalence. This has also been confirmed in our patient population. In patients with dual infection, early diagnosis of active TB is crucial in order to select the most appropriate treatment regime.

Imaging with Gallium, in the form of ^{67}Ga-citrate has served nuclear physicians well in the past in a variety of clinical situations, including granulomatous diseases (sarcoidosis and TB), lymphoma (for staging and treatment response) and various other infective- and inflammatory lung conditions (eg Pneumocystis *jiroveci* pneumonia, pneumonitis). Combinations of the afore-mentioned conditions are frequently encountered in clinical practices with a high prevalence of immunosuppression, such as ours. ^{68}Ga-citrate imaging provides the added advantages inherent to PET/CT imaging, such as improved resolution and quantification possibilities in addition to round-the-clock availability from a generator, improved logistics, bio-distribution and dosimetry. However, ^{68}Ga-citrate PET/CT has never been evaluated in the setting of indeterminate lung lesions, which makes this study the first of its kind.

^{68}Ga-citrate was prepared from a Sn-based ^{68}Ge/^{68}Ga-generator and ACD-A and all QC requirements were adhered to.

Thirty-six patients with indeterminate lung lesions were prospectively recruited, imaged and their PET/CT findings compared to histopathological diagnosis. Measurements included SUVmax, various target-to-background ratios and dual-time imaging in 20 patients. The main findings were as follows:

^{68}Ga-citrate PET demonstrates uptake in both granulomatous- and malignant lesions with significant overlap in Standardized uptake Values (SUV). In patients with TB, ^{68}Ga-citrate PET demonstrated extra-pulmonary involvement which was more extensive than that predicted by CT. It may also play a role in the evaluation of treatment response. In these findings, it is similar to ^{18}F-FDG. In contrast to ^{18}F-FDG however, ^{68}Ga-citrate demonstrated uptake in Neuro-endocrine tumours. In patients with malignancies, there was also a trend towards diffusely increased bone marrow uptake, which will require further exploration.

Importantly, imaging with ^{68}Ga-citrate did not demonstrate any uptake in patients with lung fibrosis, which may lead to a reduction of futile biopsies in this group of patients.

Limitations include the small number of patients, the absence of a comparison group with ^{18}F-FDG PET and the inability (due to ethical-and other reasons) to biopsy every lesion noted on PET. ^{68}Ga-citrate imaging appears promising in the setting of lung pathology and offers important advantages compared to ^{18}F-FDG. Larger clinical trials are required to validate afore-mentioned findings.

Keywords: ^{68}Ga-citrate; PET/CT; TB; SPN; indeterminate lung lesions; benign; malignant

Acknowledgements

Whilst growing up, my father often reminded me of the fact that nothing worthwhile doing or having, is achieved easily. These words of wisdom mirror the following words of another wise man: “Every worthwhile accomplishment, big or little, has its stages of drudgery and triumph; a beginning, a struggle and a victory” -Gandhi

I have now experienced the true meaning of these words in every sense. Starting, persevering with and completing a PhD thesis is a daunting task and one that cannot possibly be achieved without the help and support of others.

I am profoundly indebted to my promotor, Prof Mike Sathekge, without whose exceptional vision and collaborative efforts this project would not have been possible. I am immensely grateful for his shared knowledge, guidance, patience, time, support and encouragement. The brilliant example by which he leads, is truly inspirational.

I am very grateful to my Belgian co-supervisors, Prof Alex Maes and Prof Christophe Van de Wiele for their valuable time and input and to Prof Hans Pottel for his help with the statistical analysis. Thanks also to Prof Rheeder for his valuable time and suggestions.

My sincere gratitude goes to all of the staff (administrative-, medical- and nursing) at the department of Nuclear Medicine, without whom none of this would have been possible. I would like to thank the following people in particular for their efforts: Thomas Ebenhan and Brenda Mokaleng for their help with the labeling and QC of the ^{68}Gallium-citrate (often on very short notice!); Sr Cecelia Corbett for her endless support and calls to various referring doctors and patients; all of our radiographers for their willingness to perform additional scans and to write all of the images to CDs; the registrars (especially Drs Orunmuyi and Modiselle) for their help with retrieving the histology- and other results and all of the doctors for their help with obtaining consent and reporting of scans. A special word of thanks also goes to Dr Alfred Ankrah, for helping to ease my clinical workload and enabling me to finish the write-up of this thesis. Many thanks also to the registrars and consultants from the Department of Radiology for their help with the reporting of the CT scans.

I am immensely grateful to the following people for their referral of appropriate study patients: Drs Jacobs and Malefahlo from the Department of Cardiothoracic Surgery and Prof Stoltz & Sr Zeeland for patient referrals from the unit of Infectious Diseases. Thanks also to our colleagues at NECSA, in particular Otto Knoessen, for performing the HPLC on ^{68}Ga-citrate.

My deepest, most heartfelt gratitude goes to my parents, Quintus and Monica Vorster, my husband Dwayne, brother Martin, family and friends. For your unconditional love, support, encouragement, for understanding and for always believing in me. I am unbelievably blessed to have all of you in my life. Thanks to my wonderful parents for providing me with the rare privilege of a home filled with books and thought-provoking conversations, where academic literature were often being written or edited, lectures prepared and graduations attended. Thank you so much, Dad, for inspiring me with your own exceptional and brilliant academic career and Mom for always being my biggest fan and indispensible source of love, support and encouragement.

To my amazing husband, Dwayne, thank you so much for putting up with the many, many hours spent in front of my computer, for always believing in me, for encouraging me, for not allowing me to take myself too seriously and for always placing the latest helpful technology at my fingertips.